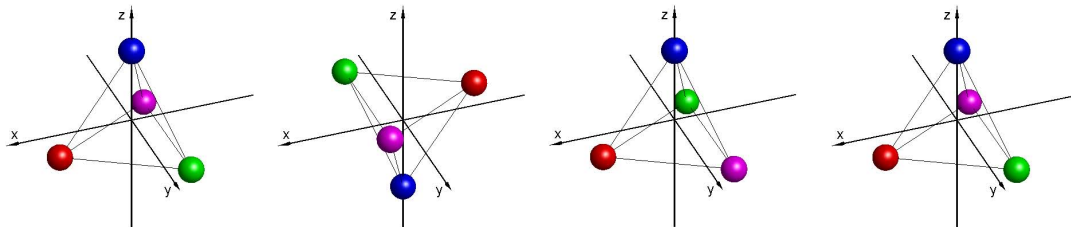# Multiply Excited Intra-shell States

Geometric and quantum-mechanical symmetries in lithium- and beryllium-like systems

Marianne Poulsen

Master's thesis

Department of Physics and Astronomy
University of Aarhus
October 2004

Acknowledgements

Many people have contributed to making my time writing this thesis interesting and joyful. First of all, I am very thankful to my supervisor, Lars Bojer Madsen, for his idea to this project and his encouragement and patience during the last year. I also owe a debt of gratitude to Jan Linderberg and Jeppe Olsen at the Department of Chemistry, University of Aarhus, for their help with the difficult theory of the permutation group.

My friends and colleagues at the University of Aarhus are likewise acknowledged for the enjoyable atmosphere in which my university studies have taken place. The five years I have spent at the Departments of Physics and Mathematics have been a pleasure because of good company provided by both staff and fellow students. In this connection it would be impossible to mention everybody I am grateful to. However, I would like to single out for special thanks the people who have been involved in 'Fysikshow' the last two years. Both the friendship and the source of inspiration have been of great importance to me. A special gratitude is also extended to my officemates over the last couple of years for bringing me apples, helping with English and making the time cheerful. Finally, I am very grateful to those of my friends who have taking part in proofreading this thesis.

Contents

Chapter 1

Introduction

1.1   Motivation

The first few decades of the previous century were gilded years in terms of atomic physics and quantum mechanics. The development was impressive and the theory reached a degree of completeness. However, modern quantum theory still relies on approximate methods for calculating atomic spectra since an exact solution to the Schrödinger equation only exists for one-electron systems. Development of high-precision experimental techniques, such as high-resolution laser spectroscopy, have opened up new and interesting fields within atomic physics over the last decades. A current interest in multiply excited states is thus strongly stimulated by a new generation of synchrotron light sources providing unprecedented brightness. In particular, multiple excitations can lead to states with unoccupied inner shells also known as hollow states. When all the inner orbitals are empty the electrons move around at relatively large distances from the nucleus in a highly correlated manner. Successful access to hollow lithium states makes studies of quadruply excited states the next step in this development. The goal of this thesis is therefore to contribute to the theoretical characterization and understanding of triply and quadruply excited states.

1.2   The study of multiply excited states

When multiply excited states are considered, electron-electron correlations become increasingly important and the conventional Hartree-Fock methods no longer apply. The Hartree-Fock method does not include the inter-electronic interaction, but considers each electron to move in the mean field generated by the nucleus and all the other electrons. The optimal wave function is found by using the variational method and therefore the theory is only effective for the calculation of the ground state and single-electron excitation part of the spectrum. Madden and Codling (1963) were the first to experimentally reveal anomalies above the first ionization threshold in helium [1]. Being the simplest possible many-electron systems, helium
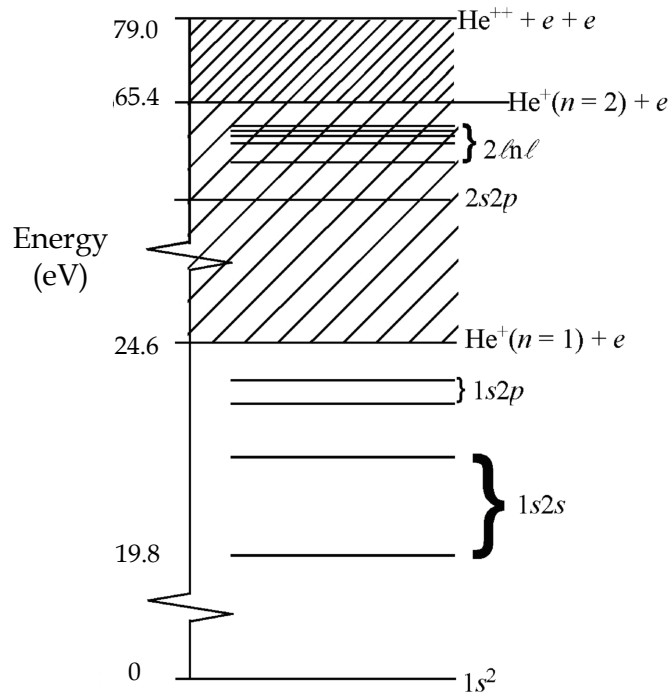
Figure 1.1: Energy level scheme showing some states of He and He$^+$. Adopted from reference [2] and adjusted with data from reference [3].

and helium-like ions have played an important role in the study of multiply excited states. Figure 1.1 gives a schematic overview of the energy levels in He and He$^+$. The energy of the first excited state is seen to be 19.8 eV above the ground state. The first ionization threshold is at 24.6 eV while the second ionization threshold is seen to be at 79 eV; in other words, the ionization energy of a ground state He$^+$ is 54.4 eV.

The photoabsorption experiment by Madden and Codling showed two important features. Firstly, there was clear evidence of discrete states embedded in the continuum. For each doubly excited state there will always be a continuum state with the same energy, as an example 2s2p and 1sϵp have the same energy (ϵ refers to a free electron and $n'l'n''l''$ denotes the principal quantum numbers and the angular momenta of the two electrons). The electron-electron interaction couples these states and as a result the doubly excited state decays by autoionization. Secondly, the experiment demonstrated that classification in terms of a single-electron configuration is impossible due to the electron-electron interaction. The $n = 2$ level of He$^+$ is degenerate (2s and 2p) and two separate series of autoionizing resonances are thus expected to converge to this limit, namely 2snp and 2pns. However, only a single series was observed. The theory of autoionization and configuration-mixing above the first ionization threshold was explained by Fano, Cooper and co-workers who pointed out that the $|2snp\rangle$ and $|2pns\rangle$ states should be described by the configuration superpositions $(|2snp\rangle \pm |2pns\rangle)/\sqrt{2}$ [4, 5, 6]. The so-called configuration-mixing fractions specify the mixing between single-electron
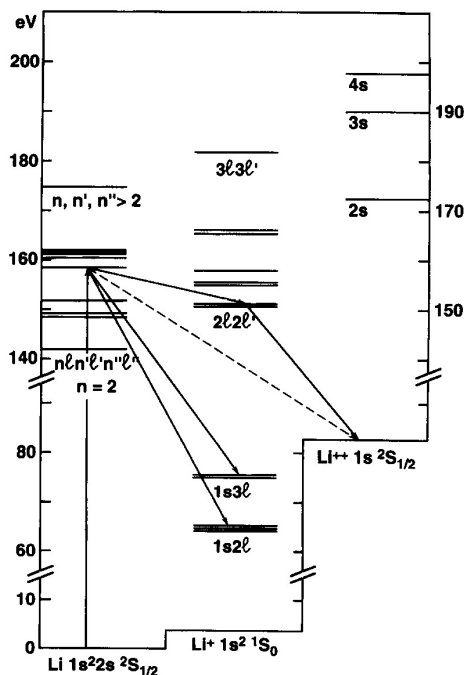
Figure 1.2: Energy level scheme showing some states of Li, Li$^+$ and Li^{++}. Adopted from reference [7].

configurations. Thus, the mixing fractions for $(|2snp\rangle \pm |2pns\rangle)/\sqrt{2}$ are 1/2 for both $|2snp\rangle$ and $|2pns\rangle$.

The Madden and Codling experiment and the accompanying theoretical discussion started an interest in electron-electron correlations in multiply excited states; an interest which has been reinforced in the course of the last decade due to the new possibilities for experimental investigation. The two-electron atom is almost completely understood and characterized, and consequently, triply excited states has been subject for recent theoretical as well as experimental investigations.

Figure 1.2 shows the energy level structure in Li, Li$^+$ and Li^{++}. In particular, we notice that triply excited states are located above the second ionization threshold. The lowest triply excited state is of ^{2}P^o symmetry and denoted Li(2s2s2p^{2}P^o) by its dominant configuration. This notation is frequently applied in the literature despite the fact that a classification in terms of a single-electron configuration is impossible. The Li(2s2s2p^{2}P^o) state is located approximately 142 eV above the Li(1s1s2s^{2}S^e) ground state. Experimentally, this energy is achieved either by collisions or by photoexcitation. The very first observation of triply excited states in three electron systems was in e^-+He scattering by Kuyatt *et al* as early as 1965 [8]. Ten years later the first measurement of triply excited states in atomic lithium was reported by Bruch *et al* [9]. They used a beam-foil technique, and their measurement was followed by another experiment by Rødbro *et al*, using collisional excitation in which the foil was replaced with a target gas, which in turn led to an improvement in energy resolution [10]. A gap of almost thirty years

elapsed from the first observation of triply excited states to the first measurement by photoabsorption by Kiernan *et al* (1994) who used the so-called dual-laser plasma technique to obtain appropriate spectra [11].

Due to the one-particle nature of the dipole operator photoexcitation of the Li(1s1s2s^{2}S^e) ground state to a triply excited state cannot occur in the absence of electron-electron interaction. Consequently, the study of these processes enables one to characterize highly correlated systems. In contrast, collision processes are not restricted by specific selection rules and optically inaccessible states can therefore be strongly populated in these processes. The different qualities in the two methods can be viewed as positive or negative depending on the purpose of the experiment and therefore the two methods complement each other.

As a result of further advances in high-resolution light sources, triply excited states in lithium have been the subject of intense studies over the last decade. Various experiments with photoexcitation have been carried out, including both photoion- and photoelectron experiments. The advantage of photoelectron spectrometry compared to the photoion technique is the possibility of leaving the system in individual final ionic states uniquely determined by the photon energy, $\hbar\omega$, and the energy of the measured electron. However, these experiments require the photon flux to be orders of magnitude higher than in photoion experiments, sadly with poorer energy resolution as a consequence. A more detailed review of experimental results on triply excited states in lithium and references to specific articles can be found in references [12, 13].

The theories describing multiply excited states may be divided into two main categories. The first contains various computational techniques yielding precise predictions of properties of atomic states such as energy levels, widths and configuration-mixing fractions. The Schrödinger equation has thus been solved in various refined basis sets, but also methods such as the hyperspherical approach have been used. These techniques add little physical insight into the correlated systems and will not be treated in this thesis. A review of the most important *ab initio* methods can be found in references [12, 13]. The second category consists of theoretical models which aim at providing more understanding in the form of physical images including geometry, symmetry considerations and electronic motion. The aim of this thesis is to present an explicit analytical construction of highly-correlated multiply excited states, a construction which, in addition to precise predictions of atomic states, provides a simple picture illustrating the underlying physics of the systems. Moreover, it will be demonstrated how multiply excited states can be classified exclusively on the basis of symmetry.

Lithium- and beryllium-like systems are chosen for our study for two reasons. Firstly, research on these states provides a possibility to test theoretical approximations for the dynamics of the electrons because of the simplicity of these systems compared to larger systems. The electrons move in a highly correlated manner and more electrons would therefore complicate the problem. Secondly, the new possibilities for a detailed experimental investigation of these states motivate the theoretical study greatly. We study the so-called intra-shell states which are hollow

states with the electrons confined to the same shell. These states are interesting since the dominant configurations of the lowest-lying triply excited lithium states and quadruply excited beryllium states are intra-shell states. In addition, intra-shell states have higher symmetry than inter-shell states in which the electrons occupy different shells.

A natural question is whether there is anything new to learn when the number of electrons is increased from three to four. The answer is yes. First of all, we gain insight into a new layer of atomic physics, since the four-electron system has been the subject of only a few studies. It is clear that the four-electron problem is related to the three- as well as the two-electron problem. Below the third ionization threshold the four-electron atom effectively behaves like the three-electron atom which essentially behaves like the two-electron atom below the second ionization threshold. However, above every ionization threshold new decay channels open up. Furthermore, the electron-electron correlations are expected to be stronger when more electrons interact. Finally, the spatial extension is an important difference between the three-electron system and larger systems. Three pointlike particles will always lie in a plane while the extent of four pointlike particles randomly placed is three dimensional.

1.3   Thesis Outline

The thesis is organized as follows. Chapters 2-4 present theoretical models and predictions for multiply excited states. Chapter 5 gives a summery and concludes. Appendixes A-C are not, as such, part of the thesis, and the latter can be read independently of these. Appendixes B-C are for readers with interest in computer programs used in making numerical calculations.

Chapter 2: This chapter demonstrates an elegant method to classify atomic states, especially multiply excited intra-shell states, exclusively on the basis of symmetry.

Chapter 3: This chapter deals with triply excited intra-shell states. Firstly, it gives an introduction to the so-called symmetric rotor model which gives an explicit analytical construction of highly correlated multiply excited states. Secondly, atomic state predictions within the symmetric rotor model are presented and compared with *ab initio* calculations.

Chapter 4: Here the symmetric rotor model is extended to quadruply excited states.

Chapter 5: Summary and concluding remarks on the thesis project in general.

Appendix A: This appendix gives a summary of the results of the representation theory of the permutation group used in chapter 2.

Appendix B: Here computer programs used in classifying atomic states in chapter 2 are discussed.

Appendix C: Here some of the computer programs used in making atomic states predictions within the symmetric rotor model in chapters 3 and 4 are discussed.

Chapter 2

Classification based on symmetry

It is well-known that symmetry plays an important role in quantum mechanics. The eigenstates of a given Hamiltonian are classified according to a set of quantum numbers, which specifies the transformation properties of the wave function under symmetry operations. In this way the spatial distribution of the wave function is constrained by the transformation properties arising from invariance under rotation, inversion and permutation of particles. Consequently, specific nodal surfaces may appear in the multidimensional coordinate space. These are called inherent nodal surfaces since they originate just from symmetry. A geometric configuration located in a nodal surface is strictly forbidden, and since the wave function is continuous the structure in a region surrounding this configuration will to a great extent be affected by the nodal surface.

This chapter demonstrates how atomic states can be classified exclusively on the basis of symmetry and therefore independent of the model describing the dynamics of the system. Hence, the resulting classification schemes are very general and useful in connection with the so-called symmetric rotor model presented in chapters 3 and 4. The classification follows the ideas presented in a number of papers by Bao *et al* [14]-[19]. However, the approach here is chosen slightly differently so that the interpretation of the results is compatible with the symmetric rotor model. Moreover, classification of six-valence-electron atoms has not been presented before. The first section introduces the use of group theory in the general setup. The second section deals with the simplest possible many-electron system, namely the two-electron system, and tends as an introduction to the method. Section three and four classify three- and four-valence-electron atoms and are thus most important to this thesis in general. Finally, the last section of this chapter presents considerations for and results of the classification of six-valence-electron atoms. This section completes the work done on classification based on symmetry and, in addition, underlines the generality of the method.

2.1 The use of group theory

Systems of identical fermions are closely connected to the permutation group, S_n, since the Pauli principle requires such systems to have permutation symmetry. Group theory in physics is the subject of several textbooks e.g. references [20, 21, 22], and the contents of this section and especially appendix A are mainly based on these references. The classification of the atomic states will rely on the claim that an antisymmetrized eigenstate of identical fermions in general can be expanded as

$$|\Psi^{LM\pi,SM_s}\rangle = \sum_i F_{Mi}^{L\pi S}\chi_{M_si}^S ,$$ (2.1)

where the summation is over all possible couplings of intermediate spin. Here L is the total angular momentum of the state, M the magnetic quantum number, π the parity, S the total spin and M_s its projection. The expansion in equation (2.1) is possible in the so-called Young-Yamanouchi basis of S_n. The theory of the permutation group will not be subject for this thesis, but the most important results of the Young-Yamanouchi theory are summarized in appendix A. For a more detailed discussion, the reader is referred to references [20, 21, 22]. For the purpose of making a classification scheme it is not important to know the explicit expressions for $F_{Mi}^{L\pi S}$ and $\chi_{M_si}^S$. The advantage of the expansion in equation (2.1) is that for a given intermediate spin coupling the contribution to the expansion is a product of a spatial function, $F_{Mi}^{L\pi S}$, and a spin function, $\chi_{M_si}^S$. This is not general for all representations; using for example the antisymmetrization operator on a random state gives a *sum* of products for each intermediate spin coupling. Since we will examine the symmetry properties of the spatial part of the wave function, the expansion in equation (2.1) is a clever choice.

We are only interested in the relative positions of the electrons and the nucleus, the overall rotation with respect to the fixed laboratory frame is not important. A body frame will therefore be defined and the spatial functions expanded through rotations as

$$F_{Mi}^{L\pi S} = \sum_{M_I} D_{M_IM}^L(-\omega)F_{M_Ii,\omega}^{L\pi S} ,$$ (2.2)

where $F_{M_Ii,\omega}^{L\pi S}$ refers to a rotated frame determined by the Euler angles $\omega = (\alpha, \beta, \gamma)$ describing rotations around fixed z, y and z axes, respectively. The Wigner functions, $D_{M_IM}^L(-\omega)$, are the matrix elements of the rotation matrix, $\mathbf{R}(-\omega)$, and M_I is the magnetic quantum number with respect to the body-fixed z axis.

2.2 Two-valence-electron atoms

Owing to its simplicity, the two-electron system is a typical textbook example. Therefore, it is appropriate to use this well-known system to introduce the methods and considerations presented in this chapter.

When atomic states are classified, it is in particular interesting to find the states with lowest energy. As argued earlier the mixing between different configurations are so great that classifications based on single products of orbitals are useless and we will only be concerned about the total angular momentum, L, the total spin, S, and the parity, π, of the states. Before we consider the symmetry of the two-electron system we recall some basic results of the Pauli exclusion principle stating that systems of identical fermions are described by antisymmetric wave functions. In the case of a system with only two electrons the spin part of the wave function is either symmetric (triplet states, $S = 1$) or antisymmetric (singlet states, $S = 0$). Hence, the total wave function for such a system splits up into a product of a symmetric (antisymmetric) spin function and an antisymmetric (symmetric) spatial function in the case of triplet (singlet) states. The separation of the spin and spatial function is special for the two-electron system and simplifies the problem to a great extent. As a consequence, the number of possible terms, $^{2S+1}L^{\pi}$, from pair of two equivalent electrons ($l_1 = l_2$) is limited by the constraint

$$L + S = \text{even integer}, \qquad \text{when } l_1 = l_2 . \tag{2.3}$$

The proof of this theorem is simple and given in several textbooks e.g. reference [21]. If we, in addition to the above statements, use the rules for coupling two angular momenta we can deduce that the terms $^1S^o$, $^3S^o$ and $^3S^e$ are forbidden by Pauli statistics. An S-state requires two equivalent electrons and, therefore, has to be of even parity, since the parity is determined as

$$\pi = (-1)^{l_1+l_2} . \tag{2.4}$$

A triplet state of zero total angular momentum is forbidden by equation (2.3) and, as a result, the only allowed S-state is $^1S^e$.

The classification method to be presented does not tell whether a state is allowed or not but whether the state is expected to belong to the low-lying part of the energy spectrum. Hence, this method screens out more states than just those forbidden by Pauli statistics. In addition to two-electron atoms the classification covers two-valence-electron atoms, since these to some extent behave like a two-electron system. The method only applies to states with the two electrons placed in the same shell such that their average distances to the nucleus are equal. Furthermore, the classification is expected to be most valuable for excited states with a high principal quantum number, $n = n_1 = n_2$, since larger distance to the nucleus increases the importance of the electron-electron interaction, and Pauli statistics play a less significant role when more one-electron orbital angular momenta are available for coupling ($l_i \leq n - 1$).

2.2.1 Symmetry considerations

Considering the potential energy of the system, the attraction to the nucleus and the electron-electron repulsion, the most favourble configuration is when the two
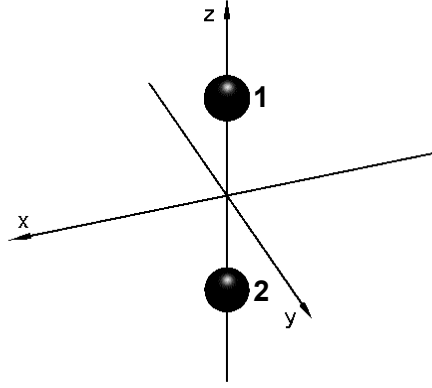
Figure 2.1: Choice of body-fixed frame for the two-electron atom. The nucleus is imagined to be localized in the origin.

electrons are placed diametrically opposite with respect to the nucleus (see figure 2.1). We therefore expect that the wave function prefers to peak at this so-called line-configuration and distribute around it. As a result, a state with an inherent nodal line localized in the line-configuration does not belong to the low-lying part of the energy spectrum.

To consider the interaction within the three-body system, a body-fixed frame is chosen as seen in figure 2.1. The choice is not random but inspired by molecular theory. The rotational state of a molecule is determined by the quantum numbers L, M and M_I which specify the total angular momentum and its projection on the z axis fixed in space and the z axis in the body-fixed frame, respectively. However, M_I is only a good quantum number if the moments of inertia with respect to the body-fixed x and y axes are the same and in this case the three-atomic molecule is called a linear rotor. This condition is only satisfied if the z axis is chosen to be the principal axis as in figure 2.1.

We see that any combination of two of the following operations leaves the system unchanged

$$\mathbf{I},\ \mathbf{P}(12),\ \mathbf{R}_\pi^y,\ \mathbf{R}_\pi^x, \tag{2.5}$$

where $\mathbf{P}(12)$ denotes a permutation of the two particles. $\mathbf{I}$ is the operator of space inversion and $\mathbf{R}_\theta^k$ is the operator of rotation about the k axis by an angle θ. The operation $\mathbf{R}_\pi^x$ is equivalent to the three successive rotations $\mathbf{R}_{-\pi/2}^y \mathbf{R}_\pi^z \mathbf{R}_{\pi/2}^y$ which is a more convenient expression since the Wigner functions of rotations are determined with respect to the fixed y and z axes. As a result, the line-configuration is invariant to the following operations

$$\mathbf{O}_a = \mathbf{I}\mathbf{P}(12)\ , \tag{2.6}$$

$$\mathbf{O}_b = \mathbf{I}\mathbf{R}_\pi^y\ , \tag{2.7}$$

$$\mathbf{O}_c = \mathbf{I}\mathbf{R}_{-\pi/2}^y \mathbf{R}_\pi^z \mathbf{R}_{\pi/2}^y\ . \tag{2.8}$$

In the case of two electrons the spin coupling is unambiguous and therefore the

wave function, $|\Psi^{LM\pi,SM_s}\rangle$, in equation (2.1) is simply given by

$$|\Psi^{LM\pi,SM_s}\rangle = F_M^{L\pi S}\chi_{M_s}^S = \left[\sum_{M_I} D_{M_I M}^L(-\omega)F_{M_I,\omega}^{L\pi S}\right]\chi_{M_s}^S . \qquad (2.9)$$

Since the line-configuration is invariant to $\mathbf{O}_a - \mathbf{O}_c$, the value of the spatial function, $F_{M_I,\omega}^{L\pi S}$, at the line-configuration has to be invariant to these operations. This value will be denoted $F_{M_I}^{L\pi S}(\text{line})$ with the subscript w left out. As a result, the wave function is constrained by the condition

$$F_{M_I}^{L\pi S}(\text{line}) = \left[\mathbf{O}_\rho F_{M_I,\omega}^{L\pi S}\right]_{\text{line}} , \qquad \rho \in \{a, b, c\} , \qquad (2.10)$$

which yields the following sets of homogeneous linear equations

$$F_{M_I}^{L\pi S}(\text{line}) = \pi G^S(\mathbf{P}(12))F_{M_I}^{L\pi S}(\text{line}) , \qquad (2.11)$$

$$F_{M_I}^{L\pi S}(\text{line}) = (-1)^L F_{-M_I}^{L\pi S}(\text{line}) , \qquad (2.12)$$

$$F_{M_I}^{L\pi S}(\text{line}) = \pi(-1)^{M_I} F_{M_I}^{L\pi S}(\text{line}) , \qquad (2.13)$$

where $G^S(\mathbf{P})$ are the Yamanouchi matrices of permutations in S_n. For smaller permutation groups these can be looked up in tables (e.g. reference [20]) and in appendix A it is demonstrated how to derive them by hand in general. Furthermore, for easy reference those matrices which are most complicated to derive are listed in appendix A. In the case of S_2 the matrices are simple and well-known, namely $G^0(\mathbf{P}(12)) = (1)$ and $G^1(\mathbf{P}(12)) = (-1)$ or, in other words, the effect of the permutation $\mathbf{P}(12)$ is to leave the spatial part of the singlet wave function unchanged and change the sign of the spatial part of the triplet wave function. The ambiguous use of the sign π should not give rise to any confusion since the context makes it clear whether π is the parity, ± 1, or the number, $\pi = 3.1415...$. The following properties of the rotation operator have been used to derive equations (2.11)-(2.13) and the corresponding equations in the following sections [23, section 3.5]

$$\mathbf{R}_\theta^z F_{M_I i}^{L\pi S} = e^{-i\theta M_I} F_{M_I i}^{L\pi S} , \qquad (2.14)$$

$$\mathbf{R}_\theta^y F_{M_I i}^{L\pi S} = \sum_{M_I'} d_{M_I' M_I}^L(\theta) F_{M_I' i}^{L\pi S} , \qquad (2.15)$$

$$d_{M_I' M_I}^L(\pi) = (-1)^{L-M_I'}\delta_{M_I'-M_I} , \qquad (2.16)$$

$$d_{M_I' M_I}^L(-\beta) = (-1)^{M_I+M_I'}d_{M_I' M_I}^L(\beta) , \qquad (2.17)$$

$$\delta_{MN} = \sum_{M'} d_{MM'}^L(\beta)d_{M'N}^L(\beta) , \qquad (2.18)$$

where $d_{M_I M_I'}^L(\beta) = D_{M_I M_I'}^L(0, \beta, 0)$. As an example we will derive equation (2.13)

from equation (2.10)

$$F_{M_I}^{L\pi S}(\text{line}) = \left[\mathbf{O}_c F_{M_I,\omega}^{L\pi S}\right]_{\text{line}} \tag{2.19}$$

$$= \left[\mathbf{IR}_{-\pi/2}^y \mathbf{R}_\pi^z \mathbf{R}_{\pi/2}^y F_{M_I,\omega}^{L\pi S}\right]_{\text{line}} \tag{2.20}$$

$$= \left[\mathbf{IR}_{-\pi/2}^y \mathbf{R}_\pi^z \sum_{M_I'} d_{M_I'M_I}^L\left(\frac{\pi}{2}\right) F_{M_I',\omega}^{L\pi S}\right]_{\text{line}} \tag{2.21}$$

$$= \left[\mathbf{IR}_{-\pi/2}^y \sum_{M_I'} (-1)^{M_I'} d_{M_I'M_I}^L\left(\frac{\pi}{2}\right) F_{M_I',\omega}^{L\pi S}\right]_{\text{line}} \tag{2.22}$$

$$= \left[\mathbf{I} \sum_{M_I'M_I''} (-1)^{M_I'} d_{M_I''M_I'}^L\left(-\frac{\pi}{2}\right) d_{M_I'M_I}^L\left(\frac{\pi}{2}\right) F_{M_I'',\omega}^{L\pi S}\right]_{\text{line}} \tag{2.23}$$

$$= \left[\mathbf{I} \sum_{M_I''} (-1)^{M_I''} F_{M_I'',\omega}^{L\pi S} \sum_{M_I'} d_{M_I''M_I'}^L\left(\frac{\pi}{2}\right) d_{M_I'M_I}^L\left(\frac{\pi}{2}\right)\right]_{\text{line}} \tag{2.24}$$

$$= \left[\pi(-1)^{M_I} F_{M_I,\omega}^{L\pi S}\right]_{\text{line}} \tag{2.25}$$

$$= \pi(-1)^{M_I} F_{M_I}^{L\pi S}(\text{line}) \ . \tag{2.26}$$

The sets of homogeneous linear equations that the coefficients, $F_{M_I,\omega}^{L\pi S}$, have to obey at the line-configuration only depend on L, π and S. The question is whether there exist nontrivial solutions to equations (2.11)-(2.13). If no solution with at least one nonzero $F_{M_I}^{L\pi S}(\text{line})$ exists for a given set of L, π and S, the term, $^{2S+1}L^\pi$, is line-inaccessible. Consequently, $|\Psi^{LM\pi,SM_s}\rangle$ is zero for any line-configuration, independent of the size and orientation of the line, and the term is not expected to belong to the low-lying energy spectrum. On the other hand, if a nontrivial solution to equations (2.11)-(2.13) exists for a given set of L, π and S, the term, $^{2S+1}L^\pi$, is line-accessible. Therefore, solving equations (2.11)-(2.13) gives a classification scheme for the two-valence-electron atoms.

2.2.2   Solution procedure and results

Owing to the simplicity of the representations, $G^S(\mathbf{P})$, for S_2 it is an easy task to solve equations (2.11)-(2.13). Equation (2.11) relates the parity and the spin multiplicity by the constraint

$$\pi = G^S(\mathbf{P}(12)) \ . \tag{2.27}$$

Consequently, the low-lying triplet states are of odd parity and the low-lying singlet states of even parity. Furthermore, equation (2.13) relates the parity to the M_I quantum number such that

$$\pi = (-1)^{M_I} \ . \tag{2.28}$$

Hence, S-states with odd parity are line-inaccessible, since $|M_I| \le L$. Equation (2.12) gives an one-to-one correspondence between $F_{-M_I}^{L\pi S}(\text{line})$ and $F_{M_I}^{L\pi S}(\text{line})$ for

Table 2.1: Classification scheme for two-valence-electron atoms, especially valid for doubly excited intra-shell states. Only line-accessible states with $L \leq 4$ are shown, and the allowed values of T are marked with x.

$\backslash T$	0	1	2	3	4
$^1S^e$	x				
$^1D^e$	x		x		
$^1F^e$			x		
$^1G^e$	x		x		x
$^3P^o$		x			
$^3D^o$		x			
$^3F^o$		x		x	
$^3G^o$		x		x	

each term and, consequently, we only have to consider the absolute value of M_I. We will see that this is a general fact for the larger systems as well, and therefore we follow the conventional notation and define $T \equiv |M_I|$. In addition, equation (2.12) shows that $M_I = 0$ is forbidden for odd values of L. Table 2.1 displays the line-accessible states with $L \leq 4$.

2.2.3 Discussion

First of all, we note that the classification scheme in table 2.1 is consistent with the conclusions from the use of Pauli statistics; thus, the only line-accessible S-state is $^1S^e$. Furthermore, it is worth considering the energy levels of doubly excited states in helium. Figure 2.2 shows the lowest-lying part of the helium spectrum for states with both electrons in the third principal shell ($n = 3$) and $L \leq 3$. As predicted the lowest-lying spectrum consists of states given in table 2.1. However, the lowest $^3P^e$ and $^1P^o$ term have lower energy than $^3F^o$. This is easy explained by Pauli statistics. When $n = 3$, three sets of one-electron angular momenta couple to $^3P^e$, namely sd, p^2 and d^2, two sets couple to $^1P^o$, namely sp and pd, while only one set couple to $^3F^o$, namely pd. Neither $^3D^o$ nor $^1F^e$ are seen in figure 2.2. The term $^1F^e$ is simply Pauli forbidden for two electrons with $n = 3$. Since $^3D^o$ is not seen, the term has higher energy than $^3F^o$ even though the only possible configuration for both states is pd. However, the classification in table 2.1 shows that two values of T are allowed for $^3F^o$ compared to only one for $^3D^o$. The rotational part of the energy spectrum for a linear rotor molecule is [25, equation 10.104]

$$E = \frac{1}{2I}(L(L+1) - T^2) , \qquad (2.29)$$

with $I = 2mr^2$ being the moment of inertia of the rotor, where r denotes the distance from the outer atoms to the center and m is the mass of the outer atoms of the molecule. Consequently, it is actually expected from a molecular viewpoint that the lowest $^3F^o$ state has lower energy than the lowest $^3D^o$ state. We will discuss the question about rotational-like energy spectrum in detail in chapter 3.
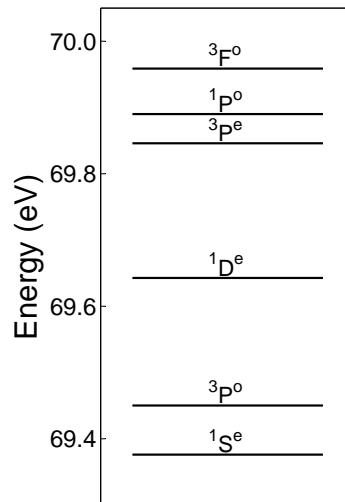
Figure 2.2: The lowest-lying part of the energy spectrum for doubly exited helium with both electrons in the third principal shell ($n = 3$) and $L \leq 3$. The energy of the states are above the ground state in He obtained using the truncated diagonalization method with hydrogenic basis functions [24].

This example showed that a combination of the symmetry-based classification and Pauli statistics gives the most correct classification. However, Pauli statistics play a less significant role for higher n where more one-electron angular momenta are available for coupling. Furthermore, the constraints arising from symmetry are expected to be even more significant when more electrons interact and the electron-electron interaction is stronger. Therefore, we expect a symmetry-based classification to be of great value for three-, four- and six-electron systems. It is also possible to classify five-valence-electron atoms using symmetry, but the constraints arising from symmetry considerations are not as strong in this case, to which we will return.

To conclude this section, we have seen a method to obtain a primary classification scheme for the two-valence-electron atoms especially valid for doubly excited states. The procedure seems a bit elaborate, but the point is that a generalization to the more complicated systems with more electrons is straightforward though more tedious.

2.3   Three-valence-electron atoms

2.3.1   Symmetry considerations

We now proceed by classifying three-valence-electron atoms using the method introduced in the previous section. The Coulomb repulsion between the outer electrons is minimized when they form an equilateral triangle (ET). To minimize the total potential energy the nucleus should be in the center of the ET, and the con-
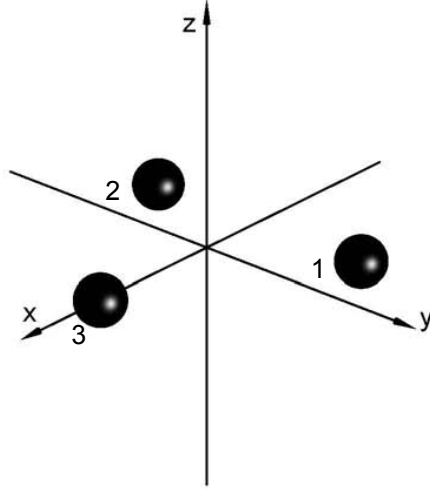
Figure 2.3: Choice of body-fixed frame for the three-valence-electron atom. The nucleus is imagined to be localized in the origin.

figuration is then confined to a plane. Therefore, the low-lying states will prefer to pursue an ET as the most probable shape i.e. the wave functions prefer to peak at the vertices of the ET and distribute around it. As a result, a state with an inherent nodal plane localized in the ET-configuration does not belong to the low-lying part of the energy spectrum. In particular, the ET-geometry is advantageous for triply excited intra-shell states, since the large distance to the nucleus increases the importance of the electron-electron interaction.

We recall that the magnetic quantum number with respect to the body-fixed z axis, M_I, only is a good quantum number if the moments of inertia with respect to the body-fixed x and y axes are the same. Therefore, the body-fixed frame is chosen so the electrons are in the xy plane with the nucleus in the origin as seen in figure 2.3. The configuration then corresponds to that of a symmetric top molecule.

Considering the symmetry of the ET we see that the configuration is invariant to the following three types of operations (see figure 2.3)

$$\mathbf{O}_d = \mathbf{R}_\pi^z \mathbf{I} \, , \tag{2.30}$$
$$\mathbf{O}_e = \mathbf{P}(132)\mathbf{R}_{2\pi/3}^z \, , \tag{2.31}$$
$$\mathbf{O}_f = \mathbf{P}(12)\mathbf{R}_\pi^y \mathbf{I} \, , \tag{2.32}$$

with the notation used in section 2.2 and $\mathbf{P}(132)$ denoting the cyclic permutation $1 \rightarrow 3 \rightarrow 2 \rightarrow 1$. In addition to $\mathbf{O}_d - \mathbf{O}_f$ the ET is invariant to other operations e.g. $\mathbf{P}(123)\mathbf{R}_{-2\pi/3}^z$, but they do not restrain the symmetry of the ET further.

Since the ET is invariant to $\mathbf{O}_d - \mathbf{O}_f$, the value of $F_{M_I i, \omega}^{L\pi S}$ at the ET-configuration, $F_{M_I i}^{L\pi S}(\text{ET})$, has to be invariant to these operations. Consequently, the wave func-

tion is constrained by the condition

$$F_{M_I i}^{L\pi S}(\text{ET}) = \left[\mathbf{O}_\rho F_{M_I i,\omega}^{L\pi S}\right]_{\text{ET}}, \qquad \rho \in \{d, e, f\}, \tag{2.33}$$

which yields the following sets of homogeneous linear equations when equations (2.14)-(2.18) are used

$$F_{M_I i}^{L\pi S}(\text{ET}) = \pi(-1)^{M_I} F_{M_I i}^{L\pi S}(\text{ET}), \tag{2.34}$$

$$F_{M_I i}^{L\pi S}(\text{ET}) = e^{-i\frac{2\pi}{3}M_I} \sum_{i'} G_{ii'}^{S}(\mathbf{P}(132)) F_{M_I i'}^{L\pi S}(\text{ET}), \tag{2.35}$$

$$F_{M_I i}^{L\pi S}(\text{ET}) = (-1)^{L} \sum_{i'} G_{ii'}^{S}(\mathbf{P}(12)) F_{-M_I i'}^{L\pi S}(\text{ET}), \tag{2.36}$$

where $G_{ii'}^{S}(\mathbf{P})$ now denotes the Yamanouchi matrix elements of permutations in S_3. The summations $\sum_{i'} G_{ii'}^{S}(\mathbf{P}) F_{M_I i'}^{L\pi S}(\text{ET})$ are results of the matrix multiplications $G^{S}(\mathbf{P}) F_{M_I}^{L\pi S}$ since the representations, $G^{S}(\mathbf{P})$, are not in general one-dimensional as in the case of S_2. The dimension of $G^{S}(\mathbf{P})$ is equal to the number of possible intermediate spins, S_{12}, arising from coupling the spin of the first and second electron. As an example, for doublet states, $S = \frac{1}{2}$, two choices of S_{12} are possible, namely $S_{12} = 1\,(i = 1)$ and $S_{12} = 0\,(i = 2)$.

   Again we note that the sets of homogeneous linear equations which the coefficients, $F_{M_I i,\omega}^{L\pi S}$, have to obey at the ET-configuration only depend on L, π and S. If no solution to equations (2.34)-(2.36) with at least one nonzero $F_{M_I i}^{L\pi S}(\text{ET})$ exists for a given set of L, π and S, then the term, $^{2S+1}L^\pi$, is ET-inaccessible. Consequently, $|\Psi^{LM\pi,SM_s}\rangle$ is zero at any ET-configuration independent of the size and orientation of the ET, and the term will not belong to the low-lying energy spectrum. On the other hand, if a nontrivial solution to equations (2.34)-(2.36) exists for a given set of L, π and S, then the term, $^{2S+1}L^\pi$, is ET-accessible. Therefore, solving equations (2.34)-(2.36) gives a classification scheme for the three-valence-electron atoms.

2.3.2 Solution procedure and results

Equation (2.34) relates the parity to the value of M_I by the condition

$$\pi = (-1)^{M_I}. \tag{2.37}$$

This relation is well-known from the theory of the symmetric top molecule, and similar to that for the linear rotor. Equations (2.35) and (2.36) depend on S_{12} through the matrix elements $G_{ii'}^{S}(\mathbf{P})$. These equations are easiest to solve for the quartet states, $S = \frac{3}{2}$. In this case there is only one possible choice for the intermediate spin coupling, namely $S_{12} = 1$. Consequently, the matrix elements of the permutations are as simple as $G_{11}^{3/2}(\mathbf{P}(jk)) = -1$ or, in other words, the effect of a permutation of two electrons is to change the sign of the spatial part of the

wave function as it should be since the quartet spin function is totally symmetric. Hence, the set of equations to be solved for $S = \frac{3}{2}$ is

$$F_{M_I 1} = e^{-i\frac{2\pi}{3}M_I} F_{M_I 1} \,, \tag{2.38}$$

$$F_{-M_I 1} = -(-1)^L F_{M_I 1} \,, \tag{2.39}$$

with $F_{M_I i}^{L\pi S}(\text{ET}) = F_{M_I i}$ in short. In particular, it is seen from equation (2.38) that M_I is constrained to values which satisfy $M_I \bmod 3 = 0$. Equation (2.39) shows that only the absolute values of M_I are of interest, as claimed earlier. Moreover, we see that $M_I = 0$ is forbidden for even values of L. If we confine the classification scheme to $L \leq 4$ there are four nonzero solutions which can be written

$$|\Psi^{LM\pi,SM_s}\rangle_{\text{ET}} \propto \left[D_{M_I M}^{L}(-\omega) - (-1)^L D_{-M_I M}^{L}(-\omega) \right] \chi_{M_s}^{2} \,, \tag{2.40}$$

since the summation in equation (2.2) disappears because there only is one allowed value of T for all $L \leq 4$. The classification scheme for the quartet states is shown in the lower part of table 2.2.

When $S = \frac{1}{2}$ equations (2.34)-(2.36) can be solved in the same manner. The task is, however, not as simple as in the case of $S = \frac{3}{2}$ since there are two possible choices of i corresponding to S_{12}. Hence, owing to the permutation elements, $G_{ii'}^{S}(\mathbf{P})$, the equations will mix the values of i. Using appendix A (or the table given in reference [20]) we see that

$$G^{1/2}(\mathbf{P}(132)) = \begin{pmatrix} -\frac{1}{2} & -\frac{\sqrt{3}}{2} \\ \frac{\sqrt{3}}{2} & -\frac{1}{2} \end{pmatrix} \,, \tag{2.41}$$

$$G^{1/2}(\mathbf{P}(12)) = \begin{pmatrix} -1 & 0 \\ 0 & 1 \end{pmatrix} \,. \tag{2.42}$$

Hence, when $S = \frac{1}{2}$ equation (2.35) reads

$$\begin{pmatrix} -\frac{1}{2}e^{-i\frac{2\pi}{3}M_I} - 1 & -\frac{\sqrt{3}}{2}e^{-i\frac{2\pi}{3}M_I} \\ \frac{\sqrt{3}}{2}e^{-i\frac{2\pi}{3}M_I} & -\frac{1}{2}e^{-i\frac{2\pi}{3}M_I} - 1 \end{pmatrix} \bar{F}_{M_I} = 0 \,, \tag{2.43}$$

with $\bar{F}_{M_I} = \begin{pmatrix} F_{M_I 1} \\ F_{M_I 2} \end{pmatrix}$. As a result,

$$F_{M_I 1} = 0 \qquad\qquad \text{if } M_I \bmod 3 = 0 \,, \tag{2.44}$$

$$F_{M_I 2} = (-1)^{M_I \bmod 3} i F_{M_I 1} \,. \tag{2.45}$$

Inserting $G^{1/2}(\mathbf{P}(12))$ in equation (2.36) we get

$$\bar{F}_{M_I} = (-1)^L \begin{pmatrix} -1 & 0 \\ 0 & 1 \end{pmatrix} \bar{F}_{-M_I} \,, \tag{2.46}$$

which in addition to equations (2.44)-(2.45) yields

$$F_{M_I 1} = -(-1)^L F_{-M_I 1} \,. \tag{2.47}$$

It is worth noting that the coefficients $F_{M_I 1}$ and $F_{M_I 2}$ only differ by a phase. For $L \leq 4$ there are seven nonzero solutions which are given in the upper part of in table 2.2.

Table 2.2: Classification scheme for three-valence-electron atoms, especially valid for triply excited intra-shell states. Only ET-accessible states with $L \leq 4$ are shown, and the allowed values of T are marked with x.

$\backslash T$	0	1	2	3	4
$^2\mathrm{P^o}$		x			
$^2\mathrm{D^o}$		x			
$^2\mathrm{D^e}$			x		
$^2\mathrm{F^o}$		x			
$^2\mathrm{F^e}$			x		
$^2\mathrm{G^o}$		x			
$^2\mathrm{G^e}$			x		x
$^4\mathrm{P^e}$	x				
$^4\mathrm{F^o}$				x	
$^4\mathrm{F^e}$	x				
$^4\mathrm{G^o}$				x	

2.3.3   Discussion

Figure 2.4 shows $3l3l'3l''$ triply excited states in the lithium-like ion He$^-$ with $L \leq 4$ ordered along each column according to the $^{2S+1}L^{\pi}$ symmetry. The energies are calculated within the frozen-r model in which the radial degrees of freedom are frozen [26]. The frozen-r model has quantitatively been justified by multiconfigurational Hartree-Fock calculations [27] and by calculations with the hyperspherical method [28]. ET-accessible states are marked with red. In general we only consider states with $L \leq 4$ since states with larger L are very restricted by Pauli statistics for smaller principal quantum numbers, n. As an example, only one set of one-electron angular momenta couple to $^2\mathrm{H^e}$ within the third principal shell, namely 3d3d3d. We see a general tendency that the energy of the lowest state of a specific symmetry is lower for lower L. This can be explained by a combination of Pauli statistics and by considering the rotational part of the energy spectrum for a symmetric top molecule. In the next chapter we return to the energy spectrum and discuss the question of rotational structure in detail. The S-states do not follow this tendency which is in agreement with the symmetry based classification. Table 2.2 shows that no S-states are ET-accessible and consequently these states are not expected to belong the lowest-lying part of the energy spectrum. Among states with a specific L we see that the lowest-lying states are ET-accessible in agreement with our predictions.

In conclusion we have classified three-valence-electron atoms and especially triply excited intra-shell states. The classification can be done in more detail by considering other symmetries than the equilateral triangle e.g. the symmetry of an isosceles triangle, but this it not of interest in connection with the symmetric rotor model.
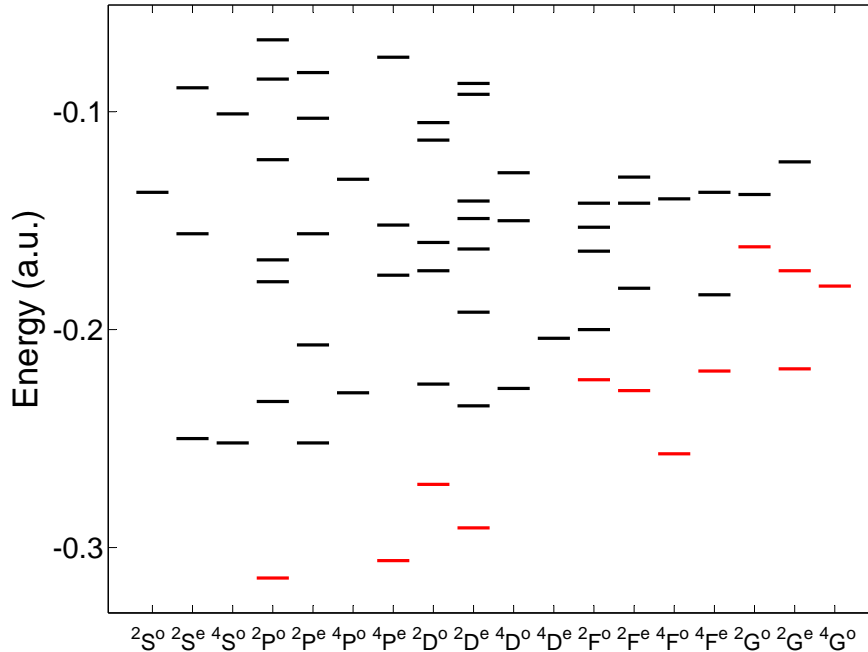
Figure 2.4: Energy levels of $3l3l'3l''$ triply excited states in He$^-$ with $L \leq 4$ calculated within the frozen-r model [26]. The states are ordered along each column according to the $^{2S+1}L^{\pi}$ symmetry. ET-accessible states are marked with red.

2.4 Four-valence-electron atoms

2.4.1 Symmetry considerations

We continue the classification with the four-valence-electron atomic states. The Coulomb repulsion between four electrons in the same shell will be minimized when the electrons are placed in the vertices of a regular tetrahedron (RTH) and, therefore, the low-lying states prefer to pursue a RTH as the most probable shape. Hence, the preferred geometric shape of the four-valence-electron atom corresponds to a spherical top.

In the classification of the two- and three-electron atoms the right choice of body-fixed frame was important. The magnetic quantum number with respect to the body-fixed z axis, M_I, is only a good quantum number if the moments of inertia with respect to the body-fixed x and y axes are the same. In contrast to the linear rotor and the symmetric top, this requirement is fulfilled for the spherical top no matter how the body frame is chosen. After all, the operations to which the RTH is invariant depend on the body frame. There are two natural choices of a body-fixed frame for the spherical top. The first shown in figure 4.2(a) has one electron placed on the z axis while the second shown in figure 4.2(b) treats all the electrons equally with respect to the z axis and is the one with highest rotational symmetry. Even though M_I will be a good quantum number no matter how the body frame is chosen, the choice is definitely important with respect to
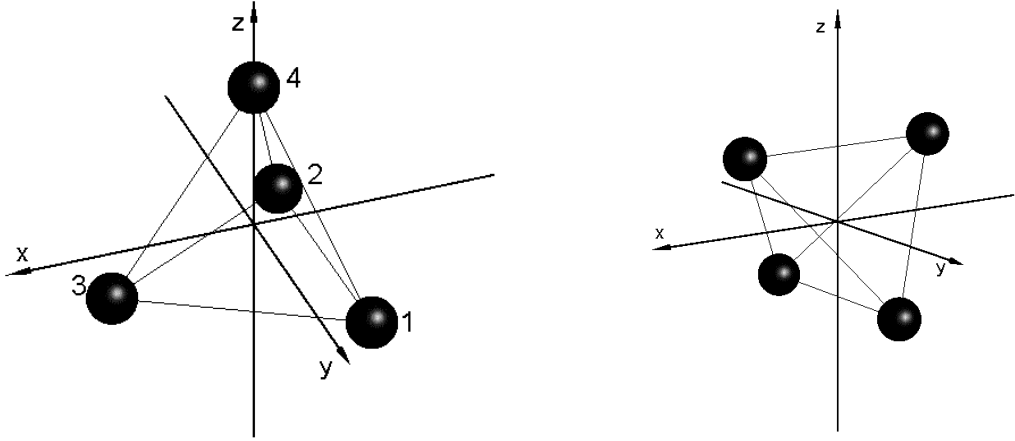
(a) One electron placed on the z axis.   (b) All electrons treated equally with respect to the z axis.

Figure 2.5: Two different choices of body-fixed frame.

numerical calculations within the symmetric rotor model discussed in chapter 4. The frame shown in figure 4.2(a) turns out to be preferred in this connection and the classification is therefore made with respect to this frame. Thus, the RTH is invariant to the following three types of operations

$$\mathbf{O}_g = \mathbf{P}(132)\mathbf{R}_{2\pi/3}^z \ , \tag{2.48}$$

$$\mathbf{O}_h = \mathbf{P}(12)\mathbf{R}_\pi^y \mathbf{I} \ , \tag{2.49}$$

$$\mathbf{O}_i = \mathbf{P}(124)\mathbf{R}_\Phi^y \mathbf{R}_{2\pi/3}^z \mathbf{R}_{-\Phi}^y \ , \tag{2.50}$$

with the notation used in section 2.2 and $\Phi = 2\arccos\left(\frac{1}{\sqrt{3}}\right) = 1.911\text{rad} = 109.5^\circ$ being the inter-electronic angle as seen from the nucleus. As an example, the effect of $\mathbf{O}_h$ is demonstrated in figure 2.6.
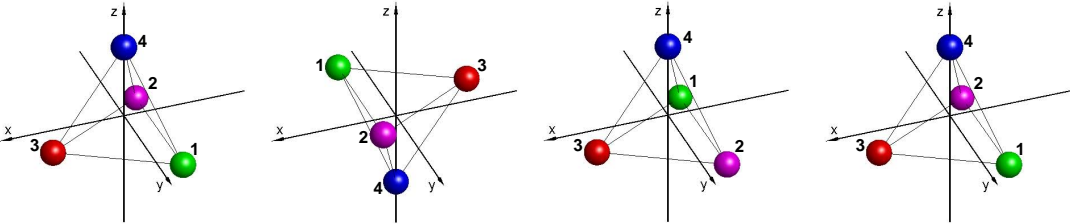
Figure 2.6: The effect of $\mathbf{O}_h = \mathbf{P}(12)\mathbf{R}_\pi^y \mathbf{I}$.

Since the RTH is invariant to the operations in equations (2.48)-(2.50), the values of $F_{M_I i,\omega}^{L\pi S}$ at the RTH-configuration, $F_{M_I i}^{L\pi S}(\text{RTH})$, have to be invariant to these operations. Hence,

$$F_{M_I i}^{L\pi S}(\text{RTH}) = \left[\mathbf{O}_\rho F_{M_I i,\omega}^{L\pi S}\right]_{\text{RTH}} \ , \qquad \rho \in \{g, h, i\} \ , \tag{2.51}$$

which gives the following sets of homogeneous linear equations when equations
(2.14)-(2.18) are used

$$F_{M_I i}^{L\pi S}(\text{RTH}) = e^{-i\frac{2\pi}{3}M_I} \sum_{i'} G_{ii'}^{S}(\mathbf{P}(132)) F_{M_I i'}^{L\pi S}(\text{RTH}) \, , \tag{2.52}$$

$$F_{M_I i}^{L\pi S}(\text{RTH}) = \pi(-1)^{L+M_I} \sum_{i'} G_{ii'}^{S}(\mathbf{P}(12)) F_{-M_I i'}^{L\pi S}(\text{RTH}) \, , \tag{2.53}$$

$$F_{M_I i}^{L\pi S}(\text{RTH}) = \sum_{M_I' i'} B_{M_I M_I'}^{L} G_{ii'}^{S}(\mathbf{P}(124)) F_{M_I' i'}^{L\pi S}(\text{RTH}) \, , \tag{2.54}$$

where $G_{ii'}^{S}(\mathbf{P})$ now denotes the Yamanouchi matrix elements of permutations in
S_4. The matrix elements, $B_{M_I M_I'}^{L}$, are given by

$$B_{M_I M_I'}^{L} = \langle LM_I' | \mathbf{R}_{\Phi}^{y} \mathbf{R}_{2\pi/3}^{z} \mathbf{R}_{-\Phi}^{y} | LM_I \rangle = \sum_{M_I''} d_{M_I'' M_I'}^{L}(\Phi) d_{M_I'' M_I}^{L}(\Phi) e^{-i\frac{2\pi}{3}M_I''} \, . \tag{2.55}$$

The procedure has so far been the same as in the three-electron case, but never-
theless a difference has shown up in the two sets of homogeneous linear equations,
equations (2.34)-(2.36) and equations (2.52)-(2.54). Equation (2.54) mixes the
values of M_I and consequently the allowed values of M_I will depend on the inter-
mediate spins in the four-electron case. Furthermore, this mixing complicates the
procedure for solving the linear system.

If equations (2.52)-(2.54) only have the trivial solution, a nodal surface will
be located in the RTH-configuration and the state is RTH-inaccessible. On the
other hand, if a nontrivial solution exists for a given set of L, π and S, the term,
$^{2S+1}L^{\pi}$, is RTH-accessible. Since the Coulomb repulsion is minimized in the RTH-
configuration, the low-lying energy spectrum is expected to consist of the RTH-
accessible states.

2.4.2 Solution procedure and results

The size and complexity of the linear systems classifying atomic states are seen to
increase with the number of electrons. Therefore, the solution of the equations for
four-electron systems is supported by numerical calculations.

In the case of $S = 2$ only one possible choice for the intermediate spin coupling
is possible, namely $S_{12} = S_{34} = 1$. Consequently, the matrix elements of the
permutations are as simple as $G_{11}^{2}(\mathbf{P}(jk)) = -1$. So in this case the set of equations
to be solved reads

$$F_{M_I 1} = e^{-i\frac{2\pi}{3}M_I} F_{M_I 1} \, , \tag{2.56}$$

$$F_{M_I 1} = -\pi(-1)^{L+M_I} F_{-M_I 1} \, , \tag{2.57}$$

$$F_{M_I 1} = \sum_{M_I'} B_{M_I M_I'}^{L} F_{M_I' 1} \, , \tag{2.58}$$

Table 2.3: RTH-accessible quintet states with $L \leq 4$ listed in the first column. The second and third column give the $F_{M_I 1}$ coefficients with $M_I \geq 0$ in the wave function in equation (2.62).

	F_{01}	F_{31}
${}^5\mathrm{S}^\mathrm{o}$	1	
${}^5\mathrm{F}^\mathrm{e}$	$\sqrt{\frac{5}{9}}$	$\sqrt{\frac{2}{9}}$
${}^5\mathrm{G}^\mathrm{o}$	$\sqrt{\frac{7}{27}}$	$-\sqrt{\frac{10}{27}}$

with $F_{M_I i}^{L\pi S}(\mathrm{RTH}) = F_{M_I i}$ in short. Equation (2.56) gives the condition

$$F_{M_I 1} = 0 \;\; \text{if} \;\; M_I \bmod 3 \neq 0 \;, \tag{2.59}$$

and equations (2.57) and (2.58) can be reduced to one equation

$$F_{M_I 1} = \frac{1}{2}(-\pi(-1)^L + 1)F_{01} + \sum_{M_I' > 0}\left(-\pi(-1)^{L+M_I'}B_{M_I - M_I'}^L + B_{M_I M_I'}^L\right)F_{M_I' 1} \;. \tag{2.60}$$

The elements $B_{M_I M_I'}^L$ are calculated numerically, and the computer program is shown and discussed in appendix B. When these elements are given it is not daunting to solve equations (2.59)-(2.60) by paper and pencil. We will go through the similar but more complicated equations for $S = 1$ and the details in the solution of equations (2.59)-(2.60) are therefore left out. The three nonzero solutions with $L \leq 4$ are listed in table 2.3. In contrast to the classification of the two- and three-valence-electron states, the ratio between the coefficients, $F_{M_I i}$, are determined when solving for the RTH-accessible states. The possibility of predicting these ratios gives, in addition to the classification scheme, the value of the wave function, $|\Psi^{LM\pi, SM_s}\rangle$, at the RTH-configuration since we have

$$|\Psi^{LM\pi, SM_s}\rangle_{\mathrm{RTH}} \propto \sum_{M_I i} D_{M_I M}^L(-\omega)F_{M_I i}^{L\pi S}(\mathrm{RTH})\chi_{M_s i}^S \;. \tag{2.61}$$

Thus, before solving the Schrödinger equation, the expressions of the wave functions at the RTH can be predicted. The determination of $|\Psi^{LM\pi, SM_s}\rangle_{\mathrm{RTH}}$ is only up to a constant depending on the size of the RTH since the set of $F_{M_I i}^{L\pi S}(\mathrm{RTH})$ is determined up to a overall constant. In the case of $S = 2$ the wave function at the RTH reads

$$|\Psi^{LM\pi, S=2, M_s}\rangle_{\mathrm{RTH}} \propto \left(\sum_{M_I} D_{M_I M}^L(-\omega)F_{M_I 1}\right)\chi_{M_s}^2 \;, \tag{2.62}$$

with the nonzero $F_{M_I 1}$ with $M_I \geq 0$ listed in table 2.3. The coefficients with $M_I < 0$ can be determined from the simple relation given in equation (2.57).

In the cases of $S = 0$ and $S = 1$ there are two and three possible choices of $i = \{S_{12}S_{34}\}$, respectively. Using appendix A to derive the matrices, $G^1(\mathbf{P})$,

equation (2.52) easily gives the following relations for $S = 1$

$$
F_{M_I 1} = 0 \qquad\qquad\qquad \text{if } M_I \bmod 3 \neq 0 , \qquad (2.63)
$$

$$
F_{M_I 2} = F_{M_I 3} = 0 \qquad\qquad \text{if } M_I \bmod 3 = 0 , \qquad (2.64)
$$

$$
F_{M_I 3} = (-1)^{M_I \bmod 3} i F_{M_I 2} . \qquad\qquad\qquad\qquad\qquad (2.65)
$$

Hence, it is seen that $F_{M_I 1}$ differs not just by a phase from $F_{M_I 2}$ and $F_{M_I 3}$; in fact, $F_{M_I 1}$ is zero whenever $F_{M_I 2}$ and $F_{M_I 3}$ are nonzero and vice versa which is seen in equations (2.63)-(2.64). Furthermore, equation (2.53) relates the values of $F_{-M_I i}$ and $F_{M_I i}$

$$
\begin{pmatrix} F_{-M_I 1} \\ F_{-M_I 2} \\ F_{-M_I 3} \end{pmatrix} = -\pi(-1)^{L+M_I} \begin{pmatrix} F_{M_I 1} \\ F_{M_I 2} \\ -F_{M_I 3} \end{pmatrix} . \qquad (2.66)
$$

Hence, equation (2.54) can be rewritten

$$
\begin{pmatrix} F_{M_I 1} \\ F_{M_I 2} \\ F_{M_I 3} \end{pmatrix} = G^S(\mathbf{P}(124)) \Bigg\{ \frac{1}{2}\big(-\pi(-1)^L + 1\big) B^L_{M_I 0} \begin{pmatrix} F_{01} \\ 0 \\ 0 \end{pmatrix}
$$
$$
+ \sum_{M'_I > 0} \Bigg[-\pi(-1)^{L+M'_I} B^L_{M_I - M'_I} \begin{pmatrix} F_{M'_I 1} \\ F_{M'_I 2} \\ -F_{M'_I 3} \end{pmatrix} + B^L_{M_I M'_I} \begin{pmatrix} F_{M'_I 1} \\ F_{M'_I 2} \\ F_{M'_I 3} \end{pmatrix} \Bigg] \Bigg\} , \quad (2.67)
$$

or expressed more compactly with equations (2.63)-(2.65)

$$
G^1(\mathbf{P}(124)) \Bigg[\frac{1}{2}(-\pi(-1)^L + 1) B^L_{M_I 0} \vec{V}_0 F_{01} +
$$
$$
\sum_{M'_I > 0} \big(-\pi(-1)^{L+M'_I} B^L_{M_I - M'_I} \vec{V}_{-M'_I} + B^L_{M_I M'_I} \vec{V}_{M'_I} \big) F_{M'_I y} \Bigg] - \vec{V}_{M_I} F_{M_I y} = 0 , \quad (2.68)
$$

with

$$
G^1(\mathbf{P}(124)) = \begin{pmatrix} -\frac{1}{3} & -\frac{\sqrt{2}}{3} & \frac{\sqrt{6}}{3} \\ -\frac{\sqrt{2}}{3} & \frac{5}{6} & \frac{\sqrt{3}}{6} \\ -\frac{\sqrt{6}}{3} & -\frac{\sqrt{3}}{6} & -\frac{1}{2} \end{pmatrix} , \qquad (2.69)
$$

$$
\vec{V}_{M_I} = \begin{pmatrix} 1 \\ 0 \\ 0 \end{pmatrix} \qquad\qquad \text{if } M_I \bmod 3 = 0 , \qquad (2.70)
$$

$$
\vec{V}_{M_I} = \begin{pmatrix} 0 \\ 1 \\ -i \end{pmatrix} \qquad\qquad \text{if } M_I \bmod 3 = 1 , \qquad (2.71)
$$

$$
\vec{V}_{M_I} = \begin{pmatrix} 0 \\ 1 \\ i \end{pmatrix} \qquad\qquad \text{if } M_I \bmod 3 = 2 , \qquad (2.72)
$$

$$
y = 1 \qquad\qquad\qquad \text{if } M_I \bmod 3 = 0 , \qquad (2.73)
$$

$$
y = 2 \qquad\qquad\qquad \text{if } M_I \bmod 3 \neq 0 . \qquad (2.74)
$$

Equation (2.68) with equations (2.69)-(2.74) and (2.65) contain all the information of the linear systems in equation (2.52)-(2.54) for $S = 1$. It is indeed possible to continue the paper and pencil work, and for small L the task is not daunting, but for larger L it is difficult to keep track of the large number of unknown variables,

Table 2.4: RTH-accessible triplet states with $L \leq 4$ listed in the first column. The second column gives the spin coupling, $i = 1$ corresponds to $S_{12} = S_{34} = 1$ and $i = 2$ to $S_{12} = 0$ and $S_{34} = 1$. The numbers in the last five columns are the $F_{M_I i}$ coefficients with $M_I \geq 0$ in the wave function in equation (2.61).

	i	F_{0i}	F_{1i}	F_{2i}	F_{3i}	F_{4i}
$^3\mathrm{P}^\mathrm{e}$	1	1				
	2		$\sqrt{\frac{1}{2}}$			
$^3\mathrm{D}^\mathrm{o}$	1	1				
	2		$-\sqrt{\frac{1}{6}}$	$\sqrt{\frac{1}{3}}$		
$^3\mathrm{F}^\mathrm{o}$	1				$\sqrt{\frac{1}{2}}$	
	2		$-\sqrt{\frac{5}{12}}$	$-\sqrt{\frac{1}{12}}$		
$^3\mathrm{F}^\mathrm{e}$	1	$\frac{2}{3}$			$\sqrt{\frac{5}{18}}$	
	2		$\sqrt{\frac{1}{12}}$	$\sqrt{\frac{5}{12}}$		
$^3\mathrm{G}^\mathrm{o}$	1	$\sqrt{\frac{20}{27}}$			$\sqrt{\frac{7}{54}}$	
	2		$\sqrt{\frac{25}{108}}$	$-\sqrt{\frac{1}{108}}$		$\sqrt{\frac{7}{27}}$
$^3\mathrm{G}^\mathrm{e}$	1				$\sqrt{\frac{1}{2}}$	
	2		$\sqrt{\frac{7}{36}}$	$-\sqrt{\frac{7}{36}}$		$-\frac{1}{3}$

$F_{M_I i}$. The solution to the reduced problem is therefore found numerically, and the computer program is seen in appendix B. To make the reading of equation (2.68) clear we consider the equation when $L = 2$. According to equations (2.63)-(2.65) there are three unknown variables, namely F_{01}, F_{12} and F_{22}, and the less compact form of equation (2.68) reads

$$\left[\begin{pmatrix} G^{\frac{1}{2}}(-\pi+1)B_{00}^2\vec{V_0} & G(\pi B_{0-1}^2\vec{V_2}+B_{01}^2\vec{V_1}) & G(-\pi B_{0-2}^2\vec{V_1}+B_{02}^2\vec{V_2}) \\ G^{\frac{1}{2}}(-\pi+1)B_{10}^2\vec{V_0} & G(\pi B_{1-1}^2\vec{V_2}+B_{11}^2\vec{V_1}) & G(-\pi B_{1-2}^2\vec{V_1}+B_{12}^2\vec{V_2}) \\ G^{\frac{1}{2}}(-\pi+1)B_{20}^2\vec{V_0} & G(\pi B_{2-1}^2\vec{V_2}+B_{21}^2\vec{V_1}) & G(-\pi B_{2-2}^2\vec{V_1}+B_{22}^2\vec{V_2}) \end{pmatrix} - \begin{pmatrix} \vec{V_0} & 0 & 0 \\ 0 & \vec{V_1} & 0 \\ 0 & 0 & \vec{V_2} \end{pmatrix} \right] \begin{pmatrix} F_{01} \\ F_{12} \\ F_{22} \end{pmatrix} = 0 \,,$$

$$(2.75)$$

with $G^1(\mathbf{P}(124)) = G$ in short.

The result is six triplet RTH-accessible states with $L \leq 4$. Table 2.4 shows the nonzero $F_{M_I i}$ with $M_I \geq 0$ for $i = 1$ and $i = 2$ and the remaining coefficients can be determined from the simple relations (2.65) and (2.66). The coefficients in table 2.4 have been normalized for each set of intermediate spin $i = \{S_{12}S_{34}\}$.

Table 2.5: RTH-accessible singlet states with $L \leq 4$ listed in the first column. The last three columns give the $F_{M_I 1}$ coefficients in the wave function (2.61) with $M_I \geq 0$.

	F_{11}	F_{21}	F_{41}
$^1\mathrm{D^o}$	$\sqrt{\frac{2}{6}}$	$\sqrt{\frac{1}{6}}$	
$^1\mathrm{D^e}$	$\sqrt{\frac{2}{6}}$	$-\sqrt{\frac{1}{6}}$	
$^1\mathrm{G^o}$	$\sqrt{\frac{2}{27}}$	$\sqrt{\frac{8}{27}}$	$-\sqrt{\frac{7}{54}}$
$^1\mathrm{G^e}$	$\sqrt{\frac{2}{27}}$	$-\sqrt{\frac{8}{27}}$	$-\sqrt{\frac{7}{54}}$

Finally, when $S = 0$ the reduced set of equations reads

$$F_{M_I 1} = \frac{1}{2}(-\pi(-1)^L + 1)F_{01}$$
$$+ \sum_{M_I' > 0} \left(-\pi(-1)^{L+M_I'} B^L_{M_I - M_I'} e^{-i\frac{2\pi}{3}M_I'} + B^L_{M_I M_I'} e^{i\frac{2\pi}{3}M_I'} \right) F_{M_i' 1} , \quad (2.76)$$

$$F_{M_I 1} = -\pi(-1)^{L+M_I} F_{-M_I 1} \tag{2.77}$$

$$F_{M_I 2} = (-1)^{M_I \bmod 3} i F_{M_I 1} , \tag{2.78}$$

which has four nonzero solutions for $L \leq 4$ found by paper and pencil. The nonzero $F_{M_I 1}$ with $M_I \geq 0$ are listed in table 2.5. The coefficients with $i = 2$ can be determined from equation (2.78) and those with negative M_I from equation (2.77).

2.4.3   Discussion

The RTH-accessible states listed in tables 2.3-2.5 are in agreement with Bao's classification in references [16, 18]. However, the allowed values of M_I are not the same in the two schemes and the sets of equations to be solved differ as well. This is a consequence of the fact that M_I is determined with respect to the body-fixed frame which is chosen differently in the two descriptions. Therefore, the allowed values of M_I indeed have to be different in the two schemes.

To conclude this section, a primary classification scheme for four-valance-electron atoms has been obtained. This scheme is particularly valid for quadruply excited intra-shell states. Especially, the $^5\mathrm{S^o}$ state is seen to be RTH-accessible. This is in agreement with reference [29] in which Komninos and Nicolaides, on basis of multiconfigurational Hartree-Fock calculations, conclude that the inter-electronic angle in the $^5\mathrm{S^o}$ state tends to that of tetrahedral geometry (109, 5º) when the excitation, n, grows. Moreover, $^5\mathrm{S^o}$ is seen to be the only RTH-accessible S-state. Figure 2.7 shows the energy spectrum of odd intra-shell S-states, $^{2S+1}\mathrm{S^o}$, in carbon calculated within the frozen-r model [30]. All valence electrons are assumed to be in the second principle shell, $n = 2$. We notice that among the three
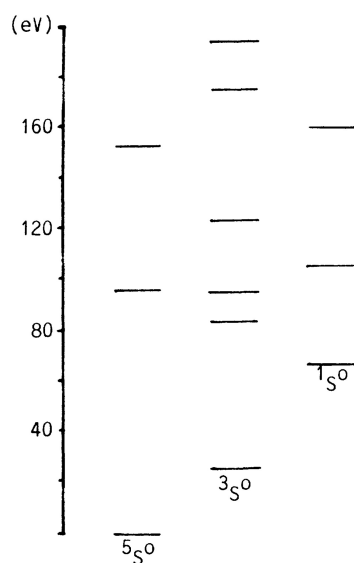
Figure 2.7: Energies of the $^5S^o$, $^3S^o$ and $^1S^o$ carbon states relative to the lowest $^5S^o$ state calculated within the frozen-r model. Adopted from reference [30].

types of symmetry, the lowest-lying state is of $^5S^o$ symmetry, in agreement with the symmetry based classification.

2.5   Six-valence-electron atoms

As stated, six-electron systems is not one of the main subjects for this thesis. Nevertheless, a little attention is directed to the problem. The previous sections have demonstrated an apt method to classify atomic states. As seen in section 2.4, the complexity of the equations arising from symmetry considerations increases significantly with the number of electrons. Consequently, the complete set for the six-electron system has not been solved until now. This section therefore completes classification based on symmetry.

2.5.1   Symmetry considerations

When we consider states with six valence electrons, the Coulomb repulsion between the outer electrons is minimized when they are placed in the vertices of a regular octahedron (ROH), as shown in figure 2.8. Like the regular tetrahedron the octahedron is a spherical top and the body-fixed frame can therefore be chosen at will. In the body-fixed frame of figure 2.8, the ROH-configuration is invariant to
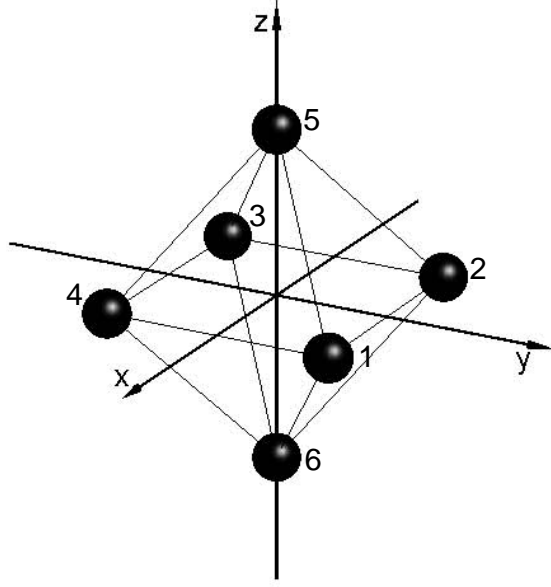
Figure 2.8: Six electrons placed in the vertices of a regular octahedron.

the following four types of symmetry operations

$$\mathbf{O}_j = \mathbf{P}(13)\mathbf{P}(24)\mathbf{P}(56)\mathbf{I} \ , \tag{2.79}$$

$$\mathbf{O}_k = \mathbf{P}(1234)\mathbf{R}^z_{-\pi/2} \ , \tag{2.80}$$

$$\mathbf{O}_l = \mathbf{P}(12)\mathbf{P}(34)\mathbf{P}(56)\mathbf{R}^y_\pi \ , \tag{2.81}$$

$$\mathbf{O}_m = \mathbf{P}(253)\mathbf{P}(146)\mathbf{R}^y_{-\theta}\mathbf{R}^z_{2\pi/3}\mathbf{R}^y_\theta \ , \tag{2.82}$$

where $\theta = \frac{1}{2}\Phi = 54.74°$. Thus, the sets of equations to be solved are determined by the condition

$$F^{L\pi S}_{M_I i}(\text{ROH}) = \left[\mathbf{O}_\rho F^{L\pi S}_{M_I i,\omega}\right]_{\text{ROH}} \ , \qquad \rho \in \{j,k,l,m\} \ , \tag{2.83}$$

and hence,

$$F^{L\pi S}_{M_I i}(\text{ROH}) = \pi \sum_{i'} G^S_{ii'}(\mathbf{P}(13)\mathbf{P}(24)\mathbf{P}(56))F^{L\pi S}_{M_I i'}(\text{ROH}) \ , \tag{2.84}$$

$$F^{L\pi S}_{M_I i}(\text{ROH}) = e^{i\frac{\pi}{2}M_I} \sum_{i'} G^S_{ii'}(\mathbf{P}(1234))F^{L\pi S}_{M_I i'}(\text{ROH}) \ , \tag{2.85}$$

$$F^{L\pi S}_{M_I i}(\text{ROH}) = (-1)^{L+M_I} \sum_{i'} G^S_{ii'}(\mathbf{P}(12)\mathbf{P}(34)\mathbf{P}(56))F^{L\pi S}_{-M_I i'}(\text{ROH}) \ , \tag{2.86}$$

$$F^{L\pi S}_{M_I i}(\text{ROH}) = \sum_{M'_I i'} H_{M_I M'_I} G^S_{ii'}(\mathbf{P}(253)\mathbf{P}(146))F^{L\pi S}_{M'_I i'}(\text{ROH}) \ , \tag{2.87}$$

with

$$H^L_{M_I M'_I} = \langle LM'_I|\mathbf{R}^y_{-\theta}\mathbf{R}^z_{2\pi/3}\mathbf{R}^y_\theta|LM_I\rangle = \sum_{M''_I} d^L_{M''_I M'_I}(\theta)d^L_{M''_I M_I}(\theta)e^{-i\frac{2\pi}{3}M''_I} \ . \tag{2.88}$$

2.5.2 Solution procedure and results

The dimension of the permutation matrices, $n = \text{size}(G^S(\mathbf{P}))$, corresponds to the number of possible ways to couple the intermediate spins, S_{12}, S_{34} and S_{56}, to the total spin, S. The number of unknown variables, $F_{M_I i}$, for each term, $^{2S+1}L^\pi$, is $n(2L+1)$ corresponding to n different spin couplings for each value of $|M_I| \leq L$. As an example, the number of unknown variables for $^3G^\pi$ is 81 since $n = 9$ when $S = 1$. Keeping track of so many unknown parameters is daunting and therefore this problem is solved numerically. Previous section showed how the unknown variables, $F_{M_I i}$, can be found explicitly. The most interesting question is, however, whether a nontrivial solution exists for a given set of L, π and S; in other words, whether the term, $^{2S+1}L^\pi$, is ROH-accessible and, thus, belongs to the low-lying part of the energy spectrum. To answer this question we have to write equations (2.84)-(2.87) in a suitable form for a computer program.

With the notation

$$\mathbf{A} = G^S(\mathbf{P}(13)\mathbf{P}(24)\mathbf{P}(56)) \,, \tag{2.89}$$

$$\mathbf{B} = G^S(\mathbf{P}(1234)) \,, \tag{2.90}$$

$$\mathbf{C} = G^S(\mathbf{P}(12)\mathbf{P}(34)\mathbf{P}(56)) \,, \tag{2.91}$$

$$\mathbf{D} = G^S(\mathbf{P}(253)\mathbf{P}(146)) \,, \tag{2.92}$$

equations (2.84)-(2.87) can be rewritten

$$[\pi\mathbf{A} - \mathbf{I}]\bar{F}_{M_I} = 0 \,, \tag{2.93}$$

$$[e^{i\frac{\pi}{2}M_I}\mathbf{B} - \mathbf{I}]\bar{F}_{M_I} = 0 \,, \tag{2.94}$$

$$\sum_{M_I' i'}[(-1)^{L+M_I'}\delta_{-M_I M_I'}\mathbf{C}_{ii'} - \delta_{M_I M_I'}\delta_{ii'}]F_{M_I' i'} = 0 \,, \tag{2.95}$$

$$\sum_{M_I' i'}[H_{M_I M_I'}\mathbf{D}_{ii'} - \delta_{M_I M_I'}\delta_{ii'}]F_{M_I' i'} = 0 \,, \tag{2.96}$$

with $\mathbf{I}$ denoting identity matrices of size n, and

$$\bar{F}_{M_I} = \begin{pmatrix} F_{M_I 1} \\ F_{M_I 2} \\ \vdots \\ F_{M_I n} \end{pmatrix} \tag{2.97}$$

Equations (2.93)-(2.94) do not mix the values of M_I and are therefore a lot simpler than equations (2.95)-(2.96). For a given value of M_I the solution to equations (2.93)-(2.94) is simply the nullity of the combined matrix

$$\begin{pmatrix} \pi\mathbf{A} - \mathbf{I} \\ e^{i\frac{\pi}{2}M_I}\mathbf{B} - \mathbf{I} \end{pmatrix} \tag{2.98}$$

To solve equations (2.95)-(2.96) we introduce more notation. The Kronecker tensor product, $\mathrm{kron}(X, Y)$, of two matrices, X and Y, is a larger matrix formed by taking all possible products between the elements of X and those of Y. If $X \in \mathrm{Mat}_{m,n}$ and $Y \in \mathrm{Mat}_{p,q}$ then $\mathrm{kron}(X, Y) \in \mathrm{Mat}_{mp,nq}$, and the elements are arranged in the following order

$$
\mathrm{kron}(X, Y) = \begin{pmatrix} X_{11}Y & X_{12}Y & \dots & X_{1n}Y \\ X_{21}Y & X_{22}Y & & \\ \vdots & & \ddots & \\ X_{m1}Y & & & X_{mn}Y \end{pmatrix}
\tag{2.99}
$$

Furthermore, let $\bar{\mathbf{F}}$ be a column vector with the $n(2L + 1)$ unknown variables, $F_{M_I i}$, arranged in the following order

$$
\bar{\mathbf{F}} = \begin{pmatrix} \bar{F}_{-L} \\ \bar{F}_{-L+1} \\ \vdots \\ \bar{F}_L \end{pmatrix}
\tag{2.100}
$$

Using the Kronecker tensor product equations (2.95)-(2.96) can be written on the compact form

$$
\begin{pmatrix} \mathrm{kron}(M, \mathbf{C}) - \mathbf{I} \\ \mathrm{kron}(H, \mathbf{D}) - \mathbf{I} \end{pmatrix} \bar{\mathbf{F}} = 0 \, ,
\tag{2.101}
$$

where $M \in \mathrm{Mat}_{2L+1,2L+1}$ only have nonzero elements on the diagonal from the left bottom to the right top, $M_{jk} = \delta_{2L+2-j,k}(-1)^{j+1}$. The identity matrices in equation (2.101) are of size $n(2L + 1)$.

The term, $^{2S+1}L^{\pi}$, is ROH-accessible if the intersection of the nullity of the matrix in equation (2.98) and the solution space to equation (2.101) is nontrivial.

The problem is now written in a suitable form to be solved numerically. The matrix in equation (2.101) is of size $2n(2L + 1) \times n(2L + 1)$ and, therefore, the dimension of the nullity is less or equal to $n(2L + 1)$. The size of the matrix in equation (2.98) is only $2n \times n$, but there are $2L + 1$ of them. Therefore, it is appropriate to organize the two solution spaces in square matrices of size $n(2L+1)$. The computer program solving the problem is shown and discussed in appendix B.

The result of this section is the following ROH-accessible states with $L \leq 4$:

$$
S = 3 : {}^{7}\mathrm{F}^{\mathrm{o}}
\tag{2.102}
$$
$$
S = 2 : {}^{5}\mathrm{D}^{\mathrm{o}}, {}^{5}\mathrm{D}^{\mathrm{e}}, {}^{5}\mathrm{F}^{\mathrm{e}}, {}^{5}\mathrm{G}^{\mathrm{o}}, {}^{5}\mathrm{G}^{\mathrm{e}}
\tag{2.103}
$$
$$
S = 1 : {}^{3}\mathrm{P}^{\mathrm{o}}, {}^{3}\mathrm{P}^{\mathrm{e}}, {}^{3}\mathrm{D}^{\mathrm{o}}, {}^{3}\mathrm{F}^{\mathrm{o}}, {}^{3}\mathrm{F}^{\mathrm{e}}, {}^{3}\mathrm{G}^{\mathrm{o}}, {}^{3}\mathrm{G}^{\mathrm{e}}
\tag{2.104}
$$
$$
S = 0 : {}^{1}\mathrm{S}^{\mathrm{o}}, {}^{1}\mathrm{S}^{\mathrm{e}}, {}^{1}\mathrm{D}^{\mathrm{e}}, {}^{1}\mathrm{F}^{\mathrm{e}}, {}^{1}\mathrm{G}^{\mathrm{o}}, {}^{1}\mathrm{G}^{\mathrm{e}}
\tag{2.105}
$$
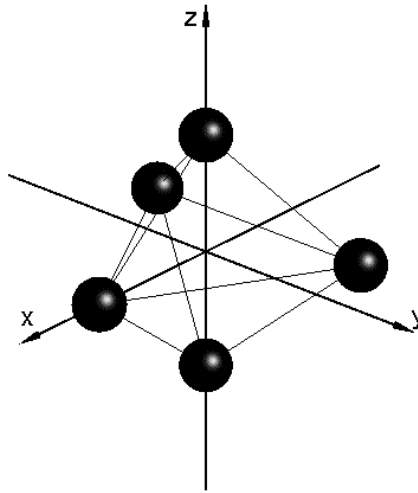
Figure 2.9: Configuration with five electrons showing some symmetry.

2.6   Five-valence-electron atoms

Before we conclude this chapter a few comments about the five-electron system are appropriate. As stated earlier, the symmetry of the five-electron system is not as high as for systems with the potential energy minimized when the electrons are placed in the vertices of a regular polyhedron in $\mathbb{R}^3$. However, the configuration showed in figure 2.9 can be used even though this configuration does not minimize the potential energy. It is, however, not the purpose of this thesis to consider other configurations than those minimizing the potential energy.

2.7   Concluding remarks

The principles in the classification method should now be very clear. First, the symmetries for a given configuration have to be found, subsequently the nodal surfaces can be determined by solving linear systems. We have seen that the difficulty in solving the equations increases significantly with the number of electrons. It is important to realize that two essential factors determine the relative energies among states of different symmetry. On one hand the geometric symmetry and on the other hand quantum-mechanical symmetry (e.g parity and the spatial permutation symmetry with respect to interchange of positions). As far as possible the system prefers the geometry minimizing the potential energy, but inherent nodal surfaces arising from quantum-mechanical symmetry may impose restrictions on this preferred geometric structure.

Finally, it should be commented that the application of this elegant method goes beyond classification of atomic states. Exactly the same method is shown to be applicable to classify states in nuclear physics [18].

Chapter 3

The three-electron symmetric rotor model

One of the main goals of this thesis is to present an explicit analytical construction of triply and quadruply excited states. This chapter gives a review of the construction of the so-called symmetric rotor for the four-body Coulomb problem. The basic idea is borrowed from the work of Madsen and Mølmer in references [31]-[34], collected in references [12, 13], but the approach presented in this thesis is not identical to their work. The aim of this chapter is a presentation of the model before proceeding to the more complicated five-body Coulomb problem in chapter 4. Moreover, the original three-electron symmetric rotor model by Madsen and Mølmer cannot be directly extended to larger systems. The description presented here has a natural extension to systems of 4, 6 and 8 electrons corresponding to the number of vertices in regular polyhedra of $\mathbb{R}^3$. This will be demonstrated in the next chapter where quadruply excited states are considered. Furthermore, some new results which have not been given by Madsen and Mølmer are presented. When this is the case, and when steps in the construction of the symmetric rotor are performed differently than in the approach of Madsen and Mølmer, a comment is made. Finally, this chapter corrects some minor mistakes in the work of Madsen and Mølmer.

3.1 Construction

We consider the Coulombic system of three electrons moving in the field of a point-like nucleus of charge Z corresponding to the nonrelativistic Hamiltonian

$$\hat{H} = \sum_{j=1}^{3} \left(\frac{-\hbar^2}{2\mu} \nabla_j^2 - \frac{Ze^2}{r_j} \right) + V_{ee} , \qquad V_{ee} = \sum_{i<j} \frac{e^2}{|\vec{r_i} - \vec{r_j}|} , \qquad (3.1)$$

where μ is the reduced electron mass and e is the electron charge. The electron-electron interaction, V_{ee}, complicates the problem to a great extent since the potential is not diagonal in a basis of antisymmetrized products of single-electron hy-

drogen configurations. Therefore, single-electron quantum numbers are not good quantum numbers and, consequently, the eigenfunctions are represented as configuration superpositions. The symmetric rotor model accounts for the electron-electron interaction by assuming that the wave function is a product of carefully chosen one-electron states.

3.1.1   The spatial part

As stated, if we consider triply excited intra-shell states the potential energy will be minimized when the electrons form a coplanar equilateral triangle (ET) with the nucleus in the center (see figure 3.1). In the ET the interaction between any electron and the remaining two is represented by a repulsive electric field along the direction, ξ, of the electron considered with respect to the nucleus. Hence, the lithium-like Hamiltonian in equation (3.1) can be approximated by a sum of hydrogenic Hamiltonians perturbed by weak external electric fields causing only intra-shell transitions

$$\hat{H} = \sum_{j=1}^{3} \left(\frac{-\hbar^2}{2\mu} \nabla_j^2 - \frac{Ze^2}{r_j} + e\vec{E}_{\xi_j} \cdot \vec{r_j} \right) , \tag{3.2}$$

with $\vec{E}_{\xi_j}$ being the electric field felt by the jth electron.

As a consequence of this assumption the wave function splits up into a product of one-electron states which is the simplest possible way to represent a many-particle wave function. The eigenstates of the hydrogenic Hamiltonian perturbed by a weak external electric field are the polarized Stark states. Thus, the very basic idea in the symmetric rotor model is that the inter-electronic interaction tends to stabilize the electrons in individual Stark states.

The Stark states, $|nkm\rangle$, are the eigenfunctions obtained when the nonrelativistic hydrogen atom Schrödinger equation is solved in parabolic coordinates. Contrary to the more well-known orbital states, $|nlm\rangle$, the Stark states retain their character in the presence of a weak electric field. The three mutually commuting operators used to effect the separation in parabolic coordinates are $\hat{H}, \hat{A}_z$ and $\hat{L}_z$ with $\hat{A}_z$ being the z component of the so-called Runge-Lenz vector [35]. The corresponding quantum numbers are the principal, parabolic and azimuthal quantum number denoted n, k and m, respectively. The values of these numbers are restricted by the following inequalities:

$$|k| \leq n - 1 , \tag{3.3}$$

$$|m| \leq n - 1 - |k| . \tag{3.4}$$

If the z axis is chosen to be in the direction of the electric field, $\vec{E}$, the energy shift from the perturbation is [36, equation 2.17]

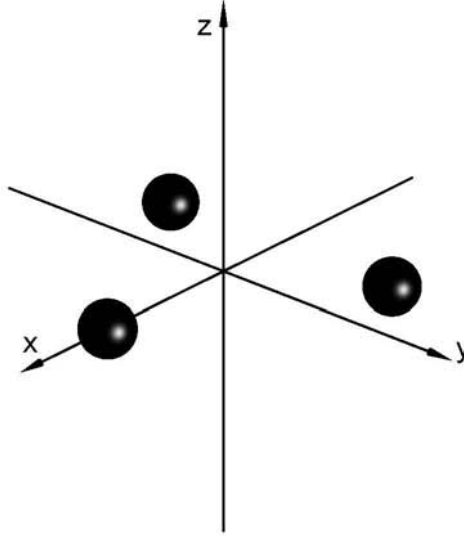$$\langle nkm|eEz|nkm\rangle = -\frac{3}{2Z}eEnk . \tag{3.5}$$

Figure 3.1: Body-fixed frame chosen with z as the principle axis. The nucleus is imagined to be localized in the origin.

Consequently, the parabolic quantum number, k, can be associated with the electric dipole moment of the atom through the relation $p_z = \frac{3}{2Z}enk$. According to equation (3.5) the largest energy shift and thus the lowest-lying state for each n is obtained when the Stark states are maximally polarized, $|n, k = n - 1, m = 0\rangle$. Therefore, it is reasonable to let the ansatz for the symmetric rotor wave function be a product of Stark states maximally polarized along ξ_i

$$|\Upsilon_R\rangle = |nn - 10\rangle_{\xi_1}|nn - 10\rangle_{\xi_2}|nn - 10\rangle_{\xi_3} . \tag{3.6}$$

This expression accounts for a considerable part of the internal interactions, but does not reflect the rotational symmetry of the problem, to which we will return.

As explained in the previous chapter, the body-fixed frame cannot be chosen randomly: the z axis has to be the principal axis for M_I to be a good quantum number. Hereafter the body-fixed x and y axes can be chosen freely. For convenience one electron is placed on the x axis, and the remaining two are rotated $q\frac{2\pi}{3}$ radians, $q = 1, 2$, about the z axis as shown in figure 3.1. If we let quantum numbers in kets without a subscript refer to quantization along the z axis the states in the xy plane, $|nn - 10\rangle_{\xi_q}$, $q = 1, 2, 3$, are related to $|nn - 10\rangle$ via the rotations

$$|nn - 10\rangle_{\xi_q} = \mathbf{R}\left(q\frac{2\pi}{3}, \frac{\pi}{2}, 0\right)|nn - 10\rangle = e^{-iq\frac{2\pi}{3}\hat{L}_z}e^{-i\frac{\pi}{2}\hat{L}_y}|nn - 10\rangle . \tag{3.7}$$

The first rotation, $e^{-i\frac{\pi}{2}\hat{L}_y}$, rotates the state $\frac{\pi}{2}$ radians about the y axis, and the second rotation, $e^{-iq\frac{2\pi}{3}\hat{L}_z}$, rotates it $q\frac{2\pi}{3}$ radians about the z axis.

The electron density for a given Stark state, $|nkm\rangle$, is $|\langle nkm|nkm\rangle|^2$. The Stark states are analytically expressible, and the maximally polarized states are
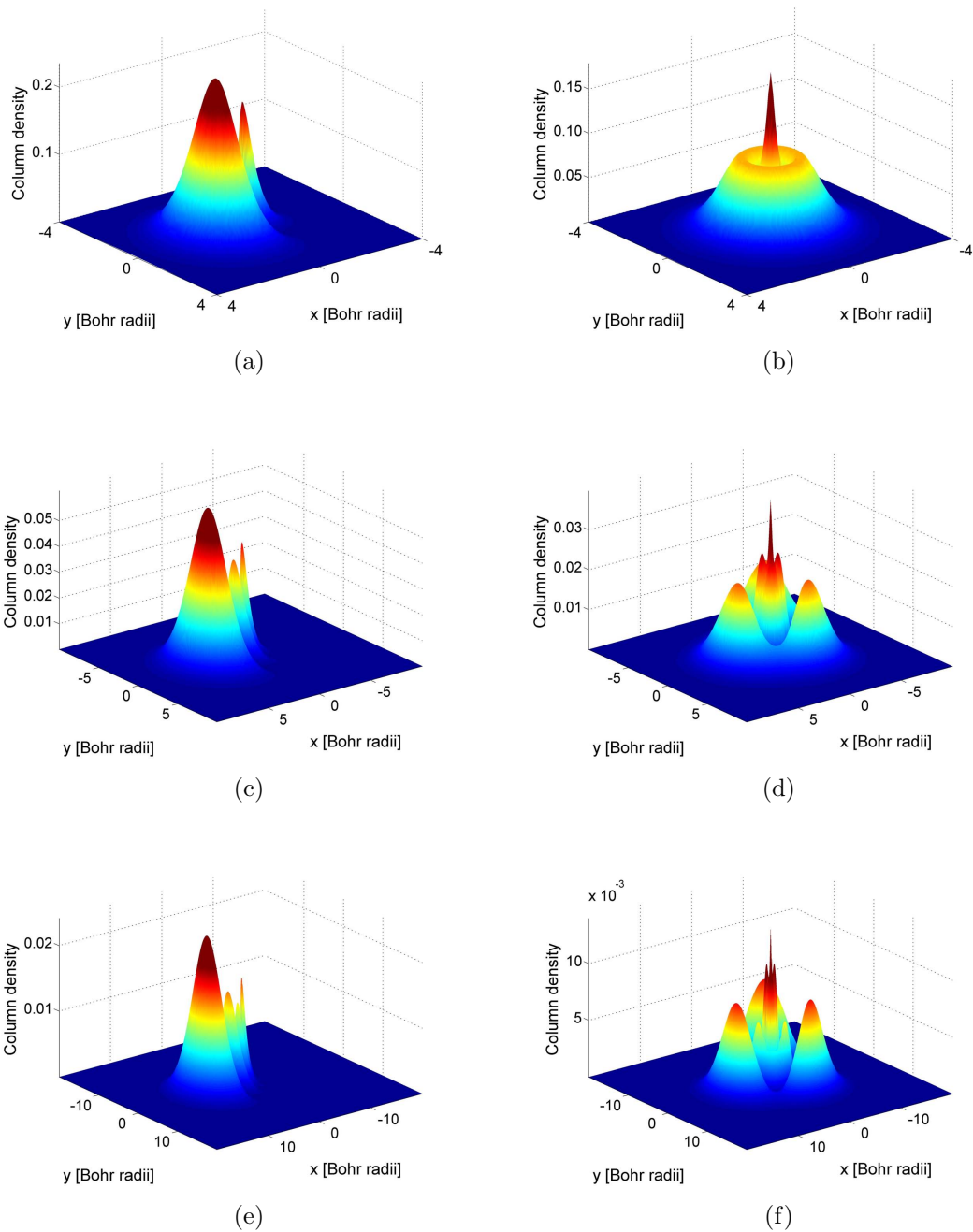
Figure 3.2: Electron density integrated over the z coordinate as a function of x and y. Figures (a), (c) and (e) show the density in the one-electron Stark states polarized along the x axis for $n = 2, 3$ and 4. Figures (b), (d) and (f) show the total density for the three electrons in equation (3.6) for $n = 2, 3$ and 4.

given as [36, equation 1.16]

$$\Psi_{n,n-1,0}(x,y,z) = \frac{1}{\sqrt{\pi n}} \frac{(Z/n)^{3/2}}{[(n-1)!]^{1/2}} e^{-Zr/n} \mathrm{L}_{n-1}\big(Z(r-z)/n\big) \,, \qquad (3.8)$$

with $r = \sqrt{x^2 + y^2 + z^2}$ and $\mathrm{L}_n(\xi)$ being Laguerre functions. Figure 3.2 displays the electron density integrated over the z coordinate as a function of x and y. Figures (a), (c) and (e) show the electron density in the one-electron Stark states polarized along the x axis for $n = 2, 3$ and 4. The asymmetric behaviour about the origin illustrates the permanent electric dipole moments of the states. Furthermore, the peak around the atomic nucleus localized at $(x, y) = (0, 0)$ reflects the attraction between the electron and the nucleus. Figures (b), (d) and (f) show the total electron density in the three-electron case for $n = 2, 3$ and 4. The threefold symmetry is reflected in these figures, and especially for $n = 3$ and $n = 4$ the density splits up into a three-pointed star. The next paragraph will show that the accumulated electron density can be expanded in spherical harmonics with the maximal azimuthal quantum number equal to twice the maximal electronic angular momentum in the given principal shell. Therefore, the full rotational symmetry for $n = 2$ can be explained as follows. When $n = 2$ the azimuthal dependence is restricted to a combination of a constant, $\exp(\pm i\phi)$ and $\exp(\pm 2i\phi)$. Hence, the threefold rotational symmetry requires that $f(\phi + \frac{2\pi}{3}) = f(\phi)$ with $f(\phi) = \mathrm{a} + \mathrm{b}\exp(i\phi) + \mathrm{c}\exp(2i\phi)$. As a result, only the constant term is compatible with the threefold rotational symmetry.

To tell us whether the model is a good characterization of the intra-shell states of the four-body Coulomb problem, the ansatz for the wave function in equation (3.6) has to be compared with experimental or numerical results. However, these results are typically given in terms of angular momentum multiplet wave functions specifying the individual angular momenta of the electrons, l_i, the total angular momentum, L, the spin multiplicity, $2S + 1$, and the parity, π. Therefore we expand the Stark states in the spherical basis, which is possible via the unitary transformation [36, equation 2.9]

$$|nkm\rangle = (-1)^{n_1} \sum_{l=0}^{n-1} \left\langle j\frac{m+k}{2} j\frac{m-k}{2} \middle| lm \right\rangle |nlm\rangle \,, \qquad (3.9)$$

with $n_1 = (n + k - (m + 1))/2$, $j = (n - 1)/2$ and $\left\langle j\frac{m+k}{2} j\frac{m-k}{2} \middle| lm \right\rangle$ being Clebsch Gordon coefficients. Hence

$$|nn-10\rangle = (-1)^{n-1} \sum_{l=0}^{n-1} \langle jjj-j|l0\rangle |nl0\rangle \,, \qquad j = \frac{n-1}{2} \,, \qquad (3.10)$$

and consequently

$$
\begin{aligned}
|nn-10\rangle_{\xi_q} &= (-1)^{n-1}\sum_{l=0}^{n-1}\langle jjj-j|l0\rangle \mathbf{R}\big(q\frac{2\pi}{3},\frac{\pi}{2},0\big)|nl0\rangle \\
&= (-1)^{n-1}\sum_{l=0}^{n-1}\langle jjj-j|l0\rangle \sum_{m=-l}^{l}|nlm\rangle\langle nlm|\mathbf{R}\big(q\frac{2\pi}{3},\frac{\pi}{2},0\big)|nl0\rangle \\
&= (-1)^{n-1}\sum_{lm}\langle jjj-j|l0\rangle D^l_{m0}\big(q\frac{2\pi}{3},\frac{\pi}{2},0\big)|nlm\rangle \,, \qquad j=\frac{n-1}{2}\,,
\end{aligned}
\tag{3.11}
$$

where the Wigner functions, $D^l_{mm'}(\alpha,\beta,\gamma)$, are the matrix elements of the rotation matrix, $\mathbf{R}(\alpha,\beta,\gamma)$. From equations (3.6) and (3.11) we get

$$
|\Upsilon_R\rangle = \sum_{\bar{l}\bar{m}}\prod_{q=1}^{3}a_q(l_qm_q)|nl_qm_q\rangle \,, \quad \bar{l}=\{l_1,l_2,l_3\}\,, \quad \bar{m}=\{m_1,m_2,m_3\}, \tag{3.12}
$$

with the a-coefficients

$$
\begin{aligned}
a_q &= (-1)^{n-1}\langle jjj-j|l_q0\rangle D^{l_q}_{m_q0}\big(q\frac{2\pi}{3},\frac{\pi}{2},0\big) \\
&= (-1)^{n-1}\langle jjj-j|l_q0\rangle d^{l_q}_{m_q0}\big(\frac{\pi}{2}\big)e^{-iq\frac{2\pi}{3}m_q}\,.
\end{aligned}
\tag{3.13}
$$

As stated, the ansatz for the wave function, $|\Upsilon_R\rangle$, is a priori constructed to be anisotropic since the electrons are oriented such, as to minimize the electron-electron repulsion. As a consequence of this break of the spatial rotational symmetry, $|\Upsilon_R\rangle$ is not an eigenstate of $\hat{L}^2$ and $\hat{L}_z$. To take into account the overall symmetry the rotational average of the intrinsic rotor, $|\Upsilon_R\rangle_\omega$, is determined

$$
|\Upsilon_R^{LMM_I}\rangle = \int d\omega D^L_{MM_I}(\omega)^*|\Upsilon_R\rangle_\omega \,, \tag{3.14}
$$

where the subscript ω refers to a rotated frame determined by the Euler angles $\omega=(\alpha,\beta,\gamma)$ and $\int d\omega$ is a shorthand notation for $\int_0^{2\pi}d\alpha\int_0^{2\pi}d\gamma\int_0^{\pi}d\beta\sin\beta$.

Now the importance of the right choice of body-fixed frame is revealed. The quantum number M_I has been added to the expression for the wave function in equation (3.14). As stated, M_I is only a good quantum number if the body-fixed frame is chosen correctly. Using symmetry chapter 2 showed that not all values of M_I satisfying $|M_I|\leq L$ are allowed. Contrary to the values of M, the allowed values of M_I depend on the term, $^{2S+1}L^\pi$.

To see that $|\Upsilon_R^{LMM_I}\rangle$, unlike $|\Upsilon_R\rangle_\omega$, is an eigenstate of $\hat{L}^2$ and $\hat{L}_z$, $|\Upsilon_R\rangle$ is formally expanded in a complete set of angular momentum eigenstates

$$
|\Upsilon_R\rangle = \sum_{L'M_I'}C_{L'M_I'}|L'M_I'\rangle \,. \tag{3.15}
$$

The intrinsic rotor is then expressed as

$$|\Upsilon_R\rangle_\omega = \sum_{L'M_I'M'} C_{L'M_I'} D^{L'}_{M'M_I'}(\omega)|L'M'\rangle \, , \tag{3.16}$$

which is substituted into equation (3.14). The orthogonality properties of the Wigner functions [23, equation 3.113]

$$\int d\omega D^I_{MM'}(\omega)^* D^J_{NN'}(\omega) = \frac{8\pi^2}{2I+1}\delta_{MN}\delta_{M'N'}\delta_{IJ} \tag{3.17}$$

then gives

$$|\Upsilon_R^{LMM_I}\rangle = \frac{8\pi^2}{2L+1}C_{LM_I}|LM\rangle \, , \tag{3.18}$$

which shows that $|\Upsilon_R^{LMM_I}\rangle$ expressed in equation (3.14) is indeed an eigenstate of $\hat{L}^2$ and $\hat{L}_z$.

To express $|\Upsilon_R^{LMM_I}\rangle$ in terms of multiplet wave functions, the expression for $|\Upsilon_R\rangle_\omega$ in equation (3.12) is substituted into equation (3.14),

$$\begin{aligned}
|\Upsilon_R^{LMM_I}\rangle &= \int d\omega D^L_{MM_I}(\omega)^*|\Upsilon_R\rangle_\omega \\
&= \int d\omega D^L_{MM_I}(\omega)^* \sum_{\bar{l}\bar{m}} a(\bar{l}\bar{m})|l_1m_1l_2m_2l_3m_3\rangle_\omega \\
&= \sum_{\bar{l}\bar{m}} a(\bar{l}\bar{m}) \int d\omega D^L_{MM_I}(\omega)^* \sum_{\bar{\mu}} D^{l_1}_{\mu_1m_1}(\omega)D^{l_2}_{\mu_2m_2}(\omega)D^{l_3}_{\mu_3m_3}(\omega)|l_1\mu_1l_2\mu_2l_3\mu_3\rangle \\
&= \sum_{\bar{l}\bar{m}\bar{\mu}} a(\bar{l}\bar{m})I(\bar{l}\bar{m}\bar{\mu}; LMM_I)|l_1\mu_1l_2\mu_2l_3\mu_3\rangle \\
&= \sum_{\bar{l}\bar{\mu}} b(\bar{l}\bar{\mu}; LMM_I)|l_1\mu_1l_2\mu_2l_3\mu_3\rangle \, , \tag{3.19}
\end{aligned}$$

where

$$b(\bar{l}\bar{\mu}; LMM_I) = \sum_{\bar{m}} a(\bar{l}\bar{m})I(\bar{l}\bar{m}\bar{\mu}; LMM_I) \, , \tag{3.20}$$

$$a(\bar{l}\bar{m}) = \prod_{q=1}^{3} a_q(l_qm_q) \, , \qquad \text{with } a_q \text{ given in equation (3.13)} \, , \tag{3.21}$$

$$\begin{aligned}
I(\bar{l}\bar{m}\bar{\mu}; LMM_I) = \frac{8\pi^2}{2L+1} \sum_{l_{12}} \Big[&\langle l_1m_1l_2m_2|l_{12}m_{12}\rangle\langle l_1\mu_1l_2\mu_2|l_{12}\mu_{12}\rangle \\
&\langle l_{12}m_{12}l_3m_3|LM_I\rangle\langle l_{12}\mu_{12}l_3\mu_3|LM\rangle \Big]. \tag{3.22}
\end{aligned}$$

Since parity, π, also is a good quantum number, an extra index can be added to $|\Upsilon_R^{LMM_I}\rangle$. So in combination with equations (3.20)-(3.22) the final expression for

the spatial part of the rotor is

$$|\Upsilon_R^{LMM_I\pi}\rangle = \sum_{\bar{l}\bar{\mu}} b(\bar{l}\bar{\mu}; LMM_I\pi)|l_1\mu_1 l_2\mu_2 l_3\mu_3\rangle \, , \tag{3.23}$$

with

$$b(\bar{l}\bar{\mu}; LMM_I\pi) = 0 \quad \text{if} \quad (-1)^{l_1+l_2+l_3} \neq \pi \, . \tag{3.24}$$

For the three-electron system it is, however, not necessary to specify parity explicitly, since we showed in section 2.3.2 that the value of M_I determines the parity by the relation $\pi = (-1)^{M_I}$. No such relation exists for the four-electron symmetric rotor. Therefore, the parity index, π, will be kept to make the extension to the four-electron system more clear.

3.1.2 The spin part

Until now we have not taken the electronic spin degrees of freedom into account. The electron-electron correlation is strongly spin dependent despite of the electron-electron interaction being spin independent (e.g. [30]). Since the Hamiltonian is spin independent the total wave function is simply a product of the spatial function, $|\Upsilon_R^{LMM_I\pi}\rangle$, and a spin function, $|\chi_{M_s}^{S_{12}S}\rangle$. The spin function specifies the total spin, S, of the three electrons and its projection, M_s, which are both conserved quantities. As in the previous chapter, the index S_{12} refers to the intermediate spin arising from coupling the spin of the first and second electron. In the presentation of the symmetric rotor model of Madsen and Mølmer, a coupling scheme which did not involve specification of any intermediate spin was used. The reason for the unconventional choice of coupling scheme was that there are no physical reasons to single out particular values of intermediate spins. However, the coupling scheme used by Madsen and Mølmer cannot be directly extended to four electrons. Therefore, the more conventional scheme is used here. This is by no means a wrong procedure as long as the final wave function does not depend on S_{12}.

The quartet states, $S = \frac{3}{2}$, are easiest to handle since they consist of a symmetric spin function and an antisymmetric spatial function. Consequently, it is not necessary to take spin into consideration and we only have to worry about antisymmetrizing the spatial function. But for the doublet states, $S = \frac{1}{2}$, we have to construct the spin function before we antisymmetrize. The ket, $|\chi_{M_s}^{S_{12}S}\rangle$, is straightforward to compose. In terms of one-electron spin functions, $|\chi_{m_{si}}^{1/2}\rangle$, we explicitly have

$$|\chi_{M_s}^{S_{12}S}\rangle = \sum_{\bar{m}_s} \left[\left\langle \frac{1}{2}m_{s1}\frac{1}{2}m_{s2}\middle| S_{12}(m_{s1}+m_{s2})\right\rangle \right.$$

$$\left. \left\langle S_{12}(m_{s1}+m_{s2})\frac{1}{2}m_{s3}\middle| SM_S\right\rangle |\chi_{m_{s1}}^{1/2}\rangle|\chi_{m_{s2}}^{1/2}\rangle|\chi_{m_{s3}}^{1/2}\rangle \right] , \tag{3.25}$$

with $\bar{m}_s = \{m_{s1}, m_{s2}, m_{s3}\}$.

3.1.3 Antisymmetrization

According to the Pauli exclusion principle the total wave function is obtained by antisymmetrizing the product state $|\Upsilon_R^{LMM_I\pi}\rangle|\chi_{M_s}^{S_{12}S}\rangle$,

$$|\Psi_{R,S_{12}}^{LMM_I\pi,SM_s}\rangle = \boldsymbol{A}\big[|\Upsilon_R^{LMM_I\pi}\rangle|\chi_{M_s}^{S_{12}S}\rangle\big] , \tag{3.26}$$

where $|\Upsilon_R^{LMM_I\pi}\rangle$ is given in equation (3.23), $|\chi_{M_s}^{S_{12}S}\rangle$ in equation (3.25) and $\boldsymbol{A}$ is the three-particle antisymmetrization operator

$$\boldsymbol{A} = \frac{1}{3!}\sum_{p=1}^{3!}(-1)^p \boldsymbol{P}_p , \tag{3.27}$$

where the sum is over all permutations of three particles. With this definition $\boldsymbol{A}$ is idempotent, $\boldsymbol{A}^2 = \boldsymbol{A}$, and Hermitian, $\boldsymbol{A}^\dagger = \boldsymbol{A}$, and thus a projection operator.

Madsen and Mølmer chose another approach to antisymmetrize the rotor. They operated directly on the intrinsic rotor, $|\Upsilon_R\rangle_\omega$. The reason was that it is possible to express the three-electron antisymmetrization operator in terms of rotations which make a simple analytical expression for the antisymmetrized wave function possible. This is, however, not the case when four electrons are considered. In contrast to the planar symmetric top, the four-electron rotor extends in three spatial dimensions. Consequently, besides rotation operators, the space inversion operator is needed to express the full four-electron antisymmetrization operator. In the case of the symmetric top space inversion is equivalent to a rotation about the z axis by π radians. It is far from simple to operate with the space inversion operator on the intrinsic rotor. To evaluate the effect the intrinsic rotor has to be expanded in angular momentum multiplet wave functions specifying the individual angular momenta of the electrons. The result turns out to be a very long and complicated expression that is extremely hard to handle. In the light of these considerations the antisymmetrization is performed by explicitly permuting the particles in the product state as expressed in equation (3.26).

After antisymmetrization, $|\Psi_{R,S_{12}}^{LMM_I\pi,SM_S}\rangle$ is still an expansion on the multiplet wave functions

$$|\Psi_{R,S_{12}}^{LMM_I\pi,SM_s}\rangle = \sum_{\bar{l}\bar{\mu}\bar{m}_s} \tilde{c}(\bar{l}\bar{\mu}\bar{m}_s, LMM_I\pi, SM_s, S_{12})|l_1\mu_1 m_{s1} l_2\mu_2 m_{s2} l_3\mu_3 m_{s3}\rangle . \tag{3.28}$$

Since S_{12} is not a good quantum number, the final expression for the three-electron symmetric rotor wave function, $|\Psi_R^{LMM_I\pi,SM_s}\rangle$, is obtained by summing the contributions for the possible values of S_{12}

$$|\Psi_R^{LMM_I\pi,SM_s}\rangle = N \sum_{i=S_{12}} |\Psi_{R,i}^{LMM_I\pi,SM_s}\rangle , \tag{3.29}$$

where N is a normalization constant. The possible values of $S_{12} \in \{0,1\}$ are determined by the relation $S = S_{12} \pm \frac{1}{2}$. However, the classification in the previous

chapter showed that the intermediate spin can be disregarded in practice when only three electrons are considered. This is seen in equation (2.45) which states that the coefficients F_{MI1} and F_{MI2} only differ by a phase. By substituting equation (3.28) into equation (3.29), $|\Psi_R^{LMM_I\pi,SM_s}\rangle$ can be expressed as

$$|\Psi_R^{LMM_I\pi,SM_s}\rangle = \sum_{\bar{l}\bar{\mu}\bar{m}_s} c(\bar{l}\bar{\mu}\bar{m}_s, LMM_I\pi, SM_s)|l_1\mu_1 m_{s1}l_2\mu_2 m_{s2}l_3\mu_3 m_{s3}\rangle \, , \quad (3.30)$$

with $|\Psi_R^{LMM_I\pi,SM_s}\rangle$ being normalized such that $\sum_{\bar{l}\bar{\mu}\bar{m}_s} |c(\bar{l}\bar{\mu}\bar{m}_s, LMM_I\pi, SM_s)|^2 = 1$.

To conclude this section a three-electron symmetric quantum state has been constructed on the basis of the assumption that the inter-electronic interaction tends to stabilize the electrons in individual Stark states. The symmetric rotor is constructed with respect to basic quantum mechanics such that the state is an antisymmetric eigenstate of $\hat{L}^2$, $\hat{L}_z$, $\hat{S}^2$, $\hat{S}_z$ and the parity operator.

3.2   Atomic state predictions

The three-electron symmetric rotor has been constructed as an analytical expression for the wave function describing triply excited intra-shell states of the three-electron atom. The model gives a simple physical image of the atomic states. To test the quality of the symmetric rotor model various predictions within the model will be presented and compared with *ab initio* calculations. This section presents analytical expressions and numerical results for predictions within the symmetric rotor model, while appendix C deals with the computer programs used in making the numerical predictions.

3.2.1   Configuration-mixing fractions

According to the shell model an atomic state of $^{2S+1}L^\pi$ symmetry is described by one set of individual electron angular momenta, $l_1l_2l_3$. In the intra-shell case of $n = 2$ eight such states are allowed by the Pauli principle and for $n = 3$ the number is 64. We have seen that the configuration mixing in a real atom is expected to be large because of the inter-electronic interaction, and the states therefore are represented as configuration superpositions. The l mixing between several multiplet states is specified by the configuration-mixing fractions which can be predicted from the analytical expression for the symmetric rotor wave function, $|\Psi_R^{LMM_I\pi,SM_s}\rangle$, in equation (3.30). Let $\bar{l}_c = (l_1l_2l_3)_c$ denote the l configuration regardless of permutation e.g. $(spp)_c = \{spp, psp, pps\}$. The configuration-mixing fractions which give the probabilities for the electrons to have specific sets of one-electron angular momenta are then defined as

$$P_{\bar{l}_c}^{LM_I\pi S} \equiv \sum_{\bar{l}\in\bar{l}_c} \sum_{\bar{\mu}\bar{m}_s} |c(\bar{l}\bar{\mu}\bar{m}_s, LMM_I\pi, SM_s)|^2 \, . \quad (3.31)$$

As an example, $P^{LM_I \pi S}_{(spp)_c}$ gives the probability that the angular momentum of one of the three electrons is zero while the angular momenta of the remaining two is one. The mixing fractions, $P^{LM_I \pi S}_{\bar{l}_p}$, do not depend on either M or M_s. This reasonable independence cannot be seen directly from the definition in equation (3.31), but is verified numerically.

The mixing fractions predicted within the symmetric rotor model are calculated for all ET-accessible terms within the $n = 3$ shell and compared with configurational calculations in table 3.1 (here the probabilities are expressed as percentages). SR denotes the symmetric rotor model, MCDF denotes the multiconfigurational Dirac-Fock calculations in reference [37] and CI denotes the configuration interaction calculations in reference [38]. The CI-results are for the lithium-like ion N^{4+} while the other predictions are for lithium. Some numbers in the CI-column are left out since the reference is ambiguous in the prediction of these numbers. Contrary to the SR-predictions the mixing fractions for a given term as predicted in references [37, 38] do not add to 100% (e.g. $^2P^o$ and $^2G^o$). The principal quantum number, n, is fixed in calculations within the symmetric rotor model (here $n = 3$) and thus the mixing fractions have to add to 100%. But the configurational calculations account for mixing with shells with higher n too. However, references [37, 38] give predictions close to 100% in favour of the intra-shell picture.

It is worth taking the so-called rotational fractions, A_T, into consideration before the results are compared further. Inspired by molecular theory, Morishita and Lin defined the rotational fraction, A_T, as a measure of the purity of a state [26]. If A_T is close to one, $T = |M_I|$ is an approximate good quantum number, and the three-electron system to some extent acts like a symmetric top. By construction M_I is a good quantum number in the symmetric rotor model. Only when the rotational fractions listed in table 3.1 are close to one do we expect agreement between the SR-predictions and the configurational calculations.

In general the symmetric rotor model not only predicts the trend in the mixing fractions, but actually compares very well with the configurational calculations. However, discrepancy is pronounced for $^2G^e_{|M_I|=2}$ and $^4F^e_{|M_I|=0}$, but in these cases the rotational fractions, A_T, are seen to be low, so the disagreement is not unexpected. The SR- and CI-predictions for the sd^2 fraction for $^4F^e$ differ by more than a factor of ten. However, according to reference [38] the $^4F^e$ state just above the lowest $^4F^e$ state consists of 99% sd^2. This explains the high sd^2 fraction predicted by SR. Since T is not an approximate good quantum number for the lowest $^4F^e$ state ($A_T = 0.68$), the symmetric rotor mixes this state with those above. Finally, the mixing fractions are seen to be independent of the nuclear charge, Z, since the CI data are for the lithium-like N^{4+} ions.

The convincing agreement between the symmetric rotor predictions and the *ab initio* calculations makes us believe that the symmetric rotor model does in fact account for the electron-electron correlations within the triply excited intrashell states. The mixing fractions presented in table 3.1 differ a little from those predicted by Madsen and Mølmer [33]. Firstly, they present mixing fractions for

Table 3.1: Configuration-mixing fractions for lithium-like ions expressed as percentages. SR denotes predictions within the symmetric rotor model for Li, MCDF multiconfigurational Dirac-Fock calculations for Li [37] and CI configuration interaction calculations for N^{4+} [38]. A_T is the rotational fraction [26].

Term	Configuration	SR	CI	MCDF	A_T
$^2P^o_{\|M_I\|=1}$	s^2p	67.04	64.0	61.8	1.00
	p^3	18.86	19.5	20.0	
	spd	11.73	13.2	13.5	
	pd^2	2.37		3.3	
$^2D^o_{\|M_I\|=1}$	spd	54.30			0.99
	p^3	40.73	37.5		
	pd^2	4.97			
$^2D^e_{\|M_I\|=2}$	sp^2	62.06	55.7		0.98
	s^2d	20.69	24.5		
	p^2d	16.07	17.2		
	sd^2	0.74			
	d^3	0.44			
$^2F^o_{\|M_I\|=1}$	spd	58.18	57.0		0.80
	pd^2	41.82			
$^2F^e_{\|M_I\|=2}$	p^2d	77.92	73.8		0.92
	sd^2	20.78	25.5		
	d^3	1.30			
$^2G^o_{\|M_I\|=1}$	pd^2	100.00	98.7		0.59
$^2G^e_{\|M_I\|=2}$	sd^2	42.33	63.2		0.59
	p^2d	31.75	10.2		
	d^3	25.93	24.3		
$^2G^e_{\|M_I\|=4}$	p^2d	74.07	74.8		0.96
	sd^2	24.69	20.8		
	d^3	1.23			
$^4P^e_{\|M_I\|=0}$	sp^2	90.78	90.1		0.68
	sd^2	4.54			
	p^2d	4.54	5.2		
	d^3	0.14			
$^4F^e_{\|M_I\|=0}$	p^2d	80.00	94.3		0.68
	sd^2	13.33			
	d^3	6.67	5.1		
$^4F^o_{\|M_I\|=3}$	spd	96.97	96.2		0.98
	pd^2	3.03			
$^4G^o_{\|M_I\|=3}$	pd^2	100.00	99.4		0.87

some even states with $M_I = -1$ e.g. $^4\mathrm{P^e}_{M_I=-1}$. These states are not allowed by symmetry since odd values of M_I are associated with odd parity. Secondly, there is a discrepancy between their presented mixing fractions and l distributions. The next section deals with the l distributions of the states and at the end of that section the disagreement in their results will be explained.

3.2.2   Distribution over l quantum numbers

The configuration-mixing fractions are closely connected to the distribution over individual angular momentum quantum numbers, l_i, in the system. Fano (1974) was the first to show interest in the l distributions [39]. He pointed out that the electron-electron interaction in the vicinity of the double-electron escape threshold leads to population of high angular momentum states. In a further consideration of the two-electron atom Drukarev (1982) derived a formula for the l distribution from the assumption that one electron is in a maximally polarized Stark state along the direction of the second electron [40]. As demonstrated earlier, the Stark states can be expanded in the spherical basis. According to equation (3.10) the relation for the maximally polarized Stark states, $|nn-10\rangle$, is

$$|nn-10\rangle = (-1)^{n-1} \sum_{l=0}^{n-1} \langle jjj-j|l0\rangle |nl0\rangle \; , \tag{3.32}$$

where $j = (n-1)/2$. Hence, the probability that the electron is found with a specific value of angular momentum, l, is the square of the coupling coefficient

$$P_D(l) = |\langle jjj-j|l0\rangle|^2 \; , \qquad j = \frac{n-1}{2} \; , \tag{3.33}$$

with D denoting Drukarev. This prediction does not, however, take into account the overall symmetry, including conserved quantum numbers.

To calculate the l distributions within the symmetric rotor model, we recall the final ansatz for the wave function given in equation (3.30)

$$|\Psi_R^{LMM_I\pi,SM_s}\rangle = \sum_{\bar{l}\bar{\mu}\bar{m}_s} c(\bar{l}\bar{\mu}\bar{m}_s, LMM_I\pi, SM_s) |l_1\mu_1 m_{s1} l_2\mu_2 m_{s2} l_3\mu_3 m_{s3}\rangle \; . \tag{3.34}$$

Hence, it is seen that the probability for one electron to have a particular value of angular momentum, l, is

$$P_{SR}(l) = \sum_{\bar{l}, l_1=l} \sum_{\bar{\mu}\bar{m}_s} |c(\bar{l}\bar{\mu}\bar{m}_s, LMM_I\pi, SM_s)|^2 \; . \tag{3.35}$$

So once the configuration-mixing fractions are determined the l distributions can be calculated. The previous section showed successful predictions of the mixing fractions and therefore this must be the case for the l distributions too.

Table 3.2: Distribution of one-electron angular momentum in Li in the $n = 3$ shell predicted within the symmetric rotor model, equation (3.35). The probabilities are expressed as percentages.

Term	$P_{SR}(s)$	$P_{SR}(p)$	$P_{SR}(d)$
${}^2\mathrm{P}^{\mathrm{o}}_{|M_I|=1}$	48.60	45.90	5.49
${}^2\mathrm{D}^{\mathrm{o}}_{|M_I|=1}$	18.10	60.48	21.41
${}^2\mathrm{D}^{\mathrm{e}}_{|M_I|=2}$	34.72	52.09	13.19
${}^2\mathrm{F}^{\mathrm{o}}_{|M_I|=1}$	19.39	33.33	47.27
${}^2\mathrm{F}^{\mathrm{e}}_{|M_I|=2}$	6.93	51.95	41.13
${}^2\mathrm{G}^{\mathrm{o}}_{|M_I|=1}$	0	33.33	66.67
${}^2\mathrm{G}^{\mathrm{e}}_{|M_I|=2}$	14.11	21.16	64.73
${}^2\mathrm{G}^{\mathrm{e}}_{|M_I|=4}$	8.23	49.38	42.39
${}^4\mathrm{P}^{\mathrm{e}}_{|M_I|=0}$	31.77	63.55	4.68
${}^4\mathrm{F}^{\mathrm{o}}_{|M_I|=3}$	4.44	53.33	42.22
${}^4\mathrm{F}^{\mathrm{e}}_{|M_I|=0}$	32.32	33.33	34.34
${}^4\mathrm{G}^{\mathrm{o}}_{|M_I|=3}$	0	33.33	66.67

Table 3.2 shows the l distributions calculated within the symmetric rotor model in the $n = 3$ shell (the probabilities are expressed as percentages). In contrast to the predicted mixing fractions fully agreement between the SR-distributions presented in table 3.2 and those predicted by Madsen and Mølmer in reference [34] is observed. Since the l distribution can be determined directly from the mixing fractions, Madsen and Mølmer presumably made a minor mistake in their calculations of the mixing fractions. To make the connection between the mixing fractions and the l distribution even more clear we consider ${}^2\mathrm{D}^{\mathrm{o}}$. In this case the possible configurations are

$$\mathrm{spd}({}^2\mathrm{D}^{\mathrm{o}}), \quad \mathrm{p}^3({}^2\mathrm{D}^{\mathrm{o}}), \quad \mathrm{pd}^2({}^2\mathrm{D}^{\mathrm{o}}). \tag{3.36}$$

Consequently, the probability that one electron is found with, for example, the angular momentum $l = 2$ is

$$P_{SR}(d) = \frac{1}{3}P_{spd} + \frac{2}{3}P_{pd^2} = \begin{cases} (0.5430 + 2 \cdot 0.0497)/3 = 0.214 & (i) \\ (0.5499 + 2 \cdot 0.0377)/3 = 0.208 & (ii) \end{cases} \tag{3.37}$$

The upper result, (i), is determined with the mixing fractions presented in table 3.1, while the lower result, (ii), is obtained with mixing fractions predicted by Madsen and Mølmer in reference [33]. We see that the result determined with the mixing fractions in table 3.1 is the one in agreement with the l distribution presented both in table 3.2 and in the work of Madsen and Mølmer [34].

Figures 3.3 and 3.4 show the l distribution calculated both within the symmetric rotor model and in Drukarev's simpler approach. The distribution is calculated for $n = 2 - 7$ for the ${}^2\mathrm{P}^{\mathrm{o}}$ state and for $n = 3 - 7$ for the ${}^2\mathrm{G}^{\mathrm{e}}$ state. These terms show the general tendency, and therefore the distribution is not shown for more

Figure 3.3: l distribution for intra-shell $^2P^o$ states in $n = 2 - 7$ manifolds. The blue columns show predictions within the symmetric rotor model, equation (3.35), and the red columns show probabilities in Drukarev's approach, equation (3.33).
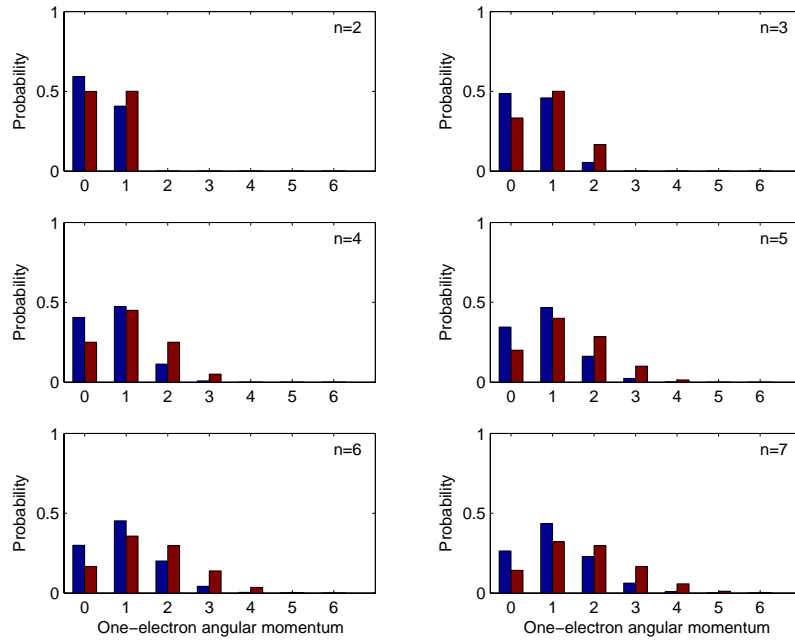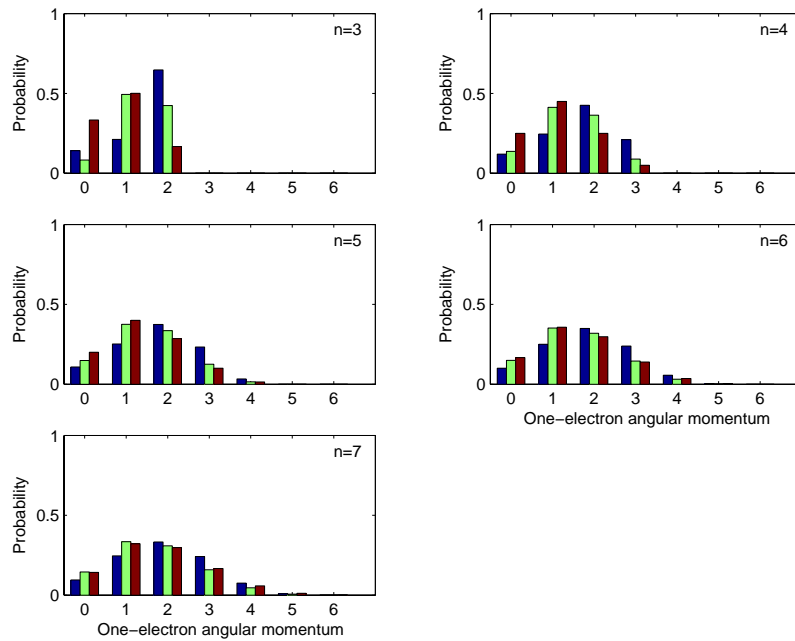

Figure 3.4: l distribution for intra-shell $^2G^e$ states in $n = 3 - 7$ manifolds. The blue and green columns show predictions within the symmetric rotor model, equation (3.35), blue in the case of $|M_I| = 2$ and green in the case of $|M_I| = 4$, and the red columns show probabilities in Drukarev's approach, equation (3.33).

states. Contrary to Drukarev's prediction the l distributions calculated within the symmetric rotor model are different for each term, $^{2S+1}L^{\pi}$. We see that the agreement between the two predictions is poor for small values of n but becomes better as n grows. Madsen and Mølmer have studied the analytical expression for the l distribution [34]. They concluded that in the limit of high n where antisymmetrization is assumed to be less significant enforcement of rotational symmetry leads to a correction but not a completely different distribution than Drukarev's. Moreover, for small n certain values of l are forbidden due to symmetry. This is, for example, the case for $^{2}G^{o}$ where $l = 0$ is Pauli forbidden (see table 3.2).

In conclusion, we have seen that it is absolutely necessary to take into account basic quantum symmetries in order to make quantitative predictions.

3.2.3 Rotational structure in the energy spectrum?

It is worth noting that the mixing fractions and the l distribution depend on the quantum number M_I. This is seen in the case of $^{2}G^{e}$ where both $|M_I| = 2$ and $|M_I| = 4$ are allowed. If the four-body problem is considered from a molecular viewpoint, the M_I-dependence is expected from the rotational energy spectrum known from the symmetric top molecule [25, equation 10.104]

$$E = \frac{1}{2I}[2L(L+1) - T^2] , \tag{3.38}$$

where the conventional notation, $T = |M_I|$, is used. Here $I = \sum_i mr_i^2$ is the moment of inertia of the molecule with respect to the z axis with r_i denoting the distance from the z axis to the ith atom. The rotational spectrum arises from the angular part of the kinetic energy operator, $\sum_i \hat{L}_i^2/2mr_i^2$, since the radii, r_i, are very localized in molecules. Deviations from equation (3.38) are associated with stretches within the molecules. Also nuclei have rotational energy spectra and here deviations from equation (3.38) are explained by considering the nucleus as being shaped as a non-spherical fluid droplet. Rotational structure in doubly excited intra-shell atomic states was reported in 1978 [41]. This was a surprising observation since electrons moving around a nucleus are not well-localized and do therefore not form a rigid rotor. It has since been discussed how to understand a classification of multiply excited intra-shell atomic states according to the rotational scheme.

Morishita and Lin (2001) identified rovibrational normal modes of the angular motions of the electrons by studying the symmetries of the three-electron problem [26]. Moreover, they calculated within the frozen-r model the 64 eigenenergies within the $n = 3$ shell in the lithium-like ion He^{-}. Figure 2.4 (see page 19) shows the result of their calculations. The ordering of the states according to $^{2S+1}L^{\pi}$ symmetries is seen to result in an erratic picture. Therefore, Morishita and Lin grouped the 64 states according to the identified normal modes. One group for example consisted of the ET-accessible states, while a nodal in the coplanar geometry was associated with a mode where the plan of the electrons oscillates with
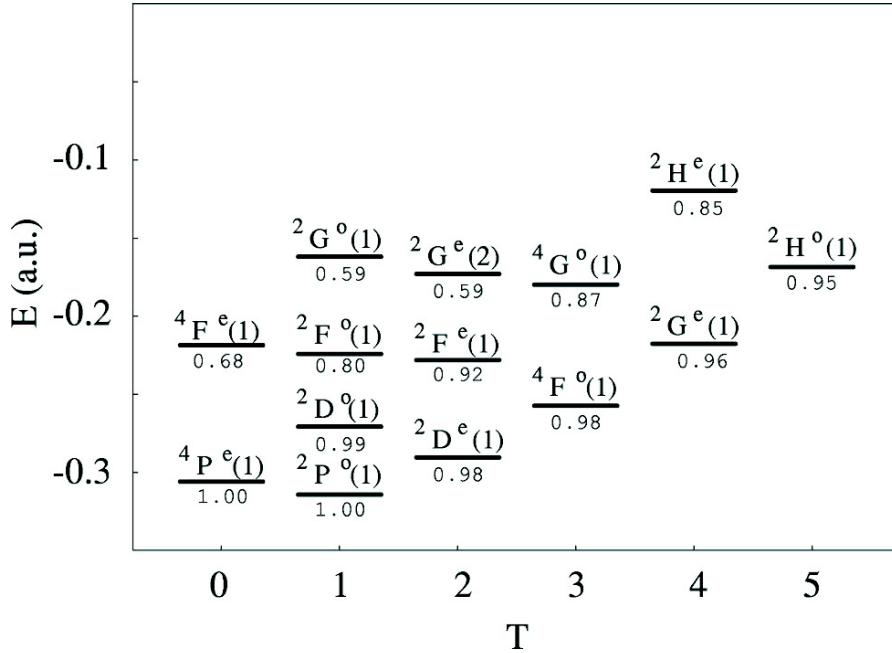
Figure 3.5: Rotational levels in He^- for triply excited ET-accessible states within the $n = 3$ shell. The number in parentheses indicates the ith state of that symmetry with 1 being the lowest. The number below each level denotes the rotational fraction, A_T. From Morishita and Lin [26].

respect to the nucleus. The ET-accessible states are those of most interest in connection with the symmetric rotor model and, in addition, those with a symmetry most like the symmetric top. A classification of these states according to the rotational fraction, A_T, is shown in figure 3.5. The figure is consistent with the qualitative predictions from equation (3.38): for fixed L the states have lower energy for high values of T, and for fixed T the energy increases as the value of L increases. However, the L and T scalings do not follow equation (3.38) since the difference in energy between two L components for fixed T is not independent of T. Moreover, as a consequence of the shell model the series in figure 3.5 terminates at $L_{max} = 5$ $\left(L = 3(n-1) = 6 \text{ is Pauli forbidden}\right)$. Such termination does not exist in molecular spectra. These deviations from the spectrum of a symmetric top molecule are, however, not unexpected since the atom does not act like a rigid rotor. This fact is also pointed out by Madsen and Mølmer in references [32, 33]. They show explicitly that the rotational constant cannot be associated with the moment of inertia of the atom since the wrong L and T scalings cause unacceptable fluctuations of the rotational constant and hence of the moment of inertia. In addition, the estimates for the mean radius from $I = \sum_i m r_i^2$ are too large. But after all, rotational structure to some extent is seen and this is not believed to be a coincidence. The symmetric top belongs to the D_{3h} point group which is isomorphic to the permutation group S_3. This fact suggests a correspondence

between the energy-level structure of the multiply excited intra-shell states of the four-body Coulomb problem and that of the symmetric top molecule.

The energy for a given state predicted within the symmetric rotor model is given by

$$
\begin{aligned}
E_n^{LM_I\pi S} &= \left\langle \Psi_R^{LM_I\pi S} \left| H \right| \Psi_R^{LM_I\pi S} \right\rangle \\
&= 3E_n + \sum_{i<j} \left\langle \Psi_R^{LM_I\pi S} \left| \frac{e^2}{r_{ij}} \right| \Psi_R^{LM_I\pi S} \right\rangle ,
\end{aligned}
\tag{3.39}
$$

with $r_{ij} = |\vec{r_i} - \vec{r_j}|$. The last equality follows from the fact that the Stark states are exact eigenstates of the single-particle part of the Hamiltonian, $\hat{H}$, given in equation (3.1). Here E_n is the Bohr Energy and the last term is the electron-electron interaction energy. It is clear from equation (3.39) that rotational structure in excited atomic states is not associated with the kinetic energy term as in a molecule, but is exclusively due to the electron-electron interaction. The term, $\left\langle \Psi_R^{LM_I\pi S} \left| \frac{e^2}{r_{ij}} \right| \Psi_R^{LM_I\pi S} \right\rangle$, scales linearly with the nuclear charge, Z, since the matrix elements of $\frac{1}{r_{ij}}$ do also. This is also in contradistinction to a rigid rotor. The moment of inertia scales with r^2 and therefore with $1/Z^2$, and hence the rotational energies of a rigid rotor scale with Z^2.

Prerequisites for rotational structure

Equation (3.39) has not been evaluated directly by Madsen and Mølmer, but they showed by an analytical examination that quantum states of many-body systems, molecular as well as nuclear or atomic, in general can have a rotational energy spectrum *irrespective* of the nature of the Hamiltonian, $\hat{H}$, if only a symmetry broken ansatz is a valid approximation for the physical state, $|\Psi\rangle$, and the particles are sufficiently localized in space [32, 33]. The method, which was an extension of the work of Peirls and Yoccoz [42], will briefly be presented here too and, in addition, minor mistakes in the presentation of Madsen and Mølmer will be corrected. The symmetric rotor is an example of a symmetry broken ansatz since the intrinsic rotor, $|\Upsilon_R\rangle_\omega$, accounts for parts of the internal interaction but not the rotational symmetry. Let us assume that a symmetry broken ansatz, $|\Psi_{sb}\rangle_\omega$, is reasonable. Angular momentum eigenstates retaining the inter-particle interaction can be constructed as in the special case of the symmetric rotor

$$
|\Psi_{sb}^{LM}\rangle = \int d\omega\, D_{MM_I}^L(\omega)^* |\Psi_{sb}\rangle_\omega .
\tag{3.40}
$$

When spin is included and the wave function is properly antisymmetrized it reads

$$
|\Psi_{sb}^{LM}\rangle = \int d\omega\, D_{MM_I}^L(\omega)^* |\Phi_{sb}\rangle_\omega ,
\tag{3.41}
$$

where

$$
|\Phi_{sb}\rangle_\omega = \boldsymbol{A}[|\Psi_{sb}\rangle_\omega |\chi_{M_s}^{S_{12}S}\rangle] ,
\tag{3.42}
$$

with the antisymmetrization operator, $\boldsymbol{A}$, given in equation (3.27). The energy eigenstates of a system described by equation (3.41) are

$$E = \frac{\langle \Psi_{sb}^{LM}|H|\Psi_{sb}^{LM}\rangle}{\langle \Psi_{sb}^{LM}|\Psi_{sb}^{LM}\rangle} = \frac{\int\int d\omega d\omega' D_{MM_I}(\omega)^* D_{MM_I}(\omega')_{\omega'}\langle \Phi_{sb}|H|\Phi_{sb}\rangle_\omega}{\int\int d\omega d\omega' D_{MM_I}(\omega)^* D_{MM_I}(\omega')_{\omega'}\langle \Phi_{sb}|\Phi_{sb}\rangle_\omega} \; . \quad (3.43)$$

The overlap functions are then defined as

$$h(\Omega) = {}_\Omega\langle \Phi_{sb}|H|\Phi_{sb}\rangle = {}_{\omega'}\langle \Phi_{sb}|H|\Phi_{sb}\rangle_\omega \quad (3.44)$$

$$n(\Omega) = {}_\Omega\langle \Phi_{sb}|\Phi_{sb}\rangle = {}_{\omega'}\langle \Phi_{sb}|\Phi_{sb}\rangle_\omega \; , \quad (3.45)$$

where Ω denotes the set of Euler angles describing the rotation $\mathbf{R}(\omega)$ followed by $\mathbf{R}^\dagger(\omega')$. The function $h(\Omega)$ is well-defined for every rotationally invariant Hamiltonian. The overlap functions can be expanded in the complete set of Wigner functions

$$h(\Omega) = \sum_{lmm'} h_{mm'}^l D_{mm'}^l(\Omega) \; , \quad (3.46)$$

$$n(\Omega) = \sum_{lmm'} n_{mm'}^l D_{mm'}^l(\Omega) \; , \quad (3.47)$$

with coefficients defined by

$$k_{mm'}^l = \frac{2l+1}{8\pi^2}\int d\Omega k(\Omega) D_{mm'}^l(\Omega)^* \; , \quad (3.48)$$

for $k = h, n$. This is seen by using the following projecting operator in equations (3.46) and (3.47)

$$\frac{2\lambda+1}{8\pi^2}\int d\Omega D_{\mu\mu'}^\lambda(\Omega)^* \; , \quad (3.49)$$

and the orthogonality proporty of the Wigner functions [23, equation 3.113]

$$\int d\Omega D_{\mu\mu'}^\lambda(\Omega)^* D_{mm'}^l(\Omega) = \frac{8\pi^2}{2l+1}\delta_{\lambda l}\delta_{\mu m}\delta_{\mu' m'} \; . \quad (3.50)$$

Since $\mathbf{R}(\Omega) = \mathbf{R}^\dagger(\omega')\mathbf{R}(\omega)$ it follows that

$$D_{mm'}^l(\Omega) = \sum_\eta D_{\eta m}^l(\omega')^* D_{\eta m'}^l(\omega) \; . \quad (3.51)$$

Inserting this relation in equations (3.46) and (3.47) and using equation (3.50) we obtain from equation (3.43)

$$E = \frac{h_{M_I M_I}^L}{n_{M_I M_I}^L} \; . \quad (3.52)$$

The point is that if the state, $|\Phi_{sb}\rangle$, is very anisotropic the overlap functions defined in equations (3.44)-(3.45) will vanish already for small values of $\Omega = (\alpha, \beta, \gamma)$. Then

it is reasonable to expand the Wigner function, $D^l_{mm'} = \langle lm|e^{-i\alpha\hat{L}_z}e^{-i\beta\hat{L}_y}e^{-i\gamma\hat{L}_z}|lm'\rangle$, in equation (3.48) to the second order in the angles and the following expression for $k^L_{M_I M_I}$ is obtained

$$k^L_{M_I M_I} = \frac{2L+1}{8\pi^2} \int d\Omega k(\Omega)\left(1 - \frac{\beta^2 L(L+1)}{4} + i(\alpha+\gamma)M_I \right.$$
$$\left. + \frac{\beta^2 M_I^2}{4} - \frac{(\alpha^2+\gamma^2)M_I^2}{2}\right) . \quad (3.53)$$

The linear M_I term disappears when $h(\Omega)$ and $n(\Omega)$ are even functions in α and γ, which is the case for wave functions which are symmetric with respect to the z axis, as for the symmetric rotor. Neglecting the linear M_I term, equations (3.52) and (3.53) give the energy in the case where the overlap functions fall off sufficiently fast

$$E = \frac{H_0 - \frac{H_{2y}}{4}L(L+1) + \left(\frac{H_{2y}}{4} - \frac{H_{2z}}{2}\right)M_I^2}{N_0 - \frac{N_{2y}}{4}L(L+1) + \left(\frac{N_{2y}}{4} - \frac{N_{2z}}{2}\right)M_I^2} , \quad (3.54)$$

where

$$K_{ny} = \int d\Omega k(\Omega)\beta^n , \quad (3.55)$$

$$K_{nz} = \int d\Omega k(\Omega)(\alpha^n + \gamma^n) , \quad (3.56)$$

with $K_n = H_n, N_n$ and $K_0 = K_{0y}$. Both the numerator and denominator in equation (3.54) show the characteristic $L(L+1)$ and M_I^2 behaviour, and if the higher-order terms and the second-order terms in the denominator are small we obtain the rotational spectrum

$$E = \frac{H_0}{N_0} + B_y L(L+1) - (B_y - 2B_z)M_I^2 , \quad (3.57)$$

with the rotational constants $B_y = (H_0 N_{2y} - H_{2y}N_0)/4N_0^2$ and $B_z = (H_0 N_{2z} - H_{2z}N_0)/4N_0^2$. For nonsymmetric wave functions equation (3.57) is supplemented with a linear M_I term. In molecules with degenerate vibrational or electronic levels such terms are in fact recognized in the energy spectrum as well [43, chapter 1.3]. The M_I dependence disappears when $B_y = 2B_z$ and we obtain the rotational spectrum for a spherical top molecule which we will return to in the next chapter.

As a result it is seen that the rotational spectrum will show up if and only if the overlap functions, $h(\theta)$ and $n(\theta)$, fall off sufficiently fast or, equivalently, the particles are sufficiently well-localized in the angular directions. The rotational constants are not necessary determined by the value of the moment of inertia, but the magnitude and even the sign depend on $H_0 N_{2i} - H_{2i}N_0$, $i = y, z$. Madsen and Mølmer studied the overlap functions for the symmetric rotor. As expected they found that the triply excited rotor states are not sufficiently localized in space to have a rotational energy spectrum.

Energy spectrum in the symmetric rotor model

To determine the energy spectrum in the symmetric rotor model[1] we have to evaluate equation (3.39) directly and thus examine the matrix elements expressing the correlation, $\left\langle \Psi_R^{LM_I\pi S} \left| \frac{e^2}{r_{ij}} \right| \Psi_R^{LM_I\pi S} \right\rangle$. For that purpose the wave function given in equation (3.30) is used

$$|\Psi_R^{LMM_I\pi,SM_s}\rangle = \sum_{\bar{l}\bar{\mu}\bar{m}_s} c(\bar{l}\bar{\mu}\bar{m}_s, LMM_I\pi, SM_s)|l_1\mu_1 m_{s1}l_2\mu_2 m_{s2}l_3\mu_3 m_{s3}\rangle \ . \quad (3.58)$$

Hence, the correlation terms read

$$\left\langle \Psi_R^{LM_I\pi S} \left| \frac{e^2}{r_{ij}} \right| \Psi_R^{LM_I\pi S} \right\rangle$$

$$= \sum_{\bar{l}_a\bar{\mu}_a\bar{m}_{sa}} \sum_{\bar{l}_b\bar{\mu}_b\bar{m}_{sb}} c(\bar{l}_a\bar{\mu}_a\bar{m}_{sa})^* c(\bar{l}_b\bar{\mu}_b\bar{m}_{sb}) \left\langle \bar{l}_a\bar{\mu}_a\bar{m}_{sa} \left| \frac{e^2}{r_{12}} \right| \bar{l}_b\bar{\mu}_b\bar{m}_{sb} \right\rangle \quad (3.59)$$

with $c(\bar{l}\bar{\mu}\bar{m}_s, LMM_I\pi, SM_s) = c(\bar{l}\bar{\mu}\bar{m}_s)$ in short. On the right-hand side of the equality sign r_{ij} has been replaced by r_{12} because the matrix elements are independent of i and j since the rotor is constructed to be antisymmetric. Thus, the general matrix elements to be calculated are of the form

$$\left\langle \bar{l}_a\bar{\mu}_a\bar{m}_{sa} \left| \frac{e^2}{r_{12}} \right| \bar{l}_b\bar{\mu}_b\bar{m}_{sb} \right\rangle$$

$$= \left\langle l_{a1}\mu_{a1} m_{sa1}l_{a2}\mu_{a2} m_{sa2}l_{a3}\mu_{a3} m_{sa3} \left| \frac{e^2}{r_{12}} \right| l_{b1}\mu_{b1} m_{sb1}l_{b2}\mu_{b2} m_{sb2}l_{b3}\mu_{b3} m_{sb3} \right\rangle \ . \quad (3.60)$$

The Coulomb repulsion, e^2/r_{12}, can be expanded in terms of Legendre polynomials $P_k(\cos\theta)$ where θ is the angle between $\vec{r_1}$ and $\vec{r_2}$. These can then be expressed as a sum over products of spherical harmonics [23, Application 4, equation 14]

$$\frac{e^2}{r_{12}} = e^2 \sum_{k=0}^{\infty} \frac{r_<^k}{r_>^{k+1}} \left(\frac{4\pi}{2k+1} \right) \sum_{q=-k}^{q=k} (-1)^q Y_{k-q}(\Omega_1)Y_{kq}(\Omega_2) \ , \quad (3.61)$$

where $r_< = \min(r_1, r_2)$ and $r_> = \max(r_1, r_2)$. With this expression equation (3.60) can be written as

$$\left\langle \bar{l}_a\bar{\mu}_a\bar{m}_{sa} \left| \frac{e^2}{r_{12}} \right| \bar{l}_b\bar{\mu}_b\bar{m}_{sb} \right\rangle$$

$$= \delta_{l_{a3}l_{b3}}\delta_{\mu_{a3}\mu_{b3}}\delta_{m_{sa1}m_{sb1}}\delta_{m_{sa2}m_{sb2}}\delta_{m_{sa3}m_{sb3}} \sum_{k=0}^{\infty} R_k(l_{a1}l_{b1}l_{a2}l_{b2})$$

$$\times \frac{4\pi}{2k+1} \sum_{q=-k}^{q=k} (-1)^q \langle Y_{l_{a1}\mu_{a1}}|Y_{k-q}|Y_{l_{b1}\mu_{b1}}\rangle \langle Y_{l_{a2}\mu_{a2}}|Y_{kq}|Y_{l_{b2}\mu_{b2}}\rangle \ , \quad (3.62)$$

---

[1]None of the considerations and calculations in this section can be found in the work of Madsen and Mølmer.

where

$$R_k(l_{a1}l_{b1}l_{a2}l_{b2})$$
$$= e^2 \int_0^\infty dr_1 r_1^2 \int_0^\infty dr_2 r_2^2 \, R_{nl_{a1}}(r_1) R_{nl_{a2}}(r_2) \frac{r_<^k}{r_>^{k+1}} R_{nl_{b1}}(r_1) R_{nl_{b2}}(r_2) \ . \quad (3.63)$$

At first sight equation (3.62) looks really difficult to handle numerically because of the infinite summation. However, the values of k and q which give rise to nonzero contributions are restricted since [23, equation 3.115]

$$\langle Y_{l_a\mu_a}|Y_{kq}|Y_{l_b\mu_b}\rangle = \left[\frac{(2k+1)(2l_b+1)}{4\pi(2l_a+1)}\right]^{\frac{1}{2}} \langle kql_b\mu_b|l_a\mu_a\rangle\langle k0l_b0|l_a0\rangle \ , \quad (3.64)$$

which gives the following selections rules

$$|l_a - l_b| \leq k \leq l_a + l_b \ , \quad (3.65)$$
$$q = \mu_a - \mu_b \ . \quad (3.66)$$

The energies, $E_{n=3}^{LM_I\pi S}$, have been calculated for all ET-accessible states with $L \leq 4$ and classified according to $T = |M_I|$. The result displayed in the upper part of figure 3.6 is presented for the first time. The scheme in the middle shows the configuration interaction calculations of Vaeck and Hansen for N^{4+} [38]. These energies are scaled by $3/7$ to take into account the different nuclear charge, Z, since it was argued that the distance between the energy levels is expected to scale with Z. Finally, the lower scheme in figure 3.6 is the calculations of Morishita and Lin for He^- in the frozen-r model scaled by $3/2$ [26]. In all three schemes the energies are given relative to the $^2P^o$ term. The scheme predicted within the symmetric rotor model (denoted SR) has even less structure of a rotational spectrum than the predictions by Morishita and Lin (ML). Only a little rotational tendency is found in the SR-scheme e.g. for fixed T the higher value of L the higher energy. In fact, all the three schemes share the tendency that higher L increases the energy for fixed T, contrary to the behaviour in ground states configurations for which Hund's rules state that for a given value of S, the term with the maximum possible value of L has lowest energy. By a further consideration of the SR-scheme we notice that for fixed L higher values of T does not necessary means lower energy as in a pure rotational spectrum. Moreover, the L and T scalings do not follow equation (3.38) like the calculations of Morishita and Lin. These deviations from the rotational spectrum are not unexpected in the light of the analysis above. None of the three schemes agree about either the relative energies or the order of the energies. The Z-scaled version of the calculations of Morishita and Lin separates the energy levels much more than the other two schemes which agree more on the quantitative level. The larger separation is, however, due to the specific choice of radius in the frozen-r model since the separation increases if the mean radius is lowered. In the next section we will see that the choice of radius in the calculations of Morishita and
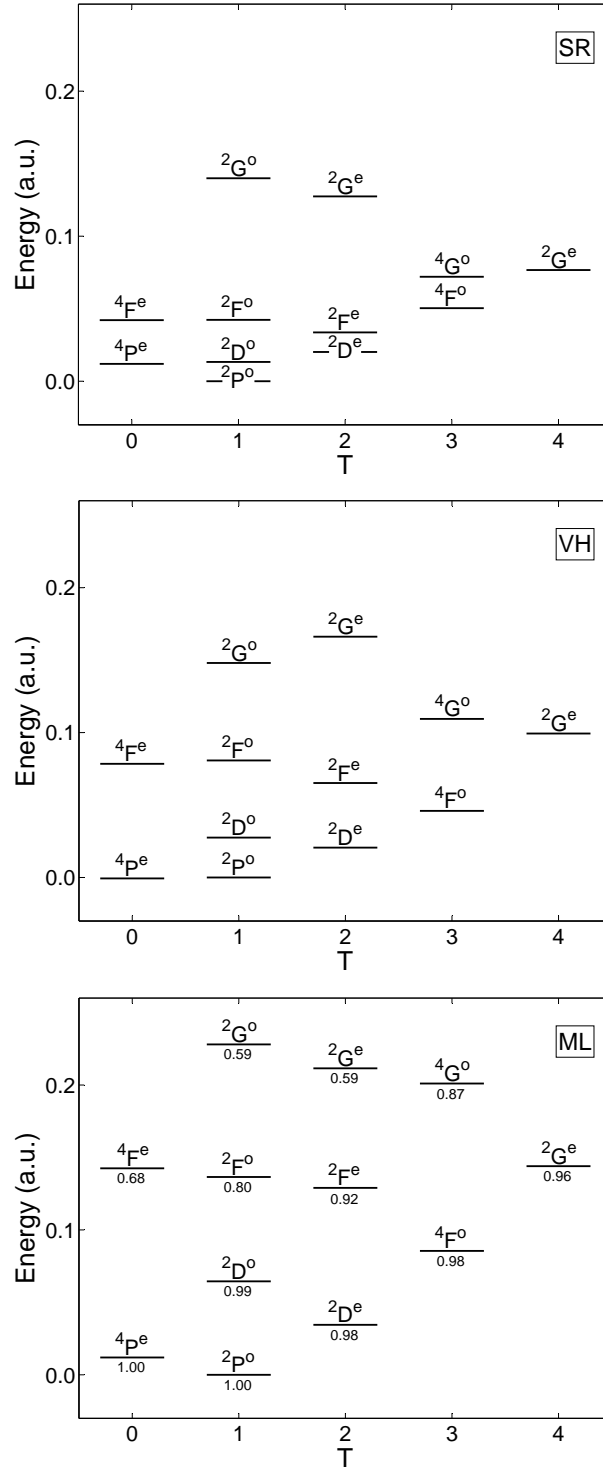
Figure 3.6: Energy levels in lithium-like atomic systems for $n = 3$ intra-shell triply excited states with $L \leq 4$. The upper scheme shows the predictions within the symmetric rotor model. The middle scheme shows Vaeck and Hansen configurational calculations for N^{4+} scaled by 3/7 [38]. Finally, the lower scheme is Morishita and Lin calculations within the frozen-r model for He^- scaled by 3/2, the number below each level denotes the rotational fraction, A_T [26].

Lin is smaller than the expectation values of the radius in the symmetric rotor model. The linear Z scaling is thus confirmed by the agreement about the relative sizes of the energies especially pronounced in the SR-scheme and the VH-scheme.

In conclusion, only a slight tendency towards rotational structure is seen in the energy spectrum of excited intra-shell atomic states. This is confirmed by the predictions within the symmetric rotor model. Such structure in atomic states is not due to rotational kinetic energy, but is a result of the electron-electron interaction. In fact any term in the Hamiltonian can a priori contribute to a rotational spectrum. However, this structure only arises if the particles are sufficiently localized in space. Even though the predictions in the previous sections confirm that the image of the three electrons forming a coplanar equilateral triangle with the nucleus in the center is correct, the failure of pure rotational structure shows that an interpretation of the picture as a rotating rigid body is wrong.

3.2.4 Expectation values of the radius

The previous sections have demonstrated convincing agreement between predictions within the symmetric rotor model and *ab initio* calculations. This agreement indeed qualifies the model both for predicting various characteristic quantities and for understanding the underlying physics of the system.

The mean radius is a measure of the size of the system [2]. In the symmetric rotor model the mean radius can be calculated in the same manner as the energy was calculated in the previous section. Due to the permutation symmetry of the system the expectation values of the radii of the three electrons are equal, hence

$$\langle r \rangle_n^{LM_I\pi S} = \langle \Psi_R^{LM_I\pi S} | r | \Psi_R^{LM_I\pi S} \rangle \tag{3.67}$$

$$= \langle \Psi_R^{LM_I\pi S} | r_1 | \Psi_R^{LM_I\pi S} \rangle \tag{3.68}$$

$$= \sum_{\bar{l}_a\bar{\mu}_a\bar{m}_{sa}} \sum_{\bar{l}_b\bar{\mu}_b\bar{m}_{sb}} c(\bar{l}_a\bar{\mu}_a\bar{m}_{sa})^* c(\bar{l}_b\bar{\mu}_b\bar{m}_{sb}) \langle \bar{l}_a\bar{\mu}_a\bar{m}_{sa} | r_1 | \bar{l}_b\bar{\mu}_b\bar{m}_{sb} \rangle \tag{3.69}$$

$$= \sum_{\bar{l}\bar{\mu}\bar{m}_s} \langle l_1 | r_1 | l_1 \rangle |c(\bar{l}\bar{\mu}\bar{m}_s)|^2 \,, \tag{3.70}$$

with

$$\langle l_1 | r_1 | l_1 \rangle = \int_0^\infty dr_1 r_1^3 R_{nl_1}(r_1)^2 = \frac{1}{2Z}\left[3n^2 - l_1(l_1+1)\right] \tag{3.71}$$

in atomic units. Hence, the expectation value of the radius is simply given by

$$\langle r \rangle_n^{LM_I\pi S} = \sum_{\bar{l}} \frac{1}{2Z}\left[3n^2 - l_1(l_1+1)\right] \sum_{\bar{\mu}\bar{m}_s} |c(\bar{l}\bar{\mu}\bar{m}_s, LMM_I\pi, SM_s)|^2 \,. \tag{3.72}$$

From this equation it is seen that the symmetric rotor model predicts the expected tendencies in the expectation values. Thus, the radius increases with higher n and

---

[2]None of the considerations and calculations in this section can be found in the work of Madsen and Mølmer.

Table 3.3: The symmetric rotor expectation values of the radii, $\langle r \rangle_n^{LM_I\pi S}$, within the $n = 3$ shell in Li. In atomic units.

$S = \frac{1}{2}$		$S = \frac{3}{2}$	
$^2\mathrm{P}^{\mathrm{o}}_{\lvert M_I\rvert=1}$	4.29	$^4\mathrm{P}^{\mathrm{e}}_{\lvert M_I\rvert=0}$	4.24
$^2\mathrm{D}^{\mathrm{o}}_{\lvert M_I\rvert=1}$	4.08		
$^2\mathrm{D}^{\mathrm{e}}_{\lvert M_I\rvert=2}$	4.19		
$^2\mathrm{F}^{\mathrm{o}}_{\lvert M_I\rvert=1}$	3.92	$^4\mathrm{F}^{\mathrm{o}}_{\lvert M_I\rvert=3}$	4.05
$^2\mathrm{F}^{\mathrm{e}}_{\lvert M_I\rvert=2}$	3.92	$^4\mathrm{F}^{\mathrm{e}}_{\lvert M_I\rvert=0}$	3.90
$^2\mathrm{G}^{\mathrm{o}}_{\lvert M_I\rvert=1}$	3.72	$^4\mathrm{G}^{\mathrm{o}}_{\lvert M_I\rvert=3}$	3.72
$^2\mathrm{G}^{\mathrm{e}}_{\lvert M_I\rvert=2}$	3.78		
$^2\mathrm{G}^{\mathrm{e}}_{\lvert M_I\rvert=4}$	3.91		

depends on the l distribution in such way that population of higher angular momentum states lowers the radius. Table 3.3 lists the calculated values of $\langle r \rangle_n^{LM_I\pi S}$ within the $n = 3$ shell. The radius is seen to depend on the value of M_I and the total spin, S, too. The radius increases with increasing M_I which e.g. is seen in the case of $^2\mathrm{G}^{\mathrm{e}}$. Quartet states are expected to have higher mean radius than doublet states due to the so-called "exchange" contribution. For the quartet states the spatial function is totally antisymmetric and therefore the electrons are constrained to stay away from each other. Unfortunately the S dependence cannot be separated from the M_I dependence in the study of table 3.3, since the same values of M_I not are allowed both for doublet and for quartet states.

Table 3.4 shows expectation values for different n. In the symmetric rotor model the calculations are performed for $^2\mathrm{P}^{\mathrm{o}}$ and $^2\mathrm{G}^{\mathrm{e}}$. These predictions are compared with the expectation value $\langle r \rangle_{n=3}$ for $^2\mathrm{P}^{\mathrm{o}}$ obtained from multiconfigurational Hartree-Fock calculations [37] and estimates used in the frozen-r model [44]. In reference [44] the radial distance of the electrons is estimated to

$$r = \frac{n^2}{Z^*} = \frac{n^2}{Z - 1/\sqrt{3}} \, , \tag{3.73}$$

with Z^* being the effective charge. Assuming Z^* to be independent of n is, however, not reasonable since Z^* is expected to lower as n increases. The predictions from the simply estimate in equation (3.73) are seen to be too low compared to the values obtained from symmetric rotor model, especially for high n. On the other hand the expectation value for $^2\mathrm{P}^{\mathrm{o}}$ obtained from multiconfigurational Hartree-Fock calculations is much greater than the one obtained in our model.

To conclude this chapter we first of all have made an explicit analytical construction of triply excited intra-shell states. The model gives a simple physical picture of the atom and, in addition, it yields precise predictions of properties of atomic states in good agreement with *ab initio* calculations. However, we have to be careful with the interpretation of the geometrical picture of the atom. Even though the model yields precise predictions, the atom does not behave like a rigid rotor. The electrons are simply not sufficiently well-localized in space.

Table 3.4: Expectation values of the radii in atomic units (Z=3). SR denotes predictions within the symmetric rotor model, MCHF denotes multiconfigurational Hartree-Fock calculations [37] and finally, frozen-r denotes estimates used in the frozen-r model which do not depend on the $^{2S+1}L^\pi$ symmetry [44].

		n=2	n=3	n=4	n=5	n=6	n=7
$^2\mathrm{P^o}$	SR	1.86	4.29	7.71	12.13	17.55	23.97
$^2\mathrm{P^o}$	MCHF		5.16				
$^2\mathrm{G^e_{|M_I|=2}}$	SR		3.78	7.07	11.47	16.88	23.30
$^2\mathrm{G^e_{|M_I|=4}}$	SR		3.91	7.32	11.74	17.16	23.57
	frozen-r	1.71	3.71	6.60	10.32	14.86	20.23

Chapter 4

The four-electron symmetric rotor model

The three-electron symmetric rotor model has been quantitatively justified by comparing predictions with *ab initio* calculations in the previous chapter. Therefore, we expect that a similar construction of a four-electron symmetric rotor will yield successful predictions for quadruply excited states. Quantitative as well as qualitative predictions will be of great value since multiply excited states of the four-electron atom is, as of yet, a practically undeveloped field of atomic physics. At present there are no experimental results available for hollow beryllium states. But in the near future there will probably be due to the great advances in resolution and brightness of light sources in the appropriate spectral region. Figure 4.1 gives an overview of the energy-level structure in Be, Be^+, Be^{2+} and Be^{3+}. The ionization thresholds are seen to be localized $9.3\,eV$, $27.5\,eV$, $181.4\,eV$ and $399.1\,eV$ above the $Be(1s^2 2s^2\,^1S^e)$ ground state [3]. The lowest quadruply excited state, $Be(2s2p^3\,^5S^o)$, lies above the third ionization threshold. Since the energy of $Be(2s2p^3\,^5S^o)$ is $266.6\,eV$ [29], the needed energy to achieve hollow beryllium is about twice the energy needed to address triply excited states in lithium.

As stated several times in the previous chapter, the original construction of the three-electron symmetric rotor cannot be directly extended to larger systems. But the construction presented in chapter 3 is straightforward to extend step by step to the four-electron system.

4.1 Construction

The ansatz for the wave function rests on the assumption that the inter-electronic interaction tends to stabilize the electrons in individual Stark states. These are chosen to be maximally polarized along the directions of the vertices in a regular tetrahedron (RTH) to account for the repulsion between the electrons. Hence, the spatial part of the four-electron rotor is

$$|\Upsilon_R\rangle = |nn-10\rangle_{\xi_1}|nn-10\rangle_{\xi_2}|nn-10\rangle_{\xi_3}|nn-10\rangle_{\xi_4}\ , \qquad (4.1)$$
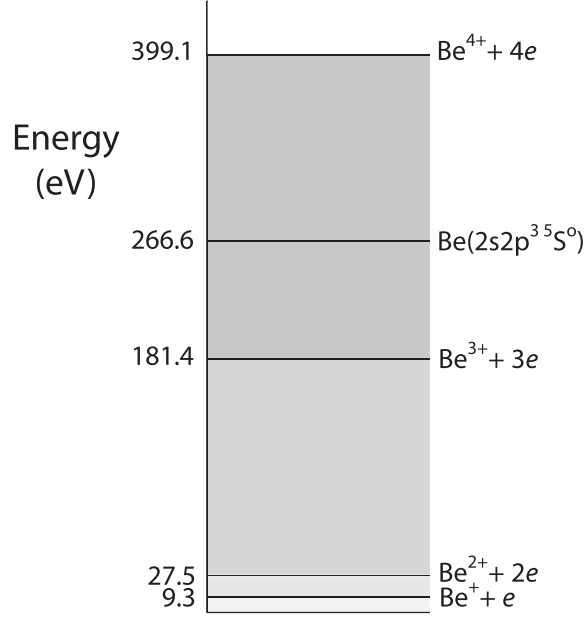
Figure 4.1: Energy level scheme for Be, Be$^+$, Be^{2+} and Be^{3+}. The threshold energies are obtained from reference [3] and the energy of Be(2s2p^3 ^{5}S^o) is obtained from multiconfigurational Hartree-Fock calculations [29].

with ξ_j being the direction of the jth electron with respect to the nucleus.

Figure 4.2 displays the two natural choices of a body-fixed frame for the spherical top. In section 2.4 we argued that M_I will be a good quantum number no matter how the body-fixed frame is chosen. But as stated, the choice is definitely important with respect to numerical calculations within the symmetric rotor model. As a consequence of rotations the analytical expression for the symmetric rotor contains many summations of Wigner functions. To minimize the number of rotations and thereby speed up the calculation process it is advantageous to choose the frame with one electron on the z axis. That is, the nucleus is placed at the origin and one electron is placed on the z axis, while the remaining three are in a plane parallel with the xy plane (see figure 4.2(a)). We still let quantum numbers in kets without a subscript refer to quantization along the z axis so the electron on the z axis is represented by the state $|nn-10\rangle$. The other three states, $|nn-10\rangle_{\xi_q}$, $q = 1, 2, 3$, are related to $|nn-10\rangle$ via the rotations

$$|nn-10\rangle_{\xi_q} = \mathbf{R}\big(q\frac{2\pi}{3}, \Phi, 0\big)|nn-10\rangle = e^{-iq\frac{2\pi}{3}\hat{L}_z}e^{-i\Phi\hat{L}_y}|nn-10\rangle \,, \qquad (4.2)$$

with $\Phi = 109.5^o$ being the inter-electronic angle as seen from the nucleus. The first rotation, $e^{-i\Phi\hat{L}_y}$, rotates the state 109.5^o about the y axis, and the second rotation, $e^{-iq\frac{2\pi}{3}\hat{L}_z}$, rotates the state through the angle $q\frac{2\pi}{3}$ about the z axis. We note that this choice of body frame only requires rotation of three of the four electrons while the frame in figure 4.2(b) would require rotation of all the four electrons.

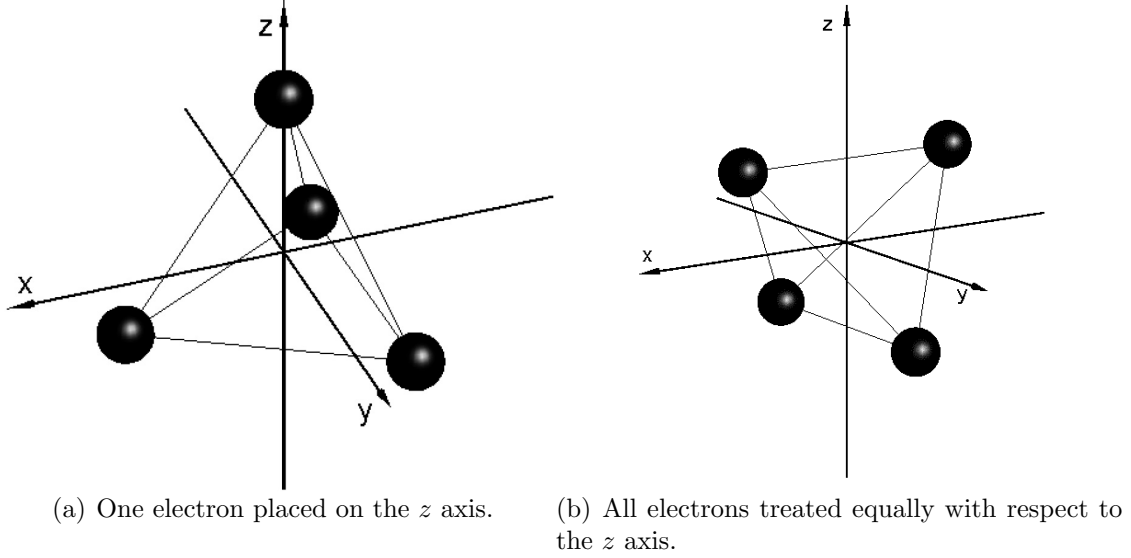(a) One electron placed on the z axis.   (b) All electrons treated equally with respect to the z axis.

Figure 4.2: Two different choices of body-fixed frame.

We recall the transformation between the maximally polarized Stark states and the spherical basis given in equation (3.10)

$$|nn-10\rangle = (-1)^{n-1} \sum_{l=0}^{n-1} \langle jjj-j|l0\rangle |nl0\rangle , \qquad j = \frac{n-1}{2} ; \qquad (4.3)$$

hence,

$$
\begin{aligned}
|nn-10\rangle_{\xi_q} &= (-1)^{n-1} \sum_{l=0}^{n-1} \langle jjj-j|l0\rangle \mathbf{R}\big(q\frac{2\pi}{3}, \Phi, 0\big)|nl0\rangle \\
&= (-1)^{n-1} \sum_{l=0}^{n-1} \langle jjj-j|l0\rangle \sum_{m=-l}^{l} |nlm\rangle \langle nlm|\mathbf{R}\big(q\frac{2\pi}{3}, \Phi, 0\big)|nl0\rangle \\
&= (-1)^{n-1} \sum_{lm} \langle jjj-j|l0\rangle D_{m0}^l\big(q\frac{2\pi}{3}, \Phi, 0\big)|nlm\rangle , \qquad j = \frac{n-1}{2} .
\end{aligned}
$$
$$(4.4)$$

So equation (4.1) with equations (4.3) and (4.4) gives

$$|\Upsilon_R\rangle = \sum_{\bar{l}\bar{m}} \prod_{q=1}^{4} a_q(l_q m_q)|nl_q m_q\rangle , \quad \bar{l} = \{l_1, l_2, l_3, l_4\} , \quad \bar{m} = \{m_1, m_2, m_3, 0\},$$
$$(4.5)$$

with the a-coefficients

$$a_q = \langle jjj-j|l_q 0\rangle D_{m_q 0}^{l_q}\big(q\frac{2\pi}{3}, \Phi, 0\big) = \langle jjj-j|l_q 0\rangle d_{m_q 0}^{l_q}(\Phi)e^{-iq\frac{2\pi}{3}m_q} , \quad q = 1,2,3,$$
$$(4.6)$$

$$a_4 = \langle jjj-j|l_4 0\rangle .$$
$$(4.7)$$

We note that the expansion in equation (4.5) is restricted by the selection rule $m_4 = 0$ as a consequence of the right choice of body frame.

The expression for the spatial part of the wave function in equation (4.5) accounts for the internal interaction but not the rotational symmetry. In the previous chapter it was shown that angular momentum eigenstates retaining the interparticle interaction can be constructed as

$$|\Upsilon_R^{LMM_I}\rangle = \int d\omega D_{MM_I}^L(\omega)^* |\Upsilon_R\rangle_\omega ,\qquad (4.8)$$

where the subscript ω refers to the rotated frame determined by the Euler angles $\omega = (\alpha, \beta, \gamma)$. Substituting expression (4.5) into equation (4.8) gives

$$\begin{aligned}
|\Upsilon_R^{LMM_I}\rangle &= \int d\omega D_{MM_I}^L(\omega)^* |\Upsilon_R\rangle_\omega \\
&= \int d\omega D_{MM_I}^L(\omega)^* \sum_{\bar{l}\bar{m}} a(\bar{l}\bar{m})|l_1m_1l_2m_2l_3m_3l_40\rangle_\omega \\
&= \sum_{\bar{l}\bar{m}} a(\bar{l}\bar{m}) \int d\omega \Big[D_{MM_I}^L(\omega)^* \\
&\qquad\qquad \sum_{\bar{\mu}} D_{\mu_1m_1}^{l_1}(\omega)D_{\mu_2m_2}^{l_2}(\omega)D_{\mu_3m_3}^{l_3}(\omega)D_{\mu_40}^{l_4}(\omega)|l_1\mu_1l_2\mu_2l_3\mu_3l_4\mu_4\rangle \Big] \\
&= \sum_{\bar{l}\bar{m}\bar{\mu}} a(\bar{l}\bar{m})I(\bar{l}\bar{m}\bar{\mu}; LMM_I)|l_1\mu_1l_2\mu_2l_3\mu_3l_4\mu_4\rangle \\
&= \sum_{\bar{l}\bar{\mu}} b(\bar{l}\bar{\mu}; LMM_I)|l_1\mu_1l_2\mu_2l_3\mu_3l_4\mu_4\rangle , \qquad (4.9)
\end{aligned}$$

where

$$b(\bar{l}\bar{\mu}; LMM_I) = \sum_{\bar{m}} a(\bar{l}\bar{m})I(\bar{l}\bar{m}\bar{\mu}; LMM_I) ,\qquad (4.10)$$

$$a(\bar{l}\bar{m}) = \prod_{q=1}^4 a_q(l_qm_q) , \qquad \text{with } a_q \text{ given in equations (4.6)-(4.7)} ,\qquad (4.11)$$

$$I(\bar{l}\bar{m}\bar{\mu}; LMM_I) = \frac{8\pi^2}{2L+1}\sum_{l_{12}}\sum_{l_{34}}\Big[\langle l_1m_1l_2m_2|l_{12}m_{12}\rangle\langle l_1\mu_1l_2\mu_2|l_{12}\mu_{12}\rangle\langle l_3m_3l_40|l_{34}m_3\rangle$$
$$\langle l_3\mu_3l_4\mu_4|l_{34}\mu_{34}\rangle\langle l_{12}m_{12}l_{34}m_3|LM_I\rangle\langle l_{12}\mu_{12}l_{34}\mu_{34}|LM\rangle \Big].$$
$$(4.12)$$

The final expression for the spatial part of the wave function is obtained by taking parity into account; hence, in combination with equations (4.10)-(4.12),

$$|\Upsilon_R^{LMM_I\pi}\rangle = \sum_{\bar{l}\bar{\mu}} b(\bar{l}\bar{\mu}; LMM_I\pi)|l_1\mu_1l_2\mu_2l_3\mu_3l_4\mu_4\rangle ,\qquad (4.13)$$

with

$$b(\bar{l}\bar{\mu}; LMM_I\pi) = 0 \quad \text{if} \quad (-1)^{l_1+l_2+l_3+l_4} \neq \pi . \tag{4.14}$$

In section 2.4 we saw that, contrary to the three-electron rotor, parity cannot be determined by the value of M_I. Therefore, equation (4.14) has to be taken into account in the numerical calculations.

The spin function, $|\chi_{M_s}^{S_{12}S_{34}S}\rangle$, is determined by coupling the spin of the first and second electron and the third and fourth electron to the intermediate spins S_{12} and S_{34}, respectively. In terms of one-electron spin functions, $|\chi_{m_{si}}^{1/2}\rangle$, the spin function reads

$$|\chi_{M_s}^{S_{12}S_{34}S}\rangle = \sum_{\bar{m}_s} \left[\left\langle \frac{1}{2}m_{s1}\frac{1}{2}m_{s2}\Big|S_{12}(m_{s1}+m_{s2})\right\rangle \left\langle \frac{1}{2}m_{s3}\frac{1}{2}m_{s4}\Big|S_{34}(m_{s3}+m_{s4})\right\rangle \right.$$

$$\left. \left\langle S_{12}(m_{s1}+m_{s2})S_{34}(m_{s3}+m_{s4})\Big|SM_S\right\rangle |\chi_{m_{s1}}^{1/2}\rangle|\chi_{m_{s2}}^{1/2}\rangle|\chi_{m_{s3}}^{1/2}\rangle|\chi_{m_{s4}}^{1/2}\rangle \right], \quad (4.15)$$

with $\bar{m}_s = \{m_{s1}, m_{s2}, m_{s3}, m_{s4}\}$. The ket, $|\chi_{M_s}^{S_{12}S_{34}S}\rangle$, specifies the total spin, S, of the four electrons and its projection, M_s, which are conserved quantities. Since the intermediate spins, S_{12} and S_{34}, are not good quantum numbers, the final wave function is obtained by summing the contributions for the possible values of S_{12} and S_{34} analogous to the construction of the three-electron rotor. We saw in chapter 2 that, contrary to the three-electron system, there is a relation between the allowed values of M_I and the intermediate spins for the four-electron system.

The total wave function is now obtained by antisymmetrizing the product state $|\Upsilon_R^{LMM_I\pi}\rangle|\chi_{M_s}^{S_{12}S_{34}S}\rangle$,

$$|\Psi_{R,S_{12}S_{34}}^{LMM_I\pi,SM_s}\rangle = \boldsymbol{A}\left[|\Upsilon_R^{LMM_I\pi}\rangle|\chi_{M_s}^{S_{12}S_{34}S}\rangle\right] , \tag{4.16}$$

where $|\Upsilon_R^{LMM_I\pi}\rangle$ is given in equation (4.13), $|\chi_{M_s}^{S_{12}S_{34}S}\rangle$ in equation (4.15) and $\boldsymbol{A}$ is the four-particle antisymmetrization operator

$$\boldsymbol{A} = \frac{1}{4!}\sum_{p=1}^{4!}(-1)^p \boldsymbol{P}_p , \tag{4.17}$$

where the sum is over all permutations of the four particles. The result is still an expansion on the multiplet wave functions

$$|\Psi_{R,S_{12}S_{34}}^{LMM_I\pi,SM_s}\rangle = \sum_{\bar{l}\bar{\mu}\bar{m}_s} \tilde{c}(\bar{l}\bar{\mu}\bar{m}_s, LMM_I\pi, SM_s, S_{12}S_{34})|l_1\mu_1 m_{s1}l_2\mu_2 m_{s2}l_3\mu_3 m_{s3}l_4\mu_4 m_{s4}\rangle.$$

$$\tag{4.18}$$

The final expression for the four-electron symmetric rotor is thus

$$|\Psi_R^{LMM_I\pi,SM_s}\rangle = N \sum_{i=\{S_{12}S_{34}\}} |\Psi_{R,i}^{LMM_I\pi,SM_s}\rangle , \tag{4.19}$$

with N being a normalization constant. The possible values of intermediate spins, S_{12} and S_{34}, are determined by the relation $\vec{S} = \vec{S_{12}} + \vec{S_{34}}$. Substituting equation (4.18) into equation (4.19) gives

$$|\Psi_R^{LMM_I\pi,SM_s}\rangle = \sum_{\bar{l}\bar{\mu}\bar{m}_s} c(\bar{l}\bar{\mu}\bar{m}_s, LMM_I\pi, SM_s)|l_1\mu_1 m_{s1}l_2\mu_2 m_{s2}l_3\mu_3 m_{s3}l_4\mu_4 m_{s4}\rangle \ ,$$

(4.20)

with $|\Psi_R^{LMM_I\pi,SM_s}\rangle$ being normalized such that $\sum_{\bar{l}\bar{\mu}\bar{m}_s} |c(\bar{l}\bar{\mu}\bar{m}_s, LMM_I\pi, SM_s)|^2 = 1$.

Since M_I is a conserved quantity the probability for a certain value of M_I has to be fixed when the intermediate spin coupling is given. This fact gives a possibility to check whether the symmetric rotor, $|\Psi_R^{LMM_I\pi,SM_s}\rangle$, is correctly constructed with respect to basic quantum-mechanical symmetries. According to equation (4.18) the probability for a given set of M_I and $i = \{S_{12}S_{34}\}$ in the symmetric rotor model is

$$P_{M_I i} = P_{M_I i}^{L\pi S} = N^2 \sum_{\bar{l}\bar{\mu}\bar{m}_s} |\tilde{c}(\bar{l}\bar{\mu}\bar{m}_s, LMM_I\pi, SM_s, i)|^2 \ . \tag{4.21}$$

For a given term, $^{2S+1}L^\pi$, we expect the probabilities, $P_{M_I i}$, determined within the symmetric rotor model to mirror those predicted in the classification schemes in tables 2.3-2.5 in section 2.4. Thus, the ratios $P_{M_I i}/P_{M'_I i}$ are compared with $|F_{M_I i}/F_{M'_I i}|^2$. The values of $P_{M_I i}/P_{M'_I i}$ are not listed since, as expected, they turned out exactly to mirror the ratios determined from the classification scheme. This result is a very good indication of the symmetric rotor being constructed correctly with respect to the rules of basic quantum mechanics.

The result of this section is an expression for the four-electron symmetric rotor. As a consequence of the preliminary work in the previous chapter the task was relatively simple. However, the length of the analytical expression for the expansion coefficients in the rotor increases when the number of electrons increases. Therefore, the task becomes more tedious when an extra electron is added and the steps in both the construction and the computer program for numerical calculations should be watched carefully.

4.2 Atomic state predictions

Chapter 3 showed successful predictions within the symmetric rotor model in the case of triply excited states, and we therefore expect the four-electron rotor to yield good predictions too. This section will for the first time present analytical expressions and numerical predictions for configuration-mixing fractions, l distributions, energies and mean radii for quadruply excited states predicted within the four-electron symmetric rotor model. Most of the computer programs used in making predictions are described and printed in appendix C.

Table 4.1: Configuration-mixing coefficients for the most important intra-shell configuration states of ^{5}S^o symmetry (coefficients predicted by either SR or MCHF to be equal to or larger than 0.05). SR denotes predictions within the symmetric rotor model. MCHF denotes multiconfigurational Hartree-Fock calculations [29]. The first column lists the single-electron configurations.

^{5}S^o	n=3		n=4		n=5		n=6	
Config.	SR	MCHF	SR	MCHF	SR	MCHF	SR	MCHF
sp^3	0.968	0.95	0.901	0.87	0.820	0.81	0.74	0.77
spd^2	0.250	0.29	0.388	0.42	0.454	0.46	0.478	0.48
sd^{2}f			0.113	0.09	0.198	0.20	0.260	0.23
spf^2					0.0632	<0.05	0.0888	<0.05
p^{2}df			0.146	0.18	0.239	0.24	0.301	0.28
pdf^2			0.0376	0.05	0.0920	0.09	0.144	0.13
d^{3}f			0.0470	0.05	0.0986	0.08	0.145	0.11
pd^{2}g							0.0750	<0.05

4.2.1 Configuration-mixing fractions

We recall the definition of the configuration-mixing fractions

$$P_{\bar{l}_c}^{LM_I\pi S} \equiv \sum_{\bar{l}\in\bar{l}_c} \sum_{\bar{\mu}\bar{m}_s} |c(\bar{l}\bar{\mu}\bar{m}_s, LMM_I\pi, SM_s)|^2 \,, \qquad (4.22)$$

where $\bar{l}_c = (l_1 l_2 l_3 l_4)_c$ denotes the l-configuration regardless of permutation and the c-coefficients are the expansion coefficients in the wave function given in equation (4.20). Since the mixing fractions express the l mixing between several multiplet states it is reasonable to call the square root of these fractions configuration-mixing coefficients. In fact, these are coefficients in expansions in refined basis sets used to diagonalize the problem in various configurational calculations.

In section 2.4 it was shown that the ^{5}S^o state is RTH-accessible in agreement with reference [29]. Table 4.1 shows a comparison between the mixing coefficients predicted within the symmetric rotor model and from multiconfigurational Hartree-Fock calculations [29]. As expected the symmetric rotor predictions compare very well with the *ab initio* calculations. This convincing agreement in the predictions makes us believe that the four-electron symmetric rotor model in fact accounts for the strong electron-electron correlations within the quadruply exited intra-shell states. Thus, it seems reasonable to expect the model to yield precise predictions of mixing coefficients for other terms as well. Table 4.2 shows configuration-mixing fractions for all RTH-accessible terms with $L \leq 4$ within the $n = 3$ shell.

There is a notable difference between tables 4.2 and 3.1 in section 3.2.1. The mixing fractions for quadruply excited intra-shell states do not depend on M_I, unlike those for triply excited intra-shell states. We will return to this point later and explain why the difference is actually expected. The mixing fractions are also

Table 4.2: Configuration-mixing fractions in Be in the $n = 3$ shell predicted within the symmetric rotor model. The probabilities are expressed as percentages.

Term	Configuration	$S = 0$	$S = 1$	$S = 2$
$^{2S+1}S^o$	sp^3			93.75
	spd^2			6.25
$^{2S+1}D^o$	s^2pd	52.65	15.29	
	sp^3	26.32	68.78	
	p^3d	15.04	9.83	
	spd^2	5.01	5.46	
	pd^3	0.97	0.65	
$^{2S+1}F^o$	s^2pd		64.90	
	spd^2		21.63	
	spd^2		12.17	
	pd^3		1.29	
$^{2S+1}G^o$	p^3d	80.10	56.59	
	spd^2	14.24	40.24	100.00
	pd^3	5.66	3.16	
$^{2S+1}P^e$	s^2p^2		60.82	
	sp^2d		20.27	
	p^4		15.21	
	p^2d^2		1.74	
	s^2d^2		1.35	
	sd^3		0.58	
	d^4		0.03	
$^{2S+1}D^e$	s^2p^2	62.04		
	p^4	15.51		
	sp^2d	14.77		
	p^2d^2	4.43		
	s^2d^2	2.95		
	sd^3	0.22		
	d^4	0.08		
$^{2S+1}F^e$	sp^2d		78.29	96.43
	s^2d^2		13.92	
	p^2d^2		7.06	
	sd^3		0.58	3.57
	d^4		0.16	
$^{2S+1}G^e$	sp^2d	41.65	76.92	
	s^2d^2	27.77		
	p^2d^2	27.52	17.95	
	sd^3	2.78	5.13	
	d^4	0.28		

Table 4.3: Distribution of one-electron angular momentum in Be in the $n = 3$ shell predicted within the symmetric rotor model, equation (4.23). The probabilities are expressed as percentages.

Term	$P_{SR}(s)$	$P_{SR}(p)$	$P_{SR}(d)$
$^5\mathrm{S^o}$	25.00	71.88	3.12
$^5\mathrm{F^e}$	25.00	48.21	26.79
$^5\mathrm{G^o}$	25.00	25.00	50.00
$^3\mathrm{P^e}$	36.30	56.62	7.07
$^3\mathrm{D^o}$	26.20	64.30	9.49
$^3\mathrm{F^o}$	37.86	31.08	31.05
$^3\mathrm{F^e}$	26.68	42.67	30.65
$^3\mathrm{G^o}$	10.06	53.30	36.64
$^3\mathrm{G^e}$	20.51	47.44	32.05
$^1\mathrm{D^o}$	34.16	45.68	20.16
$^1\mathrm{D^e}$	36.24	56.13	7.63
$^1\mathrm{G^o}$	3.56	65.05	31.39
$^1\mathrm{G^e}$	24.99	34.59	40.42

noticed to be strongly spin dependent. This is more clear in the case of quadruply excited states since there are more terms with the same L and π but different S than in the three-electron case. This confirms that even though the Hamiltonian is spin independent the electron-electron correlations are indeed spin dependent. As a consequence of Pauli statistics some configurations are even forbidden for one spin multiplicity and not for another.

4.2.2 Distribution over l quantum numbers

We recall that the probability for one electron to have a particular value of angular momentum, l, is

$$P_{SR}(l) = \sum_{\bar{l},l_1=l} \sum_{\bar{\mu}\bar{m}_s} |c(\bar{l}\bar{\mu}\bar{m}_s, LMM_I\pi, SM_s)|^2 \ . \tag{4.23}$$

Table 4.3 displays the l distributions calculated within the symmetric rotor model within the $n = 3$ shell (the probabilities are expressed as percentages). This table gives no new information, but shows the predictions in table 4.2 from another angle. It is, however, interesting to compare the results in table 4.3 with the prediction of Drukarev, $P_D(l)$, which correspond to the symmetric rotor when the overall symmetry is not taken into account. As argued in section 3.2.2, $P_D(l)$ is given by

$$P_D(l) = |\langle jjj - j|l0\rangle|^2 \ , \quad j = \frac{n-1}{2} \ . \tag{4.24}$$

Equation (4.24) shows that $P_D(l)$ does not depend on either L, S or π in contrast to the probabilities in table 4.3. Since table 4.3 illustrates that the l distribution

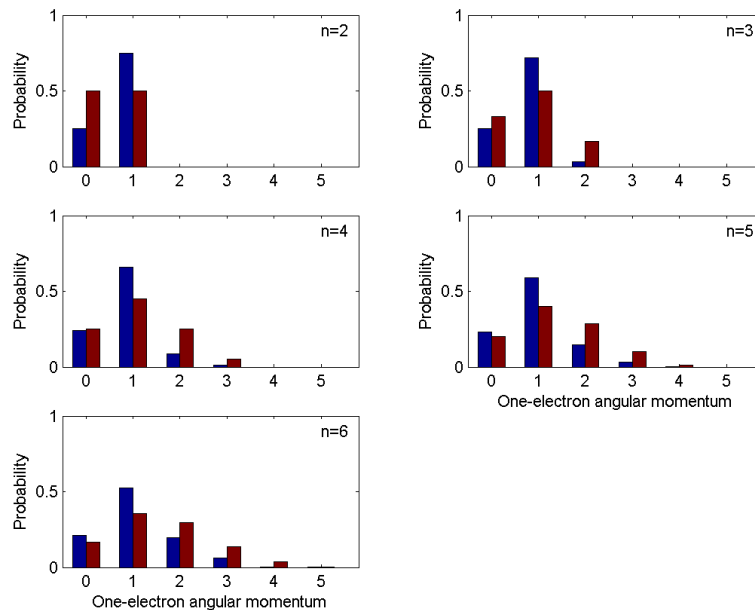Figure 4.3: l distribution for the intra-shell Be ^{5}S^o state in $n = 2 - 6$ manifolds. The blue columns show predictions within the symmetric rotor model, equation (4.23), and the red columns show probabilities in Drukarev's approach where the overall symmetry is not taken into account, equation (4.24).

strongly depends on L as well as S and π, it is absolutely necessary to take the overall symmetry into account. In other words quantum symmetries including conserved quantum numbers and antisymmetrization cannot be neglected.

Finally, figure 4.3 shows the l distribution calculated within the symmetric rotor model for the ^{5}S^o state for $n = 2 - 6$ compared with Drukarev's simpler approach. As in the three-electron case the agreement between the two predictions is better for higher excitation, n. It seems reasonable that it is more important to take the overall symmetry into account for small n when the electrons are closer to the nucleus and each other.

4.2.3 Energy spectrum

Section 3.2.3 discussed whether a rotational-like spectrum for atomic states is expected or not. We found that the rotational structure shows up in atomic as well as in molecular and nuclear many-body systems if the particles are sufficiently well-localized in space. This was not the case for the three-electron atom which turned out to be too sloppy to follow the rotational scheme. However, it was seen that the energies of triply excited states depend on the quantum number M_I, as in the energy spectrum of a rigid symmetric top. We have already noticed that the mixing fractions and l distributions for the quadruply excited states are M_I
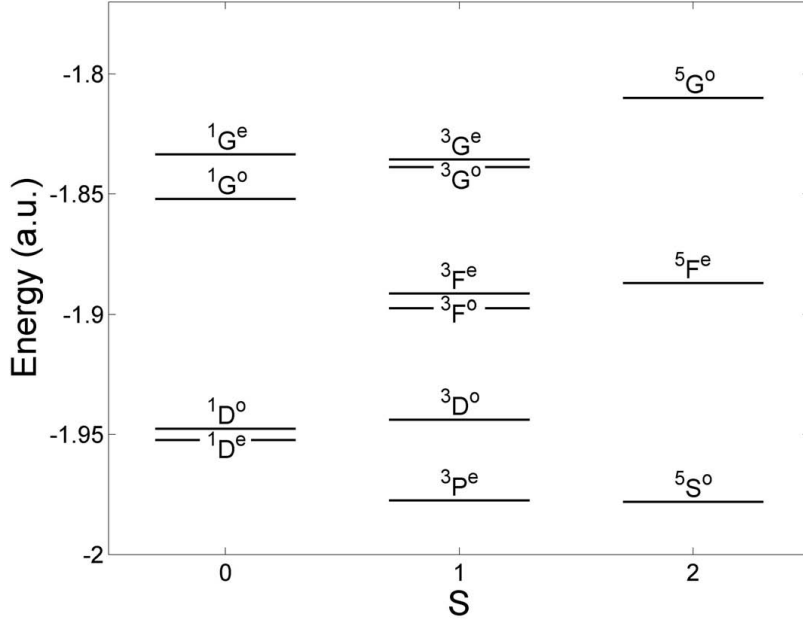
Figure 4.4: Energy levels in Be for $n = 3$ intra-shell states with $L \leq 4$ predicted within the symmetric rotor model.

independent. The energies depend on the l distribution and are therefore M_I independent too. Since no body-fixed frame is preferred, this is reasonable and also expected from the energy spectrum of a rigid spherical top. The rotational energy of the spherical top molecule reads [25, equation 10.137]

$$E = \frac{1}{2I}L(L+1) \, , \tag{4.25}$$

with $I = \sum_i mr_i^2$ being the moment of inertia of the molecule. In the light of the results and discussion in section 3.2.3 we do not expect the energy spectrum of the quadruply excited intra-shell states to follow equation (4.25). This is already confirmed since the mixing fractions and l distributions depend on both S and π unlike equation (4.25).

The energy for a given state predicted within the four-electron symmetric rotor model is

$$E_n^{LM_I\pi S} = \left\langle \Psi_R^{LM_I\pi S} \left| H \right| \Psi_R^{LM_I\pi S} \right\rangle$$
$$= 4E_n + \sum_{i<j} \left\langle \Psi_R^{LM_I\pi S} \left| \frac{e^2}{r_{ij}} \right| \Psi_R^{LM_I\pi S} \right\rangle \, , \tag{4.26}$$

with E_n being the Bohr energy and $r_{ij} = |\vec{r_i} - \vec{r_j}|$. In section 3.2.3 the correlation term, $\left\langle \Psi_R^{LM_I\pi S} \left| \frac{e^2}{r_{ij}} \right| \Psi_R^{LM_I\pi S} \right\rangle$, was evaluated and it is therefore straightforward to calculate the energies, $E_n^{LM_I\pi S}$. Figure 4.4 shows the energies for the RTH-accessible states with $L \leq 4$ within the $n = 3$ shell ordered according to the spin,

S. The energy increases with increasing L as in the rotational spectrum, but the L scaling does not follow equation (4.25). Furthermore, we see the tendency that the energy increases with increasing S, contrary to the behaviour in ground states configurations for which Hund's rules state that the term with the largest possible value of S for a given configuration has lowest energy. Finally, the energy levels split up for different parity which is expected since different parity requires different configurations.

4.2.4 Expectation values of the radius

To complete this section we calculate expectation values of the radius which give an idea of the size of the system. In section 3.2.4 an expression for expectation values of the radius within the symmetric rotor model was derived. We found

$$\langle r \rangle_n^{LM_I \pi S} = \langle \Psi_R^{LM_I \pi S} | r | \Psi_R^{LM_I \pi S} \rangle$$
$$= \sum_{\bar{l}} \frac{1}{2Z} \left[3n^2 - l_1(l_1+1) \right] \sum_{\bar{\mu} \bar{m}_s} |c(\bar{l}\bar{\mu}\bar{m}_s, LMM_I\pi, SM_s)|^2 . \qquad (4.27)$$

This expression is also valid in the case of the four-electron rotor when the right expression for the wave function is used, namely equation (4.20). Table 4.4 lists the calculated expectation values of the radius within the $n = 3$ shell. We see a general tendency towards an increase in radius with the spin multiplicity, S, as suggested in the three-electron system. The predictions for the $^{2S+1}$G^o states are exceptions. This can, however, be explained by the fact that only one configuration is allowed by Pauli statistics for ^{5}G^o, namely spd^2. Therefore, the probability for one electron to have angular momentum equal to two, $P_{SR}(d)$, is much higher for ^{5}G^o than for ^{1}G^o and ^{3}G^o, as seen in table 4.3 page 65. According to equation (4.27) higher one-electron angular momenta lower the radius, which explains the deviance of the $^{2S+1}$G^o states. Finally, it is seen that the radii in general are lower than those within the $n = 3$ shell in Li listed in table 3.3 page 55. This is reasonable since the extra electron tends to reduce the screening effect causing each electron to feel

Table 4.4: The symmetric rotor expectation values of the radii, $\langle r \rangle_{n=3}^{LM_I \pi S}$, within the $n = 3$ shell in Be. In atomic units.

Term	$S = 0$	$S = 1$	$S = 2$
$^{2S+1}$S^o			3.17
$^{2S+1}$D^o	3.11	3.14	
$^{2S+1}$F^o		3.06	
$^{2S+1}$G^o	2.98	2.97	2.94
$^{2S+1}$P^e		3.18	
$^{2S+1}$D^e	3.18		
$^{2S+1}$F^e		3.04	3.05
$^{2S+1}$G^e	2.99	3.02	

Table 4.5: Expectation values of the radii for $^5S^o$ in atomic units (Z=4). SR denotes predictions within the symmetric rotor model, MCHF denotes multiconfigurational Hartree-Fock calculations [29].

	n=2	n=3	n=4	n=5	n=6
$\langle r \rangle_{SR}$	1.31	3.17	5.75	9.07	13.12
$\langle r \rangle_{MCHF}/\langle r \rangle_{SR}$	1.31	1.23	1.21	1.20	1.19

a larger effective nuclear charge. So, even though the inter-electronic repulsion is greater when four instead of three electrons are placed in the same shell, the mean radius is lower with four electrons.

Finally, table 4.5 displays the expectation values, $\langle r \rangle_n$, for different n for $^5S^o$. The second row lists the radii determined within the symmetric rotor model while the bottom row lists the ratio between the values predicted from the multiconfigurational Hartree-Fock calculations of reference [29] and the symmetric rotor predictions. The two calculations do not agree on the size of $\langle r \rangle$, but the scaling between different n is almost the same.

This chapter demonstrated that an extension of the three-electron symmetric rotor model to four-electron atoms was possible. Thus, an explicit analytical construction of quadruply excited intra-shell states has been made. An important difference between the three- and four-electron system is the spatial extent. In chapter 3 the original construction of the symmetric rotor wave function by Madsen and Mølmer was generalized to make an extension of the model possible. Therefore, it is now straightforward to consider six- and eight-electron systems as well. The four-electron symmetric rotor model yielded atomic state predictions in good agreement with the few existing *ab initio* calculations. In addition to valuable quantitative predictions, the model gives a simple physical image of quadruply excited states.

Chapter 5

Summary and conclusions

The development in atomic physics was immense in the previous century. The photoabsorption experiment in helium by Madden and Codling in 1963 triggered forty years of intense experimental as well as theoretical investigation in multiply excited states. The experimental breakthrough in the study of triply excited states was seen in the nineties and these highly-correlated systems have since been subject for many studies. In this century, atomic physicists are challenged by quadruply excited states which, until now, have only been subject for a few theoretical studies. However, due to the rapid development in modern laser spectroscopy, access to hollow beryllium is not expected to be a long-term goal.

The aim of this thesis was to contribute to the characterization and understanding of triply and quadruply excited states through theoretical models. Firstly, this goal was achieved by illustrating how symmetry considerations and group theory are useful for classifying atomic states. Thus, chapter 2 presented an apt method to classify atomic states independent of the model describing the dynamics of the system. In particular, the classification is valid for multiply excited states. The relative energies among states of different symmetry are on one hand determined by geometric symmetry and on the other hand by quantum-mechanical symmetry. As far as possible the system prefers the geometry which minimizes the potential energy, but inherent nodal surfaces arising from quantum-mechanical symmetry may impose restrictions on this preferred geometric configuration. The symmetry based classification method was seen to be very general and classification of six-valence-electron atoms was in this thesis presented for the first time.

Secondly, the symmetric rotor model describing multiply excited intra-shell states was presented in chapters 3 and 4. The explicit analytical constructions accounting for electron-electron correlations give simple physical images of the systems. The basic idea in the model is that the inter-electronic interactions tend to stabilize the electrons in individual Stark states and, in addition, the ansatz for the wave function is supplemented to take into account basic quantum symmetries. Besides providing a qualitative understanding of multiply excited states, the model yields predictions in good agreement with *ab initio* calculations. The thesis presented a generalization of the three-electron symmetric rotor model developed

by Madsen and Mølmer, and chapter 4 demonstrated the possibility of extending the model to four-electron systems. Since quadruply excited states is, as of yet, a practically undeveloped field of atomic physics the quantitative as well as the qualitative predictions in chapter 4 are of great value. The results of the two chapters are predictions of a number of characteristic atomic properties counting configuration-mixing fractions, l distributions, energies and mean radii. In particular, these predictions illustrate the high mixing between single-electron configurations due to the inter-electronic interaction. Furthermore, the importance of quantum-mechanical symmetries was demonstrated by comparing the l distribution predicted within the symmetric rotor model and from a simpler approach not taking these symmetries into account.

Rotational-like structure in the energy spectrum was discussed in connection with the symmetric rotor predictions. In conclusion, only a slight tendency towards such a structure is found in the energy spectrum of multiply excited intra-shell states. Contrary to molecules, rotational structure in atomic states is not due to rotational kinetic energy, but is a result of the electron-electron interaction. Actually, many-body systems in general can have rotational energy spectra if the particles are sufficiently well-localized in space, but the electrons in triply and quadruply excited atomic states were found not to fulfill this requirement. Consequently, we have to be careful with the interpretation of the geometrical picture of multiply excited intra-shell states. The atom does not behave like a rigid rotor even though the symmetric rotor model yields precise predictions of the atomic states.

Currently, several new synchrotron radiation sources are being developed throughout the world. These include the Linac Coherent Light Source at Stanford and the TESLA project in Hamburg which are notable projects on free electron lasers producing x-ray radiation expected to be many orders of magnitude brighter and temporally several orders of magnitude shorter than what can be produced by x-ray sources available today. Thus, the future is wide open for a range of new studies of atomic structures.

Appendix A

Representation theory of the permutation group

"Due to the fact that group theory, especially the theory of representations and characters of the permutation group, is extremely difficult even for the specialists, there arose the tendency of opposing the so-called 'group-pest' in quantum mechanics," Soklov(1956).

The purpose of this appendix is not to go through the complete theory of the permutation group. Firstly, it would be impossible and, secondly, it is unnecessary for the purpose of the thesis. The reader is expected to be familiar with the very basic theory of the permutation group, and the aim is only to sum up the principal results of the Young-Yamanouchi theory used in chapter 2. The content of this appendix is mainly based on references [20, 21, 22].

The close connection between a system of identical fermions and the permutation group, S_n, is simply that the Pauli principle requires the system to have permutation symmetry. The classification of the atomic states in this thesis relies on the claim that an antisymmetrized eigenstate of identical fermions in general be can expanded as

$$|\Psi^{LM\pi,SM_s}\rangle = \sum_i F_{M,i}^{L\pi S} \chi_{M_S,i}^S \, , \tag{A.1}$$

where the summation is over all possible couplings of intermediate spin. This expansion is possible in the so-called Young-Yamanouchi basis.

Let us consider the permutation group S_n. A *partition* is the splitting-up of n into a sum of integers, λ_i, satisfying

$$\lambda_1 + \lambda_2 + \cdots + \lambda_h = n \, , \qquad \lambda_1 \geq \lambda_2 \geq \cdots \geq \lambda_h \, . \tag{A.2}$$

The partitions of $n = 4$ are $[4], [3,1], [2,2] \equiv [2^2], [2,1,1] \equiv [2,1^2]$ and $[1,1,1,1] \equiv [1^4]$. A partition can be pictured as a *Young diagram* which is an arrangement of n cells in h rows; each row begins with the same vertical line and the number of cells in successive rows are $\lambda_1 \geq \lambda_2 \geq \cdots \geq \lambda_h$. The Young diagrams for $n = 4$ are

$$[4] \ \square\square\square\square \qquad [31] \ {\small\begin{array}{c}\square\square\square\\\square\end{array}} \qquad [22] \ {\small\begin{array}{c}\square\square\\\square\square\end{array}} \qquad [21^2] \ {\small\begin{array}{c}\square\square\\\square\\\square\end{array}} \qquad [1^4] \ {\small\begin{array}{c}\square\\\square\\\square\\\square\end{array}} \tag{A.3}$$

There is a one to one correspondence between the inequivalent irreducible representations of S_n and the partitions. In addition, the dimension of an irreducible representation is equal to the number of *Young tableaux* that can be constructed from the corresponding partition. A Young tableau is a Young diagram with the numbers $j = 1, 2 \ldots, n$ arranged in the cells such that the numbers increases as one moves to the right and one goes down. The Young tableaux for the partition [31] are

$$[31] \qquad \begin{smallmatrix}123\\4\end{smallmatrix} \qquad \begin{smallmatrix}124\\3\end{smallmatrix} \qquad \begin{smallmatrix}134\\2\end{smallmatrix} \tag{A.4}$$

The Young tableaux give the *Young-Yamanouchi basis vectors*, $Y_i^{[\lambda]}$. The wave function in equation (A.1) is expanded in the Young-Yamanouchi basis. Further insight in the basis functions is not necessary for the purpose of this thesis. However, the *Yamanouchi matrix elements* of the irreducible representations, $G_{ii'}^{[\lambda]}(P)$, are important.

An irreducible representation of S_n represented by a partition $[\lambda]$ is reducible with respect to its subgroup $S_{n-1} \subset S_n$. The result is that the representatives, $G^{[\lambda]}(P)$, of elements P belonging to the subgroup S_{n-1} are on block-diagonal form

$$G^{[\lambda_1 \ldots \lambda_j \ldots \lambda_h]}(P) = \sum_{j=h}^{1} \bigoplus G^{[\lambda_1 \ldots \lambda_j - 1 \ldots \lambda_h]}(P) , \qquad P \in S_{n-1} , \tag{A.5}$$

where the summation is restricted to partitions, which means $\lambda_j - 1 \geq \lambda_{j+1}$. As an example we consider the partition [42] of S_6

$$G^{[42]}(P) = \left(\begin{array}{c|c} G^{[41]}(P) & \\ \hline & G^{[32]}(P) \end{array} \right) , \qquad P \in S_5 . \tag{A.6}$$

Thus, the irreducible matrices of all elements of S_n can be found once those of the $n - 1$ generators of S_n, $(12), (23), \ldots, (n - 1, n)$, are known, since we in addition to equation (A.5) have the relations

$$(j, j + \nu) = (j + 1, j + \nu)(j, j + 1)(j + 1, j + \nu) , \tag{A.7}$$

$$(\alpha\beta\gamma\delta) = (\alpha\beta)(\beta\gamma)(\gamma\delta) . \tag{A.8}$$

There is a simple rule for finding the Yamanouchi matrix elements of the generators of S_n, $G_{ii'}^{[\lambda]}(j, j + 1) = \langle Y_i^{[\lambda]} | (j, j + 1) | Y_{i'}^{[\lambda]} \rangle$, $j = 1, \ldots, n - 1$. Consider the Young-Yamanouchi basis vectors $Y_i^{[\lambda]}$ and find the numbers j and $j+1$ in the corresponding Young tableau.

1. If j and $j + 1$ are in the same column/row of the Young tableau $Y_i^{[\lambda]}$ then

$$G_{ii'}^{[\lambda]}(j, j + 1) = \pm 1 \tag{A.9}$$

2. If j and $j + 1$ are neither in the same column nor the same row of the Young tableau $Y_i^{[\lambda]}$ then

$$G_{ii'}^{[\lambda]}(j, j + 1) = \begin{cases} 1/\sigma , & i' = i \\ -\sqrt{\sigma^2 - 1}/|\sigma| , & \text{when } Y_{i'}^{[\lambda]} = (j, j + 1)Y_i^{[\lambda]} \\ 0 & \text{otherwise} , \end{cases} \tag{A.10}$$

where σ is the axial distance given by

$$\sigma = r_{j+1} - r_j - (c_{j+1} - c_j) \,, \tag{A.11}$$

with $r_j, r_{j+1}(c_j, c_{j+1})$ being row(column) numbers of j and $j+1$ in the Young tableau $Y_i^{[\lambda]}$.

The phase convention varies from textbook to textbook, the one used here is in agreement with the tables in reference [20].

Let us consider the case of four electrons with total spin $S = 1$. First we have to find a partition corresponding to $S = 1$, which can be done with the formula

$$S = \frac{1}{2}(\lambda_1 - \lambda_2) \,, \tag{A.12}$$

with $\lambda_1 + \lambda_2$ equal to the number of electrons. In the case of $n = 4$ and $S = 1$ we see that the partition [31] fulfills the requirements. To find $G^{[31]}(34)$ we consider the Young tableaux in equation (A.4) and use equation (A.9) and (A.10)

$$G_{11}^{[31]}(34) = \langle {}^{123}_4|(34)|{}^{123}_4\rangle = \frac{1}{3} \,, \tag{A.13}$$

$$G_{12}^{[31]}(34) = \langle {}^{123}_4|(34)|{}^{124}_3\rangle = -\frac{\sqrt{8}}{3} \,, \tag{A.14}$$

$$G_{13}^{[31]}(34) = \langle {}^{123}_4|(34)|{}^{134}_2\rangle = 0 \,, \tag{A.15}$$

$$G_{22}^{[31]}(34) = \langle {}^{124}_3|(34)|{}^{124}_3\rangle = -\frac{1}{3} \,, \tag{A.16}$$

$$G_{23}^{[31]}(34) = \langle {}^{124}_3|(34)|{}^{134}_2\rangle = 0 \,, \tag{A.17}$$

$$G_{33}^{[31]}(34) = \langle {}^{134}_2|(34)|{}^{134}_2\rangle = -1 \,. \tag{A.18}$$

Since the Yamanouchi matrices are symmetric, it is enough to determine the elements of the upper triangles.

A.1   Yamanouchi matrices

With the given prescription, all Yamanouchi matrix elements can be found as demonstrated. However, for easy reference the matrices for the generators $(n-1, n)$ of S_2, S_3, S_4, S_5 and S_6 are listed here [1]. When these are given the rest can easily be found using (A.6)-(A.8).

S_2

$$G^0(\mathbf{P}(12)) = (1) \tag{A.19}$$

$$G^1(\mathbf{P}(12)) = (-1) \tag{A.20}$$

---

[1]The Yamanouchi matrix elements for $S_2 - S_5$ and some of those for S_6 are adopted from reference [20]. The remainder for S_6 is derived by hand using the prescription in this appendix.

S_3

$$G^{3/2}(\mathbf{P}(23)) = (-1) \tag{A.21}$$

$$G^{1/2}(\mathbf{P}(23)) = \begin{pmatrix} \frac{1}{2} & -\frac{\sqrt{3}}{2} \\ -\frac{\sqrt{3}}{2} & -\frac{1}{2} \end{pmatrix} \tag{A.22}$$

S_4

$$G^{2}(\mathbf{P}(34)) = (-1) \tag{A.23}$$

$$G^{1}(\mathbf{P}(34)) = \begin{pmatrix} \frac{1}{3} & -\frac{2\sqrt{2}}{3} & 0 \\ -\frac{2\sqrt{2}}{3} & -\frac{1}{3} & 0 \\ 0 & 0 & -1 \end{pmatrix} \tag{A.24}$$

$$G^{0}(\mathbf{P}(34)) = \begin{pmatrix} -1 & 0 \\ 0 & 1 \end{pmatrix} \tag{A.25}$$

S_5

$$G^{3/2}(\mathbf{P}(45)) = (-1) \tag{A.26}$$

$$G^{3/2}(\mathbf{P}(45)) = \begin{pmatrix} \frac{1}{4} & -\frac{\sqrt{15}}{4} & 0 & 0 \\ -\frac{\sqrt{15}}{4} & -\frac{1}{4} & 0 & 0 \\ 0 & 0 & -1 & 0 \\ 0 & 0 & 0 & -1 \end{pmatrix} \tag{A.27}$$

$$G^{1/2}(\mathbf{P}(45)) = \begin{pmatrix} -1 & 0 & 0 & 0 & 0 \\ 0 & \frac{1}{2} & 0 & -\frac{\sqrt{3}}{2} & 0 \\ 0 & 0 & \frac{1}{2} & 0 & -\frac{\sqrt{3}}{2} \\ 0 & -\frac{\sqrt{3}}{2} & 0 & -\frac{1}{2} & 0 \\ 0 & 0 & -\frac{\sqrt{3}}{2} & 0 & -\frac{1}{2} \end{pmatrix} \tag{A.28}$$

S_6

$$G^{3}(\mathbf{P}(56)) = (-1) \tag{A.29}$$

$$G^{2}(\mathbf{P}(56)) = \begin{pmatrix} \frac{1}{5} & -\frac{\sqrt{24}}{5} & 0 & 0 & 0 \\ -\frac{\sqrt{24}}{5} & -\frac{1}{5} & 0 & 0 & 0 \\ 0 & 0 & -1 & 0 & 0 \\ 0 & 0 & 0 & -1 & 0 \\ 0 & 0 & 0 & 0 & -1 \end{pmatrix} \tag{A.30}$$

$$G^1(\mathbf{P}(56)) = \begin{pmatrix} -1 & 0 & 0 & 0 & 0 & 0 & 0 & 0 & 0 \\ 0 & \frac{1}{3} & 0 & 0 & -\frac{2\sqrt{2}}{3} & 0 & 0 & 0 & 0 \\ 0 & 0 & \frac{1}{3} & 0 & 0 & -\frac{2\sqrt{2}}{3} & 0 & 0 & 0 \\ 0 & 0 & 0 & \frac{1}{3} & 0 & 0 & -\frac{2\sqrt{2}}{3} & 0 & 0 \\ 0 & -\frac{2\sqrt{2}}{3} & 0 & 0 & -\frac{1}{3} & 0 & 0 & 0 & 0 \\ 0 & 0 & -\frac{2\sqrt{2}}{3} & 0 & 0 & -\frac{1}{3} & 0 & 0 & 0 \\ 0 & 0 & 0 & -\frac{2\sqrt{2}}{3} & 0 & 0 & -\frac{1}{3} & 0 & 0 \\ 0 & 0 & 0 & 0 & 0 & 0 & 0 & -1 & 0 \\ 0 & 0 & 0 & 0 & 0 & 0 & 0 & 0 & -1 \end{pmatrix}$$

(A.31)

$$G^0(\mathbf{P}(56)) = \begin{pmatrix} -1 & 0 & 0 & 0 & 0 \\ 0 & -1 & 0 & 0 & 0 \\ 0 & 0 & -1 & 0 & 0 \\ 0 & 0 & 0 & 1 & 0 \\ 0 & 0 & 0 & 0 & 1 \end{pmatrix}$$

(A.32)

Appendix B

Computer programs used in classifying atomic states

A consistent linear system is analytically solvable. For large systems it is, however, a difficult task to keep track of all the unknown variables. This appendix deals with the computer programs used in classifying atoms with four and six valence electrons. The programs are all written in Matlab 6.5.

B.1 Four-valence-electron atoms: Triplet states

The program classifying the four-valence-electron atoms with total spin $S = 1$ is seen in the end of this section. The running time is about 0.2 s. The program consists of the following routines which must be stored in the same directory:

clas41.m is the main program called by clas41(L, π). The function determines whether the term, ${}^3L^\pi$, is RTH-accessible and calculates the coefficients $F_{M_I i}$. The input parameter L has to be a positive integer less or equal to four. The program can be adjusted to accept larger values of L. The output is a statement which tell whether the term, ${}^3L^\pi$, is RTH-accessible or RTH-inaccessible. If the state is RTH-accessible the nontrivial solution space is found, and the coefficients are ordered in vectors, $\bar{F}_i = \begin{pmatrix} F_{-Li} \\ \vdots \\ F_{Li} \end{pmatrix}$, and given as output. Furthermore, the squared coefficients, $|F_{M_I i}|^2$, are given as rational numbers determined with the Matlab function rats which uses a continued fraction algorithm to approximate floating-point values by ratios of small integers. In this way both the signs and fractions in table 2.4 page 24 are determined. clas41.m calls the function B_elem.m.

B_elem.m called by B_elem(L) arranging the matrix elements, $B^L_{M_I M'_I}$, in equation (2.55) in a square matrix of size $2L+1$. B_elem.m calls the subroutine blqp.m.

blqp.m called by blqp(L, M_I, M'_I) calculates the matrix elements, $B^L_{M_I M'_I}$, in equa-

tion (2.55). hlqp.m loads the matrix wrot_mw2 calculated with wrot_mw2.m.

wrot_mw2.m calculates the Wigner functions $d^l_{mn}\left(2\arccos\left(\frac{1}{\sqrt{3}}\right)\right)$ and arranges them in a square matrix denoted wrot_mw2. A variable, s, determines the number of Wigner functions to be calculated by $l < $ s. wrot_mw2.m calls the function rot.m.

rot.m called by $rot(l,m,n,a)$ calculates the Wigner functions $d^l_{mn}(a)$. These are calculated by using formula (3.66) given in reference [23].

Computer program: Classification N=4, S=1

Contents

- function clas41=clas41(L,p)
- function B_elem=B_elem(L)
- function blqp=blqp(L,q,p)
- wrot_mw2.m
- function rot=rot(j,m,w,a)

function clas41=clas41(L,p)

```
v0=[1;0;0];
v1=[0;1;-i];
v2=[0;1;i];

G=[-2, -2*sqrt(2), 2*sqrt(6); -2*sqrt(2), 5, sqrt(3); ...
    -2*sqrt(6), -sqrt(3), -3]/6; %G(124)
B=B_elem(L);

A=zeros(3*(L+1),L+1);
for y=1:L+1 %All positive values of MI
    A(3*(y-1)+1:3*y,1)=G*(0.5*(-p*(-1)^L+1)*B(L+y,L+1)*v0);
    A(3*(y-1)+1:3*y,2)=G*(p*(-1)^L*B(L+y,L)*v2+B(L+y,L+2)*v1);
    if L>1
        A(3*(y-1)+1:3*y,3)=G*(-p*(-1)^L*B(L+y,L-1)*v1+B(L+y,L+3)*v2);
    end
    if L>2
        A(3*(y-1)+1:3*y,4)=G*(p*(-1)^L*B(L+y,L-2)*v0+B(L+y,L+4)*v0);
    end
    if L>3
        A(3*(y-1)+1:3*y,5)=G*(-p*(-1)^L*B(L+y,L-3)*v2+B(L+y,L+5)*v1);
    end
end
```

```
d=zeros(3,1);

if L==1
    H=[v0,d; d,v1];
end
if L==2
    H=[v0,d,d; d,v1,d; d,d,v2];
end
if L==3
    H=[v0,d,d,d; d,v1,d,d; d,d,v2,d; d,d,d,v0];
end
if L==4
    H=[v0,d,d,d,d; d,v1,d,d,d; d,d,v2,d,d; d,d,d,v0,d; d,d,d,d,v1];
end

S=A-H; %The homogeneous system to be solved

if size(null(S))>0
    display('RTH-accessible')

    F=null(S,'r'); %The elements in F are F_01 F_12 F_22 F_31 F_42

    %Ordering the output

    %i=1
    F_01=F(1);
    if L>2
        F_31=F(4);
    else
        F_31=0;
    end

    %i=2
    F_12=F(2);
    if L>1
        F_22=F(3);
    else
        F_22=0;
    end
    if L>3
        F_42=F(5);
    else
        F_42=0;
```

```
    end

    %i=3
    F_13=-i*F_12;
    F_23=i*F_22;
    F_43=-i*F_42;

    if L==1
        F_M1=[0; F_01; 0];
        F_M2=[p*(-1)^L*F_12; 0; F_12];
        F_M3=[-p*(-1)^L*F_13; 0; F_13];
    end
    if L==2
        F_M1=[0; 0; F_01; 0; 0];
        F_M2=[-p*(-1)^L*F_22; p*(-1)^L*F_12; 0; F_12; F_22];
        F_M3=[p*(-1)^L*F_23; -p*(-1)^L*F_13; 0; F_13; F_23];
    end
    if L==3
        F_M1=[p*(-1)^L*F_31; 0; 0; F_01; 0; 0; F_31];
        F_M2=[0; -p*(-1)^L*F_22; p*(-1)^L*F_12; 0; F_12; F_22; 0];
        F_M3=[0; p*(-1)^L*F_23; -p*(-1)^L*F_13; 0; F_13; F_23; 0];
    end
    if L==4
        F_M1=[0; p*(-1)^L*F_31; 0; 0; F_01; 0; 0; F_31; 0];
        F_M2=[-p*(-1)^L*F_42; 0; -p*(-1)^L*F_22; p*(-1)^L*F_12; 0; ...
                F_12; F_22; 0; F_42];
        F_M3=[p*(-1)^L*F_43; 0; p*(-1)^L*F_23; -p*(-1)^L*F_13; 0; ...
                F_13; F_23; 0; F_43];
    end

    N1=sqrt(sum(abs(F_M1).^2));
    N2=sqrt(sum(abs(F_M2).^2));
    N3=sqrt(sum(abs(F_M3).^2));

    F_M1=F_M1/N1 %Normalization
    F_M1_2rat=rats(abs(F_M1).^2)
    F_M2=F_M2/N2
    F_M2_2rat=rats(abs(F_M2).^2)
    F_M3=F_M3/N3
    F_M3_2rat=rats(abs(F_M3).^2)

else
    display('RTH-inaccessible')
end
```

function B_elem=B_elem(L)

```
A=zeros(2*L+1,2*L+1);

for x=-L:L
    for y=-L:L
        i=L+1+x;
        j=L+1+y;
        A(i,j)=blqp(L,x,y);
    end
end

B_elem=A;
```

function blqp=blqp(L,q,p)

```
load wrot_mw2 wrot_mw2;

cp=complex(0,2*pi/3);
y=0;

for x=-L:L
    k=(L+1)*L+x+1;
    h=(L+1)*L+q+1;
    g=(L+1)*L+p+1;
    y=y+wrot_mw2(k,h)*wrot_mw2(k,g)*exp(-cp*x);
end

blqp=y;
```

wrot_mw2.m

```
%Wigner functions arranged in a suitable matrix

s=7; %li<s;
wrot_mw2=zeros(s^2,s^2);

for A=0:s-1
    for a=-A:A
        for b=-A:A
            k=(A+1)*A+a+1;
            h=(A+1)*A+b+1;
            wrot_mw2(k,h)=rot(A,a,b,2*acos(1/sqrt(3)));
        end
    end
```

```
end

save wrot_mw2 wrot_mw2;


function rot=rot(j,m,w,a)

f1=0; for k=max([0,w-m]):min([j-m,j+w])
     t1=prod(1:j-m-k);
     t2=prod(1:j+w-k);
     t3=prod(1:k+m-w);
     t4=prod(1:k);
     t5=(cos(a/2))^(2*j+w-m-2*k);
     t6=(-sin(a/2))^(m-w+2*k);
     f1=f1+(-1)^k*t5*t6/(t1*t2*t3*t4);
end;


g1=prod(1:j+w);
g2=prod(1:j-w);
g3=prod(1:j+m);
g4=prod(1:j-m);


if abs(m)>j | abs(w)>j
   rot=0;
else
   rot=sqrt(g1*g2*g3*g4)*f1;
end;
```

B.2   Six-valence-electron atoms

The program classifying the six-valence-electron atoms seen in the end of this section consists of the following routines which must be stored in the same directory:

clas6.m is the main program called by clas6(S, L, π). The output of the function is a statement which tell whether the term, $^{2S+1}L^\pi$, is ROH-accessible or ROH-inaccessible. The program finds the nullity of the matrices in equations (2.98) and (2.101), arranges the solution spaces in the matrices F and K and, finally, intersects the two solution spaces. clas6.m calls the function H_elem.m and loads data in the files mat61.mat, mat62.mat and mat63.mat. The running time for clas6.m is about 0.1 s.

mat61.mat, mat62.mat, mat63.mat are files with the permutation matrices **A**, **B**, **C** and **D** in equations (2.89)-(2.92). These are determined from the permutation matrices listed in appendix A and equations (A.5), (A.7) and (A.8).

H_elem.m called by H_elem(L) arranges the elements, $H^L_{M_I M'_I}$, in equation (2.88) in a square matrix of size $2L + 1$. H_elem.m calls the subroutine hlqp.m.

hlqp.m called by hlqp(L, q, p) calculates the elements, $H^L_{M_I M'_I}$, in equation (2.88), which apart from an angle, are similar to the elements, $B^L_{M_I M'_I}$, in equation (2.55). Therefore, hlqp.m is analogous to blqp.m apart from loading the matrix wrot_mw calculated with wrot_mw.m instead of wrot_mw2.

wrot_mw.m calculates the Wigner functions $d^l_{mn}\left(\arccos\left(\frac{1}{\sqrt{3}}\right)\right)$ and arranges them in a square matrix denoted wrot_mw. The variable, s, determines the number of Wigner functions to be calculated by $l < $ s. wrot_mw.m calls the function rot.m which is described and printed in previous section.

Computer program: Classification N=6

Contents

- function clas6=clas6(S,L,p)
- function H_elem=H_elem(L)
- function hlqp=hlqp(L,q,p)
- wrot_mw.m

function clas6=clas6(S,L,p)

```
if S==0
    load mat60 A B C D;
end
if S==1
    load mat61 A B C D;
end
if S==2
    load mat62 A B C D;
end
if S==3
    A=-1;
    B=-1;
    C=-1;
    D=1;
end

d=size(A); dimS=d(1);
F=zeros(dimS*(2*L+1),dimS*(2*L+1));
```

```
%Solution to the equations arising from Oj and Ok

for y=1:dimS:dimS*(2*L+1)
    x=y-1+dimS;
    Q=(y-1)/dimS-L;
    v=complex(0,pi/2*mod(Q,4));
    if abs(v)<0.0000001
        v=0;
    end
    if sum(sum(abs([p*A-eye(dimS);exp(v)*B-eye(dimS)])))<00000.1
        F(y:y+dimS-1,y:y+dimS-1)=eye(dimS);
    elseif size(null([p*A-eye(dimS);exp(v)*B-eye(dimS)]))>0
        g=size(null([p*A-eye(dimS);exp(v)*B-eye(dimS)]));
        F(y:y+dimS-1,y:y+g(2)-1)=null([p*A-eye(dimS);exp(v)*B-eye(dimS)]);
    else
        F(y:y+dimS-1,y:y+dimS-1)=zeros(dimS,dimS);
    end
end

%Solution to the equations arising from Ol and Om

M=zeros(2*L+1,2*L+1); for y=1:2*L+1
    for k=1:2*L+1
        Qy=y-(L+1);
        Qk=k-(L+1);
        if Qy==-Qk
            M(y,k)=(-1)^(L+Qy);
        end
    end
end

H=H_elem(L);

N=null([kron(M,C)-eye((2*L+1)*dimS);kron(H,D)-eye((2*L+1)*dimS)]);

%Intersection of the two solutions

K=[F N];
[m,n]=size(K);
for t=1:n
    if K(:,n-t+1)==zeros(m,1)
        K(:,n-t+1)=[];
    end
end
```

```
[m,n]=size(K);
if n>0
    W=null(K);
    [mW,nW]=size(W);
    if nW>0
        disp('ROH-accessible');
    else
        disp('ROH-inaccessible (no nontrivial solution)');
    end
else
    disp('ROH-inaccessible (no nontrivial solution)');
end


function H_elem=H_elem(L)

A=zeros(2*L+1,2*L+1);

for x=-L:L
    for y=-L:L
        i=L+1+x;
        j=L+1+y;
        A(i,j)=hlqq(L,x,y);
    end
end

H_elem=A;


function hlqp=hlqp(L,q,p)

load wrot_mw wrot_mw;

cp=complex(0,2*pi/3);
y=0;

for x=-L:L
    k=(L+1)*L+x+1;
    h=(L+1)*L+q+1;
    g=(L+1)*L+p+1;
    y=y+wrot_mw(k,h)*wrot_mw(k,g)*exp(-cp*x);
end

hlqp=y;
```

wrot_mw.m

```
%Wigner functions arranged in a suitable matrix

s=7; %l<s;
wrot_mw=zeros(s^2,s^2);

for A=0:s-1
    for a=-A:A
        for b=-A:A
            k=(A+1)*A+a+1;
            h=(A+1)*A+b+1;
            wrot_mw(k,h)=rot(A,a,b,acos(1/sqrt(3)));
        end
    end
end

save wrot_mw wrot_mw;
```

Appendix C

Computer programs used in making symmetric rotor predictions

This appendix presents some of the computer programs used in making predictions within the symmetric rotor model. The model gives analytical expressions for the wave functions, configuration-mixing fractions, l distributions, energies and mean radii and, therefore, all atomic states predictions can in principle be calculated with paper and pencil. However, the expressions arise from a model and it is therefore pointless to make predictions with infinite decimals. Furthermore, the calculations are so demanding that paper and pencil work is far too time-consuming. Actually, the running times for the computer programs turn out to be quite long due to the many summations. Typical running times are given in the end of the first section. The programs for the three-electron symmetric rotor are simpler but otherwise analogous to the four-electron case. The running time increases considerably with the number of summations and is therefore more than a factor of ten larger for the four-electron system than for the three-electron system. This appendix presents most of the programs to make predictions within the four-electron symmetric rotor model and thus illustrates the ideas in the programs in general.

The general routines to be presented accept quantum numbers for all terms, $^{2S+1}L^\pi$. For quintet states the wave function splits up into a product of a spatial part and a spin part, and it is therefore advantageous to use simplified programs which do not include spin. The running time is thereby reduced by more than a factor of ten and, consequently, demanding calculations can be done within a reasonable time frame.

C.1   Description of four-electron rotor programs

The program used to calculate expansion coefficients in the wave function, l distributions, energies and mean radii within the four-electron symmetric rotor model is

printed in next section (for-loops are squeezed a little to save space). The program written in Matlab 6.5 consists of the following routines which must be stored in the same directory:

rotor4.m is the main program called by rotor4($n, L, M_I, \pi, S, S_{12}, S_{34}$). The input variables are the quantum numbers specifying the state. The output is independent of the intermediate spins, S_{12} and S_{34}, as long as $\vec{S} = \vec{S_{12}} + \vec{S_{34}}$ and the spin coupling is compatible with the value of M_I. Tables 2.3-2.5 in section 2.4.2 give the relation between the allowed values of M_I and the intermediate spins. The program has been tested for quantum numbers up to $n = 6$.
The output of the function is

> N: Normalization constant. The term is ETH-inaccessible if N is zero.
> P_s, P_p, ..., P_i: l distribution, $P_{SR}(l)$, given in equation (4.23).
> radius: Mean radius, $\langle r \rangle_n^{LM_I\pi S}$, given in equation (4.27).
> energy: Energy, $E_n^{LM_I\pi S}$, given in equation (4.26).

rotor.m calculates the expansion coefficients, $c(\bar{l}\bar{\mu}\bar{m}_s, LMM_I\pi, SM_s)$, in the symmetric rotor wave function in equation (4.20). The coefficients are ordered in a four dimensional array according to the basis $|l_1\mu_1m_{s1}l_2\mu_2m_{s2}l_3\mu_3m_{s3}l_4\mu_4m_{s4}\rangle$ and the wave function is properly antisymmetrized and normalized. Furthermore, the l distribution is determined, and the function calls the functions mr.m and energy4.m to determine the mean radius and the energy. These calls do not have to be included. The running time for energy4 is quite long and it is therefore advantagous to omit this call. Furthermore, the function, rotor4, calls the subroutines b_elem4.m and spin4.m. Finally, data are loaded from the files ClGh.mat and wrot_4e.mat. ClGh is a matrix with Clebsch Gordon coefficients ordered as follows; $\langle AaBb|Cc \rangle = \text{ClGh}(2A(A+1)+a+1, 2B(B+1)+b+1, 2C(C+1)+c+1)$. These coefficients are calculated with the program clebsch.m [45], which is not printed here. The dimension of ClGh sets the upper limit for the input variable n and can be adjusted. wrot_4e is a vector with the Wigner functions, $d_{m0}^l\left(2\arccos(\frac{1}{\sqrt{3}})\right)$, calculated with a program analogous to wrot_mw.m and wrot_mw2.m described in appendix B. Both ClGh and wrot_4e are defined to be global variables which means that assignment to these variables is available to all the functions declaring them global.

b_elem4.m called by b_elem4($n, l_1, l_2, l_3, l_4, \mu_1, \mu_2, \mu_3, \mu_4, L, M, M_I, \pi$) is a spin independent function calculating the spatial part of the expansion coefficients, $b(\bar{l}\bar{\mu}; LMM_I\pi)$, given in equations (4.10) and (4.14). b_elem4.m calls i_elem4.m and a_elem4.m.

i_elem4.m called by i_elem4($l_1, l_2, l_3, l_4, m_1, m_2, m_3, m_4, \mu_1, \mu_2, \mu_3, \mu_4, L, M, M_I$) calculates the elements, $I(\bar{l}\bar{m}\bar{\mu}; LMM_I)$, in equation (4.12).

a_elem4.m called by a_elem4($n, l_1, l_2, l_3, l_4, m_1, m_2, m_3, m_4$) calculates the elements,

$a(\bar{l}\bar{m})$, in equation (4.11).

spin4.m called by spin4($S, M_S, S_{12}, S_{34}, m_{s1}, m_{s2}, m_{s3}, m_{s4}$) calculates the spin function, $|\chi_{M_s}^{S_{12}S_{34}S}\rangle$, in equation (4.15).

radius.m called by mr(C) calculates the mean radius, $\langle r \rangle_n^{LM_I\pi S}$, given in equation (4.27). The input variable, C, is a matrix determined by rotor4.m containing squared absolute values of the expansion coefficients, $|c(\bar{l}\bar{\mu}\bar{m}_s, LMM_I\pi, SM_s)|^2$. A variable, Z, specifying the nuclear charge can be changed if beryllium-like ions are considered. Furthermore, the program can be adjusted to be able to calculate the radius for principal quantum numbers higher than $n = 6$.

energy4.m called by energy4(A) returns the term, $\left\langle \Psi_R^{LM_I\pi S} \left| \frac{1}{r_{12}} \right| \Psi_R^{LM_I\pi S} \right\rangle$, in equation (4.26). The energy is determined as $E_n^{LM_I\pi S} = \left[-\frac{1}{2}\frac{Z^2}{n^2}N + Z \cdot cor \sum_{i=1}^{N-1} i \right]$, with Z denoting the nuclear charge, N the number of electrons ($N = 4$ for beryllium-like ions) and $cor = \left\langle \Psi_R^{LM_I\pi S} \left| \frac{1}{r_{12}} \right| \Psi_R^{LM_I\pi S} \right\rangle$. The input variable, A, is a matrix determined by rotor4.m containing the expansion coefficients, $c(\bar{l}\bar{\mu}\bar{m}_s, LMM_I\pi, SM_s)$. For quintet states when the electronic spin does not have to be included in the for-loops the program is slightly different but analogous. The function loads data in the file En_mat.mat. The programs to calculate these data are described below.

En_mat.m arranges the terms, $\frac{4\pi}{2k+1}R_k(l_{a1}l_{b1}l_{a2}l_{b2})(-1)^q\langle Y_{l_{a1}\mu_{a1}}|Y_{k-q}|Y_{l_{b1}\mu_{b1}}\rangle \times \langle Y_{l_{a2}\mu_{a2}}|Y_{kq}|Y_{l_{b2}\mu_{b2}}\rangle$, in equation (3.62) in the matrix En_mat. En_mat.m calls the function K.m

K.m called by K($n, l_{a1}, m_{a1}, l_{a2}, m_{a2}, l_{b1}, m_{b1}, l_{b2}, m_{b2}, k, q$) calculates the term, $\frac{4\pi}{2k+1}R_k(l_{a1}l_{b1}l_{a2}l_{b2})(-1)^q\langle Y_{l_{a1}\mu_{a1}}|Y_{k-q}|Y_{l_{b1}\mu_{b1}}\rangle\langle Y_{l_{a2}\mu_{a2}}|Y_{kq}|Y_{l_{b2}\mu_{b2}}\rangle$, in equation (3.62). K.m uses the Matlab function dblquad to evaluate double integrals numerically. dblquad(@fun, $x_{min}, x_{max}, y_{min}, y_{max}$, tol, method, $p1, p2, ...$) evaluates the double integral fun(x, y) over the rectangle $x_{min} \le x \le x_{max}$, $y_{min} \le y \le y_{max}$. The function fun($x, y$) must accept a vector x and a scalar y and return a vector of values of the integrand. The variable, tol, specifies the tolerance with 1.0e-6 being default, and the variable, method, specifies the integration method with [] denoting default. Finally, $p1, p2, ...$ pass extra parameters to fun($x, y, p1, p2, ...$). In addition, K.m calls the functions r_int.m and gaunt.m

r_int.m called by r_int($r_1, r_2, n, l_{a1}, l_{a2}, l_{b1}, l_{b2}, k$) returns a vector with values of the function to be integrated in equation (3.63). The input variable r_1 has to be a vector while r_2 has to be a scalar. r_int.m calls radf.m.

radf.m called by radf(r, n, l) returns the value of the radial function, $R_{nl}(r)$, in r.

radf.m calls the function laguerre.m.

laguerre.m called by laguerre(v, a, x) returns the generalized Laguerre function, $L_v^a(x)$ [46, equation 22.3.9]. laguerre.m calls the function bino.m.

bino.m called by bino(n,k) calculates the binomial coefficient $\binom{n}{k}$.

gaunt.m called by gaunt$(l_a, \mu_a, k, q, l_b, \mu_b)$ returns the matrix element, $\langle Y_{l_a \mu_a} | Y_{kq} | Y_{l_b \mu_b} \rangle$, given in equation (3.64). gaunt.m calls the function clebsch.m not printed here.

C.1.1 Typical running times on a Intel Pentium 4, 2.67 GHz with 512 MB RAM

The running time for rotor4 with energy4 omitted varies with n, the typical time is about 40 s for $n = 2$, 825 s for $n = 3$ and 15,500 s (or 4.3 hours) for $n = 4$. Just to load ClGh adjusted to $n = 6$ takes about 30 s, since the size of the file ClGh.mat in this case is no less than 261 MB. The running time to calculate ClGh is then about two hours. The running time for energy4 is about 2,650 s for $n = 3$. To calculate the data in the file En_mat.mat requires about 8 hours when En_mat is adjusted to be useful for $n = 2$ and $n = 3$. The running time for a program analogous to rotor4 for quintet states varies from about 30 s for $n = 2$ to about 19 hours for $n = 6$. The time to calculate the energy is not different for quintet states. Finally, the running time for the equivalent three-electron program, rotor3, is about 30 s for $n = 2$ and 75 s for $n = 3$.

C.2 Computer programs: Four-electron atomic states

C.2.1 Main program, rotor4.m, and subroutines

Contents

- function rotor4=rotor4(n,L,MI,p,S,S12,S34)
- function b_elem4=b_elem4(n,l1,l2,l3,l4,w1,w2,w3,w4,L,M,MI,p)
- function i_elem4=i_elem4(l1,l2,l3,l4,m1,m2,m3,m4,w1,w2,w3,w4,L,M,MI)
- function a_elem4=a_elem4(n,l1,l2,l3,l4,m1,m2,m3,m4)
- function spin4=spin4(S,MS,S12,S34,s1,s2,s3,s4)
- function radius=mr(C)
- function energy4=energy4(A);

function rotor4=rotor4(n,L,MI,p,S,S12,S34)

```
load ClGh ClGh
global CGh;
```

```
CGh=ClGh;
load wrot_4e wrot_4e
global wr;
wr=wrot_4e;

M=0;
MS=S;

R=zeros(2*n^2,2*n^2,2*n^2,2*n^2); %4D array
for l1=0:n-1
for m1=-l1:l1
for l2=0:n-1
for m2=-l2:l2
for l3=0:n-1
for m3=-l3:l3
for l4=0:n-1
for m4=-l4:l4
for s1=-0.5:0.5 %ms for the first electron
for s2=-0.5:0.5
for s3=-0.5:0.5
for s4=-0.5:0.5
    x=2*((l1+1)*l1+m1+1)+s1-0.5;
    y=2*((l2+1)*l2+m2+1)+s2-0.5;
    z=2*((l3+1)*l3+m3+1)+s3-0.5;
    q=2*((l4+1)*l4+m4+1)+s4-0.5;
    R(x,y,z,q)=b_elem4(n,l1,l2,l3,l4,m1,m2,m3,m4,L,M,MI,p)...
        *spin4(S,MS,S12,S34,s1,s2,s3,s4);
    %Permutation of two particles (6 uneven operations)
    p12_R(y,x,z,q)=R(x,y,z,q);
    p13_R(z,y,x,q)=R(x,y,z,q);
    p14_R(q,y,z,x)=R(x,y,z,q);
    p23_R(x,z,y,q)=R(x,y,z,q);
    p24_R(x,q,z,y)=R(x,y,z,q);
    p34_R(x,y,q,z)=R(x,y,z,q);
    %Permutation of two + two particles (3 even operations)
    p_12_34_R(y,x,q,z)=R(x,y,z,q);
    p_13_24_R(z,q,x,y)=R(x,y,z,q);
    p_14_23_R(q,z,y,x)=R(x,y,z,q);
    %Cyclic permutation of three particles (8 even operations)
    c123_R(z,x,y,q)=R(x,y,z,q);
    c132_R(y,z,x,q)=R(x,y,z,q);
    c124_R(q,x,z,y)=R(x,y,z,q);
    c142_R(y,q,z,x)=R(x,y,z,q);
    c134_R(q,y,x,z)=R(x,y,z,q);
```

```
    c143_R(z,y,q,x)=R(x,y,z,q);
    c234_R(x,q,y,z)=R(x,y,z,q);
    c243_R(x,z,q,y)=R(x,y,z,q);
    %Cyclic permutation of four particles (6 uneven operations)
    c1234_R(q,x,y,z)=R(x,y,z,q);
    c1243_R(z,x,q,y)=R(x,y,z,q);
    c1324_R(q,z,x,y)=R(x,y,z,q);
    c1342_R(y,q,x,z)=R(x,y,z,q);
    c1423_R(z,q,y,x)=R(x,y,z,q);
    c1432_R(y,z,q,x)=R(x,y,z,q);
end end end end end end end end end end end end

Anti=R... %Antisymmetrizing
    -p12_R-p13_R-p14_R-p23_R-p24_R-p34_R...
    +p_12_34_R+p_13_24_R+p_14_23_R...
    +c123_R+c132_R+c124_R+c142_R+c134_R+c143_R+c234_R+c243_R...
    -c1234_R-c1243_R-c1324_R-c1342_R-c1423_R-c1432_R;

%Probabilities ordered according to the basis: |l1m1 l2m2 l3m3 l4m4>
%i.e. disregarding the electronic spin
C=zeros(n^2,n^2,n^2,n^2);
for a=1:n^2
for b=1:n^2
for c=1:n^2
for d=1:n^2
for e=-1:0
for f=-1:0
for g=-1:0
for h=-1:0
    C(a,b,c,d)=C(a,b,c,d)+abs(Anti(2*a+e,2*b+f,2*c+g,2*d+h))^2;
end end end end end end end end

N=sum(sum(sum(sum(C))))
A=Anti/sqrt(N);
C=C/N; %Normalizing
T=sum(sum(sum(C)));
%The elements in T are the probabilities for one |nlm> electron

%l distribution
P_s=T(:,:,1,1) P_p=T(:,:,1,2)+T(:,:,1,3)+T(:,:,1,4)
if n>2
    P_d=T(:,:,1,5)+T(:,:,1,6)+T(:,:,1,7)+T(:,:,1,8)+T(:,:,1,9)
else
    P_d=0
```

```
end
if n>3
    P_f=T(:,:,1,10)+T(:,:,1,11)+T(:,:,1,12)+T(:,:,1,13)+T(:,:,1,14)+...
        T(:,:,1,15)+T(:,:,1,16)
else
    P_f=0
end
if n>4
    P_g=T(:,:,1,17)+T(:,:,1,18)+T(:,:,1,19)+T(:,:,1,20)+T(:,:,1,21)+...
        T(:,:,1,22)+T(:,:,1,23)+T(:,:,1,24)+T(:,:,1,25)
else
    P_g=0
end
if n>5
    P_h=T(:,:,1,26)+T(:,:,1,27)+T(:,:,1,28)+T(:,:,1,29)+T(:,:,1,30)+...
        T(:,:,1,31)+T(:,:,1,32)+T(:,:,1,33)+T(:,:,1,34)+T(:,:,1,35)+...
        T(:,:,1,36)
else
    P_h=0
end
P_i=1-P_s-P_p-P_d-P_f-P_g-P_h

radius=mr(C)
energycor=real(energy4(A));
energy=-32/n^2+24*energycor

save filename A C N T P_s P_p P_d P_f P_g P_i radius energy


function b_elem4=b_elem4(n,l1,l2,l3,l4,w1,w2,w3,w4,L,M,MI,p)

h=0;
if p~=-1 & p~=1
    display('parity, p, must be -1 or 1')
elseif p~=(-1)^(l1+l2+l3+l4);
    b_elem4=0;
else
for m1=-l1:l1
for m2=-l2:l2
for m3=-l3:l3
    h=h+a_elem4(n,l1,l2,l3,l4,m1,m2,m3,0)*...
        i_elem4(l1,l2,l3,l4,m1,m2,m3,0,w1,w2,w3,w4,L,M,MI);
end end end
    b_elem4=h;
end
```

```
function i_elem4=i_elem4(l1,l2,l3,l4,m1,m2,m3,m4,w1,w2,w3,w4,L,M,MI)

global CGh;

j=0;
if MI~=m1+m2+m3+m4 | M~=w1+w2+w3+w4
    i_elem4=0;
else
    for l12=abs(l1-l2):(l1+l2)
    for l34=abs(l3-l4):(l3+l4)
    if (l12+1)*l12*2+m1+m2+1>0 & (l34+1)*l34*2+m3+m4+1>0 ...
        & (l12+1)*l12*2+w1+w2+1>0 & (l34+1)*l34*2+w3+w4+1>0 ...
        & abs(l12-l34)<L+1 & l12+l34>L-1
        j=j+CGh((l1+1)*l1*2+m1+1,(l2+1)*l2*2+m2+1,(l12+1)*l12*2+m1+m2+1)...
        *CGh((l3+1)*l3*2+m3+1,(l4+1)*l4*2+m4+1,(l34+1)*l34*2+m3+m4+1)...
        *CGh((l1+1)*l1*2+w1+1,(l2+1)*l2*2+w2+1,(l12+1)*l12*2+w1+w2+1)...
        *CGh((l3+1)*l3*2+w3+1,(l4+1)*l4*2+w4+1,(l34+1)*l34*2+w3+w4+1)...
        *CGh((l12+1)*l12*2+m1+m2+1,(l34+1)*l34*2+m3+m4+1,(L+1)*L*2+MI+1)...
        *CGh((l12+1)*l12*2+w1+w2+1,(l34+1)*l34*2+w3+w4+1,(L+1)*L*2+M+1);
    else
        j=j;
    end end end
    i_elem4=8*pi^2*j/(2*L+1);
end


function a_elem4=a_elem4(n,l1,l2,l3,l4,m1,m2,m3,m4)

global CGh;
global wr;

j=(n-1)/2;

cp=complex(0,2*pi/3);

a1=CGh((j+1)*j*2+j+1,(j+1)*j*2-j+1,(l1+1)*l1*2+1)*wr((l1+1)*l1+m1+1)*...
    exp(-cp*m1);
a2=CGh((j+1)*j*2+j+1,(j+1)*j*2-j+1,(l2+1)*l2*2+1)*wr((l2+1)*l2+m2+1)*...
    exp(cp*m2);
a3=CGh((j+1)*j*2+j+1,(j+1)*j*2-j+1,(l3+1)*l3*2+1)*wr((l3+1)*l3+m3+1);
a4=CGh((j+1)*j*2+j+1,(j+1)*j*2-j+1,(l4+1)*l4*2+1);

if l1>n-1 | l2>n-1 | l3>n-1 | l4>n-1 | l1<0 | l2<0 | l3<0 | l4<0 |
m1>abs(l1) | m2>abs(l2) | m3>abs(l3) | m4>abs(l4)
    display('wrong input in a_elem4')
```

```
else
    a_elem4=a1*a2*a3*a4;
end
```

function spin4=spin4(S,MS,S12,S34,s1,s2,s3,s4)

```
global CGh;

if abs(s1+s2)>S12 | abs(s3+s4)>S34 | MS~=s1+s2+s3+s4
    spin4=0;
else
    spin4=CGh(2*S12*(S12+1)+s1+s2+1,2*S34*(S34+1)+s3+s4+1,2*S*(S+1)+MS+1)...
        *CGh(2.5+s1,2.5+s2,2*S12*(S12+1)+s1+s2+1)...
        *CGh(2.5+s3,2.5+s4,2*S34*(S34+1)+s3+s4+1);
end
```

function radius=mr(C)

```
Z=4;
h=size(C);
h=h(1);

y=0;
for a=1:h
    if a==1
        l=0;
    elseif a>1 & a<5
        l=1;
    elseif a>4 & a<10
        l=2;
    elseif a>9 & a<17
        l=3;
    elseif a>16 & a<26
        l=4;
    elseif a>25 & a<37
        l=5;
    else
        l=6;
    end
    for b=1:h
    for c=1:h
    for d=1:h
        y=y+(3*h-l*(l+1))/(2*Z)*C(a,b,c,d);
    end end end
```

```
end

radius=y;
```

function energy4=energy4(A);

```
load En_mat.mat

s=size(A)./2;
n=sqrt(s(1));
h=0;

for la1=0:n-1
for la2=0:n-1
for la3=0:n-1
for la4=0:n-1
for ma1=-la1:la1
for ma2=-la2:la2
for ma3=-la3:la3
for ma4=-la4:la4
for sa1=-0.5:0.5
for sa2=-0.5:0.5
for sa3=-0.5:0.5
for sa4=-0.5:0.5
    sb1=sa1;
    sb2=sa2;
    xa=2*((la1+1)*la1+ma1+1)+sa1-0.5;
    xa2=(la1+1)*la1+ma1+1;
    ya=2*((la2+1)*la2+ma2+1)+sa2-0.5;
    ya2=(la2+1)*la2+ma2+1;
    za=2*((la3+1)*la3+ma3+1)+sa3-0.5;
    qa=2*((la4+1)*la4+ma4+1)+sa4-0.5;
    for lb1=0:n-1
    for lb2=0:n-1
    for mb1=-lb1:lb1
    for mb2=-lb2:lb2
        xb=2*((lb1+1)*lb1+mb1+1)+sb1-0.5;
        xb2=(lb1+1)*lb1+mb1+1;
        yb=2*((lb2+1)*lb2+mb2+1)+sb2-0.5;
        yb2=(lb2+1)*lb2+mb2+1;
        for j=min(abs(la1-lb1),abs(la2-lb2)):max((la1+lb1),(la2+lb2))
        for m=-j:j
            z=(j+1)*j+m+1;
            if -ma1+mb1~=m | ma2-mb2~=m | j<abs(la1-lb1) | ...
```

```
                    j<abs(la2-lb2) | j>abs(la1+lb1) | j>abs(la2+lb2)
                h=h;
            else
                h=h+conj(A(xa,ya,za,qa))*A(xb,yb,za,qa)...
                    *En_mat(n,xa2,ya2,xb2,yb2,z);
            end
        end end
    end end end end
end end end end end end end end end end end end

energy4=h;
```

C.2.2   Program: Calculating En_mat

Contents

- function En_mat()
- function K=K(n,la1,ma1,la2,ma2,lb1,mb1,lb2,mb2,k,q);
- function r_int=r_int(r1,r2,n,la1,la2,lb1,lb2,k);
- function radf=radf(r,n,j);
- function laguerre=laguerre(v,a,x);
- function bino=bino(n,k);
- function gaunt=gaunt(la,ma,L,M,lb,mb)

function En_mat()

```
nmax=3;

En_mat=zeros(nmax,nmax^2,nmax^2,nmax^2,nmax^2,(2*nmax-1)^2);

for n=2:nmax
for la1=0:n-1
for la2=0:n-1
for ma1=-la1:la1
for ma2=-la2:la2
    xa=(la1+1)*la1+ma1+1;
    ya=(la2+1)*la2+ma2+1;
    for lb1=0:n-1
    for lb2=0:n-1
    for mb1=-lb1:lb1
    for mb2=-lb2:lb2
        xb=(lb1+1)*lb1+mb1+1;
        yb=(lb2+1)*lb2+mb2+1;
        for k=0:2*(n-1)
        for m=-k:k
```

```
            z=(k+1)*k+m+1;
            En_mat(n,xa,ya,xb,yb,z)=...
                K(n,la1,ma1,la2,ma2,lb1,mb1,lb2,mb2,k,m);
        end end
    end end end end
end end end end end

save En_mat
```

function K=K(n,la1,ma1,la2,ma2,lb1,mb1,lb2,mb2,k,q);

```
p=(4*pi/(2*k+1))*...
    dblquad(@r_int,eps,100,eps,100,10^-5,[],n,la1,la2,lb1,lb2,k);
w=(-1)^q*gaunt(la1,ma1,k,-q,lb1,mb1)*gaunt(la2,ma2,k,q,lb2,mb2);
K=p*w;
```

function r_int=r_int(r1,r2,n,la1,la2,lb1,lb2,k);

```
r2_vec=zeros(size(r1))+r2;
%Vector with the same length as r1 and the value of r2 in all entrances

r_int=r1.^2.*r2.^2.*conj(radf(r1,n,la1)).*conj(radf(r2,n,la2)).*...
    radf(r1,n,lb1).*radf(r2,n,lb2).*(min(r1,r2_vec)).^k./...
    (max(r1,r2_vec)).^(k+1);
```

function radf=radf(r,n,j);

```
za=1;
f1=prod(1:(n-j-1));
f2=prod(1:(n+j));

radf=n^(-1)*sqrt(za*f1/f2)*(2*za/n)*(2*r*za/n).^(j).*...
    laguerre(n-j-1,2*j+1,2*r*za/n).*exp(-r*za/n);
```

function laguerre=laguerre(v,a,x);

```
h=x*0;
for y=0:v;
    h=h+(-1)^y*bino(v+a,v-y)*x.^y/prod(1:y);
end
laguerre=h;
```

function bino=bino(n,k);

```
if k<n+1;
```

```
    u=prod(1:n)/(prod(1:k)*prod(1:(n-k)));
else
    u=0;
end
bino=u;
```

function gaunt=gaunt(la,ma,L,M,lb,mb)

```
if -ma+M+mb~=0 | la+L-lb<0 | lb-L+lb<0 | -la+L+lb<0
    gaunt=0;
else
    gaunt=(-1)^(ma+mb)*sqrt((2*la+1)*(2*L+1)/(2*lb+1)/(4*pi))...
        *clebsch(la,-ma,L,M,lb,-mb)*clebsch(la,0,L,0,lb,0);
end
```

Bibliography

[1] R. P. Madden and K. Codling, Phys. Rev. Lett. **10**, 516 (1963).

[2] J. J. Leventhal, http://www.umsl.edu/ jjl/homepage/chapters/Chap_10.doc.

[3] N. database, http://physics.nist.gov/cgi-bin/AtData/levels_form.

[4] U. Fano, Phys. Rev. **124**, 1866 (1961).

[5] J. W. Cooper, U. Fano, and F. Prats, Phys. Rev. Lett. **10**, 518 (1963).

[6] U. Fano and J. W. Cooper, Phys. Rev. A **137**, 1364 (1965).

[7] F. J. Wuilleumier, S. Diehl, D. Cubaynes, J.-M. Bizau, and E. T. Kennedy, J. Electron Spectrosc. **88**, 41 (1998).

[8] C. E. Kuyatt, J. A. Simpson, and S. R. Mielczarek, Phys. Rev. **138**, A385 (1965).

[9] R. Bruch, G. Paul, J. Andrä, and L. Lipsky, Phys. Rev. A **12**, 1808 (1975).

[10] M. Rødbro, R. Bruch, and P. Bisgaard, J. Phys. B: At. Mol. Phys. **12**, 2413 (1979).

[11] L. M. Kiernan, E. T. Kennedy, J.-P. Mosnier, J. T. Costello, and B. F. Sonntag, Phys. Rev. Lett. **72**, 2359 (1994).

[12] L. B. Madsen, J. Phys. B: At. Mol. Opt. Phys. **36**, R223 (2003).

[13] L. B. Madsen, Dr. thesis, Department of Physics and Astronomy, University of Aarhus (2003).

[14] C. G. Bao, W. F. Xie, and C. D. Lin, J. Phys. B: At. Mol. Opt. Phys. **27**, L193 (1994).

[15] C. G. Bao, Phys. Rev. A **50**, 2182 (1994).

[16] C. G. Bao, Commun. Theor. Phys. **29**, 491 (1996).

[17] C. G. Bao, X. Yang, and C. D. Lin, Phys. Rev. A **55**, 4168 (1997).

[18] C. G. Bao, Phys. Lett. A **250**, 123 (1998).

[19] C. G. Bao, Phys. Rev. Lett. **82**, 61 (1999).

[20] M. Kotani, A. Amemiya, E. Ishiguro, and T. Kimura, *Tables of Molecular Integrals* (MARUZEN Co. Ltd., Tokyo, 1963).

[21] M. Weissbluth, *Atoms and Molecules* (Academic Press, San Diego, 1978).

[22] J. Q. Chen, *Group Representation Theory for Physicts* (World Scientific, Singapore, 1989).

[23] R. N. Zare, *Angular Momentum* (Wiley and sons, 1988).

[24] L. Lipsky, E. R. Anania, and M. J. Conneely, At. Data Nucl. Data Tables **20**, 127 (1977).

[25] B. H. Bransden and C. J. Joachain, *Physics of Atoms and Molecules* (Pearson Education, 1983), 2nd ed.

[26] T. Morishita and C. D. Lin, Phys. Rev. A **64**, 052502 (2001).

[27] Y. Komninos, M. Chryros, and C. A. Nicolaides, Phys. Rev. A **38**, 3182 (1988).

[28] T. Morishita and C. D. Lin, Phys. Rev. A **59**, 1835 (1999).

[29] Y. Komninos and C. A. Nicolaides, Phys. Rev. A **50**, 3782 (1994).

[30] C. G. Bao, Phys. Rev. A **47**, 1752 (1993).

[31] L. B. Madsen and K. Mølmer, Phys. Rev. Lett. **87**, 133002 (2001).

[32] L. B. Madsen and K. Mølmer, Phys. Rev. A **64**, 060501(R) (2001).

[33] L. B. Madsen and K. Mølmer, Phys. Rev. A **65**, 022506 (2002).

[34] L. B. Madsen and K. Mølmer, J. Phys. B: At. Mol. Opt. Phys. **36**, 769 (2003).

[35] J. F. Baugh, D. A. Edmonds, P. T. Nellesen, C. E. Burkhardt, and J. J. Leventhal, Am. J. Phys. **65**, 1097 (1997).

[36] K. Mølmer, Master's thesis, Department of Physics and Astronomy, University of Aarhus (1987).

[37] Y. Azuma, F. Koike, J. W. Cooper, T. Nagata, G. Kutluk, E. Shigemasa, R. Wehlitz, and I. A. Sellin, Phys. Rev. Lett. **79**, 2419 (1997).

[38] N. Vaeck and J. E. Hansen, J. Phys. B: At. Mol. Opt. Phys. **25**, 883 (1992).

[39] U. Fano, J. Phys. B: At. Mol. Opt. Phys. **7**, L401 (1974).

[40] G. F. Drukarev, Sov. Phys, -JETP **56**, 532 (1982).

[41] M. E. Kellman and D. R. Herrick, J. Phys. B: At. Mol. Opt. Phys. **11**, L755 (1978).

[42] R. E. Peierls and J. Yoccoz, Proc. Phys. Soc., London, Sect. A) **70**, 381 (1957).

[43] G. Herzberg, *Molecular Spectra and Molecular Structure, III. Electronic Spectra and Electronic Structure of Polyatomic Molecules* (D. Van Nostrand Company, Princeton New Jersey, 1966).

[44] S. Watanabe and C. D. Lin, Phys. Rev A **36**, 511 (1986).

[45] L. B. Madsen, Private communication.

[46] M. Abramowitz and I. A. Stegun, *Handbook of Mathematical Functions* (Dover, USA, 1964).